

MASSACHUSETTS INSTITUTE OF TECHNOLOGY
LINCOLN LABORATORY

**DESIGN AND TEST OF A MULTICHANNEL
Ka-BAND RADIOMETER FOR THICKNESS
MEASUREMENT OF OIL FILMS ON WATER**

T.J. MURPHY
Group 47

O.B. McMAHON
Group 84

PROJECT REPORT OSR-1

6 JANUARY 1997

No distribution of this report shall be made to DTIC.

Transmittal outside the Department of Defense, other than initial distribution to DoD contractors, must have prior approval of the Lincoln Laboratory Program Manager.

No secondary distribution is authorized without prior written approval of the Lincoln Laboratory Program Manager.

ABSTRACT

This report describes the design and laboratory test of the Ka-band Oil Spill Radiometric Measurement System. This system is a second-generation design based on that of the Frequency Scanning Radiometer (FSR) that was tested at OHMSETT (the National Oil Spill Response Test Facility) in October 1994.

The design philosophy for this instrument was to use commercially available, off-the-shelf parts for the unit. In contrast to the FSR that stepped-and-sampled 16 frequencies over time, the Oil Spill Radiometric Measurement System measures 12 channels simultaneously. A detailed description of the receiver operation is contained in this report.

This instrument was tested under laboratory controlled conditions using a small "calibrated" test tank on three different occasions. Oil-on-water thicknesses from 0.0 to 10.0 mm were measured, and the results compare favorably with theoretical predictions. Measurement of unknown thicknesses of oil were completed and the resulting estimates matched those of the operator. The report contains detailed comparisons between the measured data and the theoretical predictions.

Based on the successful operation of this instrument during laboratory testing, this equipment should be tested using conditions similar to the October 1994 FSR tests at OHMSETT. Recommendations are also included for increasing the instrument receiver performance, as well as for the further development of automatic oil thickness estimation algorithms.

TABLE OF CONTENTS

Abstract	iii
List of Illustrations	vii
List of Tables	vii
1. INTRODUCTION	1
2. OIL SPILL RADIOMETER	3
2.1 Theory of Operation	3
2.2 Receiver Noise Temperature	9
2.3 Calibration	10
3. TEST DESCRIPTION AND RESULTS	15
3.1 Test Description	15
3.2 Results	16
4. CONCLUSIONS/RECOMMENDATIONS	21
4.1 Conclusions	21
4.2 Recommendations	21
REFERENCES	23
APPENDIX A – RECEIVER NOISE TEMPERATURE COMPUTATION	25
APPENDIX B – ANALYSIS OF RADIOMETRIC BRIGHTNESS TEMPERATURE VERSUS FREQUENCY PLOTS	27

LIST OF ILLUSTRATIONS

Figure No.		Page
1	Photograph of Ka-band Oil Spill Radiometric measurement system.	4
2	Photograph of receiver electronics.	5
3	System block diagram.	7
4	Plot of receiver noise temperature versus measurement frequency.	10

LIST OF TABLES

Table No.		Page
1	List of Parts	8
2	Results from 12 August 1996 Test	18
3	Results from 16 August 1996 Test	19
4	Results from 21 August 1996 Test	20

1. INTRODUCTION

The Oil Spill Radiometer is a wideband, multichannel, Ka-band (26–40 GHz) radiometer designed to estimate the thickness of oil films on water under all weather conditions. The Oil Spill Radiometer is a second generation instrument designed with parameters that closely match the operational parameters of the Frequency Scanning Radiometer (FSR), the initial proof-of-concept instrument tested at OHMSETT (the National Oil Spill Response Test Facility) in October 1994 [1,2].

This report describes the Ka-band Oil Spill Radiometer and initial laboratory testing to verify instrument operation. Section 2 describes the design and testing of the radiometer hardware. Section 3 discusses the controlled laboratory testing and results of the oil-on-water measurements. Section 4 provides conclusions and recommendations.

The details concerning the computation of the receiver noise temperature are given in Appendix A. All of the data sets collected during the instrument verification testing are included in Appendix B with comments detailing the analysis of each data set.

2. OIL SPILL RADIOMETER

Figure 1 is a photograph of the Ka-band Oil Spill Radiometric Measurement System. Figure 2 shows a close-up of the receiver electronics, which are housed in a weather-resistant, briefcase-type enclosure measuring 32 X 16 in. The antenna protrudes from one end of the enclosure and all the electrical connections (power, waveguide switch control, and the 12 detected channels) are mounted on the opposite end. The analog-to-digital (A/D) converter electronics and laptop computer, which are mated together as a separate unit, complete the system. An equipment cart was modified to transport the system and support the receiver electronics box during data collection activities.

The Oil Spill Radiometer is designed around the system parameters of the Frequency Scanning Radiometer (FSR) described in Hover et al. [1]. The FSR was a single-channel radiometer capable of operating at selected frequencies over the entire Ka-band (26–40 GHz). The instantaneous system bandwidth of the FSR receiver was approximately 500 MHz, with channel selection provided by a controllable frequency oscillator. Conversely, the Oil Spill Radiometer is a 12-channel instrument; each channel has a 250 MHz instantaneous bandwidth, and a fixed frequency oscillator is used for downconversion. The FSR required approximately 12 s to scan through 16 specified frequencies; the parallel receiver channel design of the Oil Spill Radiometer requires less than 1 s to acquire the sample data for the 12 channels. In both units, sampled voltage is converted to radiometric brightness temperature using a standard calibration algorithm.

The remainder of this section discusses specific details concerning the design of the Oil Spill Radiometer.

2.1 THEORY OF OPERATION

The Oil Spill Radiometer is a total-power radiometer. A block diagram of the instrument is shown in Figure 3; Table 1 lists the parts, manufacturers, and part numbers. The key receiver front-end components are a 26–40-GHz low-noise preamplifier, full-waveguide-band single-balanced mixer, and a second stage intermediate frequency (IF) low-noise amplifier.

The Oil Spill Radiometer operates by first collecting the thermal radiation incident in the antenna footprint and amplifying this weak signal using a wide-band low-noise preamplifier. The feed horn/waveguide combination acts as a high-pass filter that allows Ka band energy to pass to the first amplification stage. The preamplifier operates over the 26–40-GHz band, has a gain of 29 dB, and noise figure of 2.0. This amplified signal (the

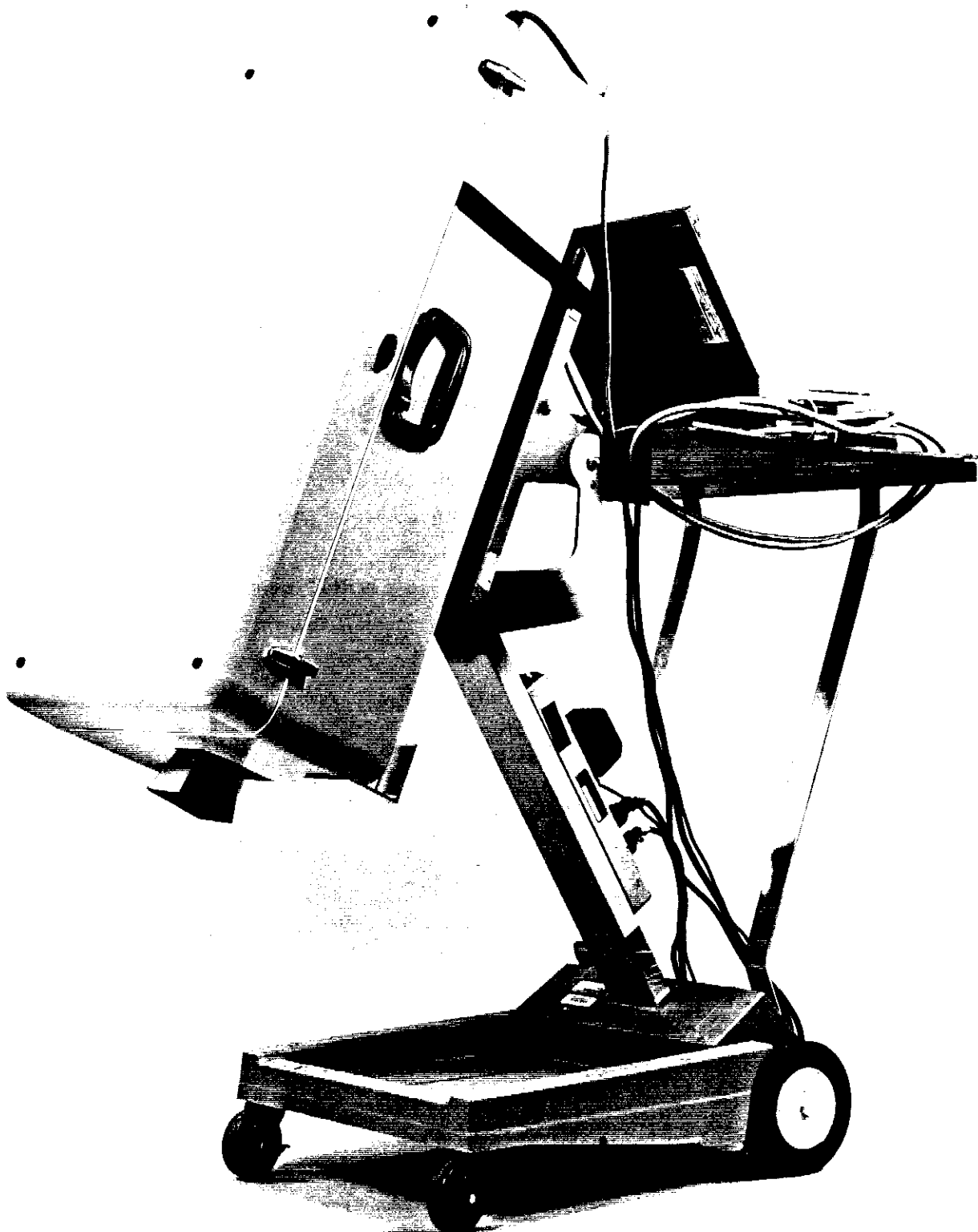


Figure 1. Ka-band Oil Spill Radiometric measurement system.

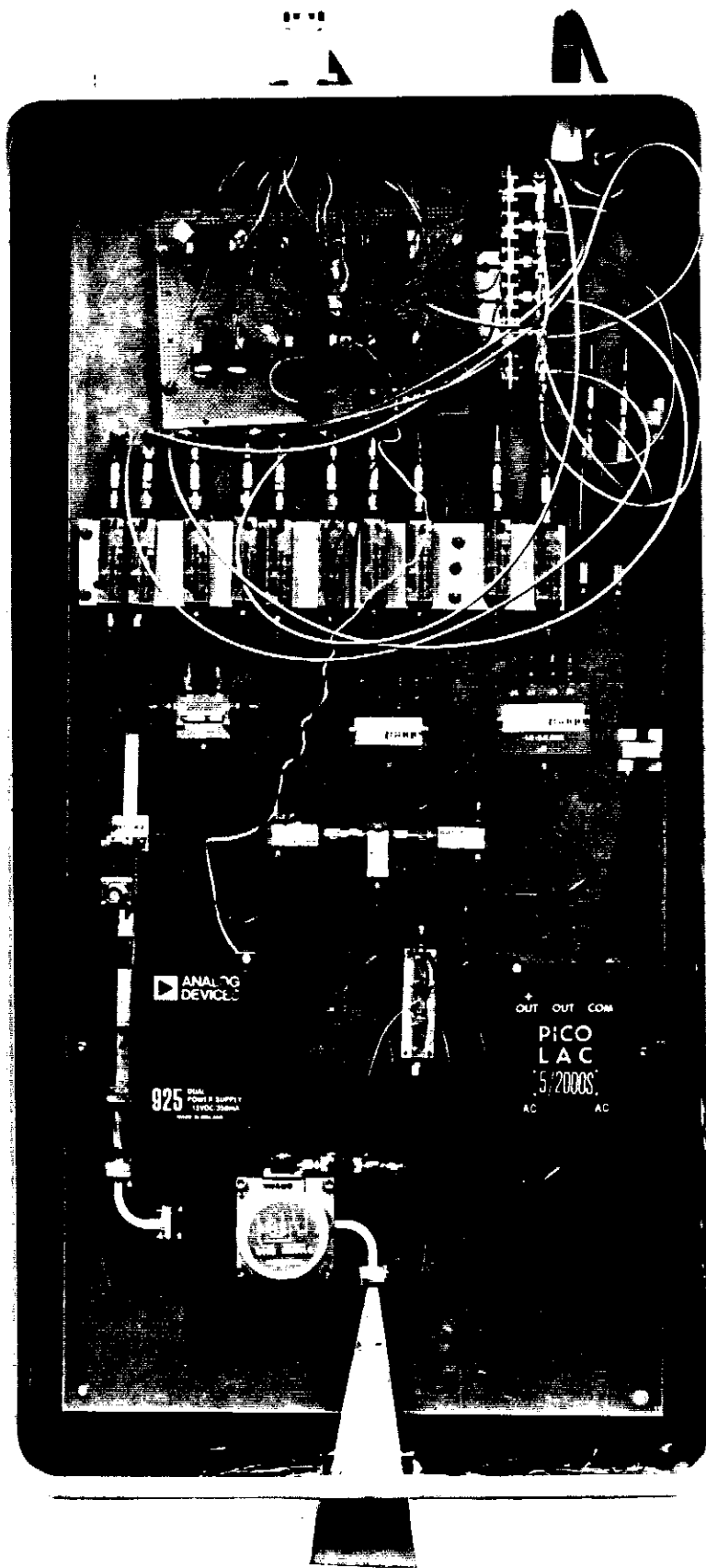


Figure 2. Receiver electronics.

lower sideband) is then mixed with a fixed local oscillator (LO) frequency (41 GHz) to obtain the difference frequency, also called the intermediate frequency. This IF signal occupies the frequency band from 1–14 GHz representing the energy contained in the 40–27-GHz band respectively. The IF amplifier has a gain of 45 dB and a noise figure of 4 dB. After IF amplification, the 1–14-GHz signal is split twice using power dividers to create four channels containing a 1–14-GHz signal. The next set of power dividers splits the power into three channels namely 1.1–4.9 GHz, 6–9.3 GHz, and 10.4–14 GHz. At each power splitter output, 250-MHz bandpass filters define each of the 12 frequency bands of interest, spaced at 1.1-GHz intervals beginning at 1.6 GHz. This represents the Ka-band energy collected by the antenna starting at 39.4 GHz and decreasing by intervals of 1.1 GHz. The signal in each of the 12 channels is then detected, or converted to a dc voltage proportional to the power incident in each 250-MHz channel bandwidth. This voltage is then low-pass-filtered through a buffer amplifier and integration stage before A/D conversion. The low-pass filter is used to reduce noise while the integration stage acts to increase the signal level prior to A/D conversion.

The A/D converter samples at a rate up to 3 KHz as set by the laptop computer controller. The samples can be time-averaged over a selected interval to reduce spurious noise response. The operator can choose to view a continuous scan of the plot of measured brightness temperature versus sample frequency, or choose to generate a single sweep for data recording purposes. The data file that is saved consists of a date/time stamp, operator comments about the sweep, and the channel number, sample frequency, and measured brightness temperature for each of the 12 channels. Another option in the laptop software allows the operator to remove (and replace with an interpolated value) any extremely noisy or 'dead' channels. Also included in the software is the instrument calibration algorithm.

The components used for internal calibration include the waveguide switch, noise source, terminated waveguide section, and directional coupler. The waveguide switch in its normal position connects the antenna output to the preamplifier input. A control signal from the A/D board causes the switch to change positions, thus connecting the calibration sources to the preamplifier. When the noise source is not powered, the waveguide termination acts as a room temperature calibration source. When power is applied to the noise source (using a control signal from the A/D board), this device acts as a very hot temperature source. The directional coupler acts as an attenuator to bring the noise source temperature into the expected operational temperature range of the radiometer. By taking measurements on these two known temperatures, the voltage measured at each detector output can be associated with radiometric temperature. Because two points (hot and cold) are known, linear interpolation techniques can be used to determine the radiometric temperatures measured from the oil-on-water measurements. The calibration methodology is discussed in Section 2.3.

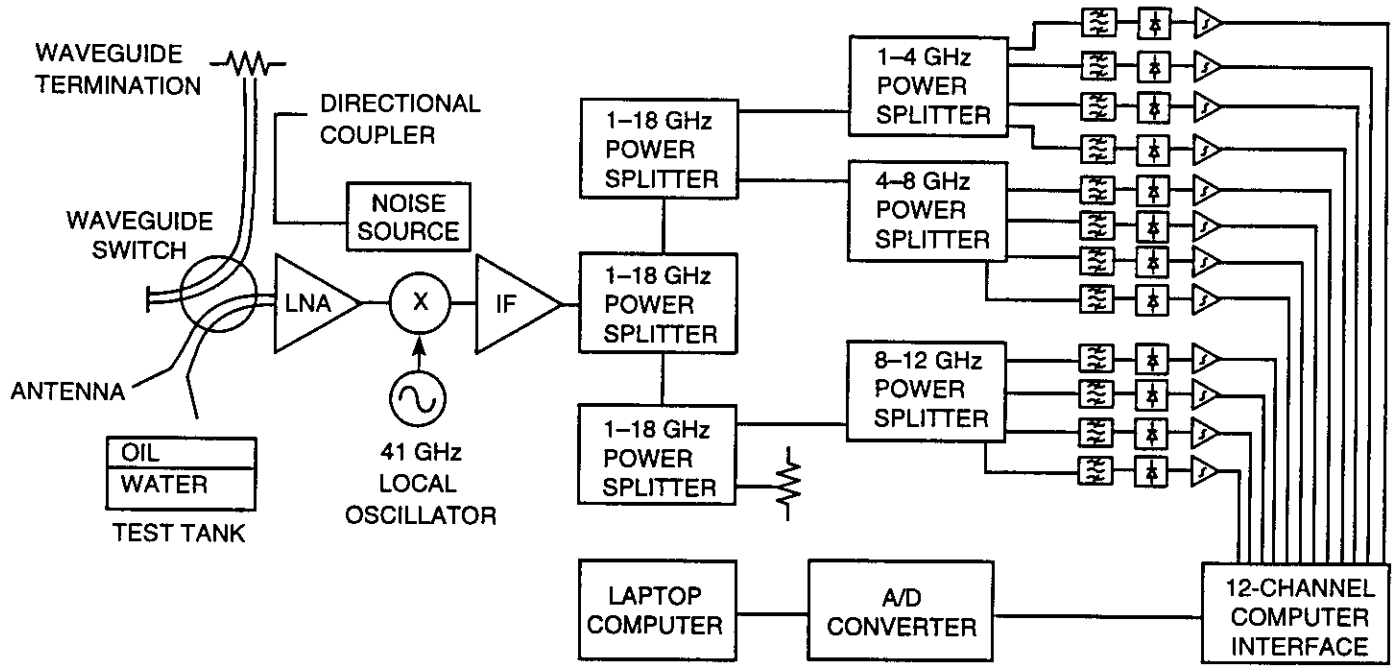


Figure 3. Block diagram.

TABLE 1
Detailed Parts Listing for the Ka-Band Oil Spill Radiometer

Description	Manufacturer	Part Number	Quantity
Antenna	Microwave Assoc.	572S	1
Waveguide Switch	Waveline	1077E	1
26 - 40 GHz Amp.	Miteq	JS4-26004000-30-5	1
1 - 18 GHz Amp.	Miteq	JS33-02001600-40-5P	1
Mixer	Spacek Labs Inc.	MKa8	1
Local Oscillator	Spacek Labs Inc.	GQ-410	1
Power Divider			
2 - 18 GHz	Sage	4232	3
1 - 4 GHz	Sage	4124	1
4 - 8 GHz	Sage	4234A	1
8 - 14 GHz	Sage	4144	1
SMA Termination	Weinshel	M1406A	1
Detector	M/A Com Inc.	2086-6000-00	12
Bandpass Filters	Daden Anthony Assoc. Inc.	CS13700-250-4SS	1
		CS12600-250-4SS	1
		CS11500-250-4SS	1
		CS10400-250-4SS	1
		CS9300-250-4SS	1
		CS8200-250-4SS	1
		CS7100-250-4SS	1
		CS6000-250-4SS	1
		CS4900-250-4SS	1
		CS3800-250-4SS	1
		BA2700-250-4SS	1
		BA1600-250-4SS	1
Power Supplies			
15 Volt	Analog Devices	925	1
5 Volt	Pico Lac	5/2000S	1
Buffer Amp.	MIT/LL		12
A/D Converter	IOtech	DaqBook 216, DBK19 Card	1
Computer	Texas Instruments	Travelmate 4000 WINSX	1
Noise Source	Noise/Com	NC5128	1
Directional Coupler	Microwave Assoc.	7728	1
WG Termination	AeroTech	28-201	1
Equipment Case	Skydyne	6840C	1
Equipment Cart	Tektronics	K212	1
Misc. Items	MIT/LL or Local Vendor		
Waveguide Pieces			
Semi-rigid Coax			
SMA Coax Cables			
Heat Sinks			
AC Power Cord/Receptacle/Power Strip			
Wire/Cables/Connectors			
Mounting Plate/Misc. Hardware			

2.2 RECEIVER NOISE TEMPERATURE

The sensitivity of the Oil Spill Radiometer is characterized by the receiver noise temperature, which, for this type of receiver is computed by using the amplifier gains, mixer conversion loss, and noise figures of the amplifiers and mixers. The major component of the receiver noise temperature is the first stage in the receiver; in this case, it is the Ka-band low-noise preamplifier. The computation for the receiver noise temperature (T_R) is [3] (see also Appendix A):

$$T_R = T_{RF} + \frac{T_M}{G_{RF}} + \frac{T_{IF}}{G_{RF}G_M}. \quad (1)$$

In this equation, T_{RF} is the noise temperature of the RF preamplifier, G_{RF} is its gain; T_M is the noise temperature of the mixer, G_M is its single-sideband gain; and T_{IF} is the noise temperature of the IF amplifier. The noise figures and gains of these devices are typically expressed in decibels and must be converted to natural numbers using the following relation:

$$N = 10^{(dB/10)}, \quad (2)$$

where N is the resulting natural number, and dB is the number expressed in decibels.

Typically, noise temperature for a device is expressed as a noise figure. To convert to noise temperature, the following relation is used:

$$T = (F - 1)T_0, \quad (3)$$

where T is the noise temperature, F is the noise figure (the dB units converted to a natural number), and T_0 is the expected operating temperature in degrees Kelvin.

Applying Equation 1 using the manufacturers' specifications for noise figures and gains, the computed receiver noise temperature for the Oil Spill Radiometer is 177 K; the details of this computation are shown in Appendix A. The receiver noise temperature is measured for each of the 12 channels. A plot of measured receiver noise temperature versus frequency is shown in Figure 4.

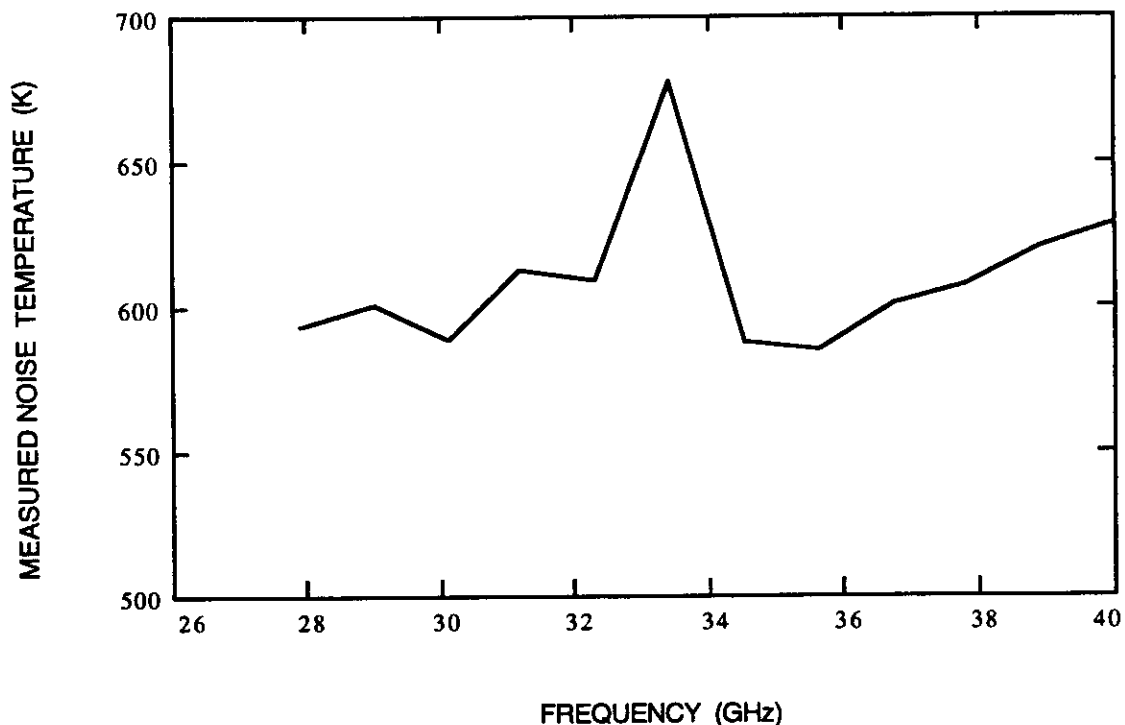


Figure 4. Measured receiver noise temperature versus frequency.

The plot of the measured receiver noise temperature versus frequency shows that most of the points fall between 580 K and 630 K. The only outlying point, 33.4 GHz, has a receiver noise temperature of 678 K; this higher noise temperature may be due to a performance characteristic of the 4–8 GHz signal splitter. Overall, these receiver noise temperature values are higher than predicted, indicating that there is more internal noise being generated than anticipated. The receiver noise temperature of this radiometer is approximately 200 K lower than the receiver noise temperature of the FSR [1]. This indicates that this radiometer has more sensitivity than the FSR.

2.3 Calibration

The system is calibrated at the start of each experiment, or when the operator detects drift (characterized by hotter or colder temperatures across the band) in the instrument's gain characteristics. Two thermal loads of different temperature (T_H and T_C) are placed in front of the antenna feed horn. The hot load is a blackbody radiator (a piece of microwave-absorbing material or Eccosorb) at ambient temperature. Thus T_H is the ambient temperature converted to degrees Kelvin. The cold thermal load is a piece of Eccosorb

placed in a bath of liquid nitrogen. Thus T_C is the temperature of the liquid nitrogen, namely 77 K. The voltage measured at the output of each of the detectors, V_H or V_C , is proportional to the radiometric brightness temperature, T_H or T_C , of the input radiation as given by

$$V_H = (T_R + t_1 T_H) G_T \quad (4)$$

$$V_C = (T_R + t_1 T_C) G_T, \quad (5)$$

where T_R is the receiver (i.e., electronics) noise temperature of the system, t_1 is the power transmission characteristic of the waveguide switch between the antenna and the RF low-noise preamplifier when the switch is in position 1, and G_T is a proportionality factor that includes the overall system gain. (The term T_R relates to the power transmission characteristics of the feed horn (i.e., antenna) and the waveguide switch between free space and the RF low-noise preamplifier.)

If the calibration procedure relied solely on the use of liquid nitrogen and ambient temperature measurements through the antenna feed horn, the transmission through the waveguide switch could be neglected because a waveguide switch would not be used; however, because internal calibration becomes necessary for the system as it matures into an airborne capable sensor, the transmission characteristics through the two different paths of the waveguide switch become important.

The calibration proceeds with the computation of the Y -factor. The ratio of V_H to V_C is used to compute this Y -factor for each of the 12 receiver channels:

$$Y = \frac{V_H}{V_C}. \quad (6)$$

Substitution of the V_H and V_C terms yields

$$Y = \frac{T_R + t_1 T_H}{T_R + t_1 T_C}. \quad (7)$$

By solving for T_R , the receiver noise temperature can be computed for each receiver channel:

$$T_R = \frac{t_1 \times (T_H - Y T_C)}{Y - 1} = \frac{t_1 \times [T_H - \frac{V_H}{V_C} T_C]}{\frac{V_H}{V_C} - 1}. \quad (8)$$

For oil on water measurements, V_{OUT} is proportional to the radiometric brightness temperature (T^B) as given by

$$V_{OUT} = (T_R + t_1 T^B) G_T. \quad (9)$$

The T^B can be computed for each channel, assuming unity for t_1 (i.e., no power loss through the waveguide switch), as

$$T^B = \frac{V_{OUT}}{V_H} - T_R = \frac{V_{OUT}}{V_H} [T_H + T_R] - T_R. \quad (10)$$

The T^B computation would be complete if the hot/cold load calibration through the antenna were an acceptable procedure; however, to alleviate the need for liquid nitrogen, an internal calibration method was developed. The internal calibration uses a calibrated “hot” noise source (T_H) and a terminated waveguide load at room temperature (T_C). If the transmission characteristics for the internal calibration path are now taken into account by allowing t_1 to characterize the waveguide switch in the internal calibration position, Equation 10 characterizes the internal calibration noise temperature (T_R). The path through the antenna and waveguide switch in position 2 (with transmission characteristic t_2) must also be taken into account by introducing Eccosorb at ambient temperature (T_A) in front of the antenna feed horn, and considering the waveguide switch transmission characteristics (t_2). The computation of the adjusted receiver noise temperature (T_R') proceeds in a manner similar to the computation described earlier in this section. Namely,

$$V_A = (T_R' + t_2 T_A) G_T \quad (11)$$

and computing the Y -factor for the internal calibration/antenna correction

$$\frac{V_A}{V_H} = \frac{T_R' + t_2 T_A}{T_R + t_1 T_H}. \quad (12)$$

Solving for the adjusted receiver noise temperature:

$$T_R' = \frac{V_A}{V_H} (T_R + t_1 T_H) - t_2 T_A. \quad (13)$$

The computation of the oil on water radiometric brightness temperature is slightly more complicated than the liquid nitrogen calibration case. Here the radiometric brightness temperature (T^B) is related to the measured voltage (V_M) as

$$V_M = (T_R' + t_2 T^B) G_T. \quad (14)$$

Computing the Y -factor

$$\frac{V_M}{V_H} = \frac{T_R' + t_2 T^B}{T_R + t_1 T_H}. \quad (15)$$

Solving for the brightness temperature yields

$$T^B = \frac{1}{t_2} \left[\frac{V_M}{V_H} (T_R + t_1 T_H) - T_R \right]. \quad (16)$$

For the multichannel radiometer calibration using the internal hot/cold loads, it is imperative that the hot load temperature (T_H), and the waveguide switch transmission characteristics (t_1 and t_2) are carefully measured at each radiometer measurement frequency. Currently, the through-antenna hot/cold load calibration is used as the primary calibration procedure; the development of the internal calibration procedure is continuing.

3. TEST DESCRIPTION AND RESULTS

This section describes the rooftop testing procedures used to verify the operation of the Ka-band Oil Spill Radiometric Measurement System. Data analysis methods were similar to those described in Murphy et al. [2]. Appendix B contains plots of the raw data, smoothed curve, and best theoretical fit (thickness estimate) of the radiometric brightness temperature (T^B) versus measurement frequency for three different collection days. One of the collections was performed as part of the equipment demonstration for the sponsor's Technical Representative. The raw results and declared thickness using the thickness estimation algorithm [2], as well as the results from a visual analysis of the T^B versus frequency curves are presented in tabular format; plots of the actual data are shown in Appendix B.

3.1 TEST DESCRIPTION

The Oil Spill Radiometric Measurement System must have a clear reflection path from the antenna feed horn to the sky via the reflection from the water/oil surface. Because of this geometry, the Radiometric Measurement System must be used outdoors. For instrument verification testing the equipment is brought to the roof of one of the Lincoln Laboratory buildings (namely, on the walkway between Buildings A and B.) From this vantage, the Radiometric Measurement System has a clear view of the sky.

Testing commences after the equipment has had some time to warm up and reach normal operating temperatures. Once the equipment warm-up is complete, a cold/hot load calibration is performed; for these verification measurements the cold load is Eccosorb bathed in liquid nitrogen, and the hot load is Eccosorb at ambient temperature. The hot/cold load calibration procedure is detailed in Section 2.3.

After the hot/cold load calibration is complete, water-only measurements are taken. Using the scan function of the instrument, the operator can observe the measurements in real-time, and can record a measurement scan when steady-state conditions are observed.

The test continues with the measurement of known oil thicknesses on water. The test tank is calibrated such that 100 ml of oil corresponds to 1 mm oil thickness. The operator adds oil, typically in increments of 1 mm, to the measurement tank, waits for a steady state condition, then collects a measurement scan. Diesel oil was used for all the laboratory tests.

If the result of the measurement scan agrees with the known thickness (and previous scanning results), one or a number of scans are recorded. After the maximum thickness is measured (typically 10 mm), oil absorbent cloths are used to remove an unknown quantity of oil from the test tank surface. The data sets are recorded on the laptop computer hard disk and include a comment by the operator concerning an estimate of the oil thickness.

After the test, the data sets are transferred from the laptop computer hard disk to a floppy disk for postcollection analysis. The VAX computer system located in the Surveillance Systems Group runs the analysis software. Data files are transferred from the floppy disk to the VAX system hard disk. The analyst uses the oil thickness estimation algorithm software to compare the measured data against a family of theoretical T^B vs frequency curves. If the analyst agrees with the algorithm estimate, no action is necessary; if the analyst believes that a different thickness estimate would better fit the data, different estimates can be investigated until the best fit is chosen. The outputs from this software are (1) a tabular form showing the raw results from each method used in the algorithm, the declared estimate, the method used to obtain the declaration, and the analyst's estimate; and (2) plots of T^B vs frequency of the raw data, a smoothed curve [a third-order polynomial, least-mean-squares (LMS) fit], and the analyst's choice of the estimated thickness.

3.2 TEST RESULTS

The Oil Spill Radiometric Measurement System was used to collect oil thickness data on three different days: 12 August, 16 August, and 21 August. The detailed results of each recorded measurement scan are shown in Appendix B as T^B vs. frequency plots followed by a description of curve fit and thickness estimated. The remainder of this section describes the overall results with the data presented in tabular form, with comments based on each collection day.

Each tabular entry contains (1) the file name; (2) the raw results from the thickness estimation algorithm, consisting of an LMS result, a correlation (CORR) result, a Mean/Slope (MN/SL) result, as well as the algorithm declared thickness (EST) and the methods used to generate a declared thickness (METHOD); (3) the result obtained by visual analysis of each curve by a data analyst (VIS); and (4) a comment relating to the fit of the curve, or why the analyst chose a thickness different from the algorithm estimate. The highlighted blocks in the raw results fields (LMS, CORR, MN/SL) closely match the final visual estimate. The

water-only measurements that are used as a reference background for each day are also listed in the tables.

3.2.1 12 August 1996 Results

Table 2 contains the results from the 12 August tests. The first number in the file naming convention specifies the expected oil thickness, e.g., 4MM812A.DAQ specifies that a volume of oil equal to a uniform layer of 4 mm was poured into the test tank.

The results using the water reference 0MM812.DAQ were poor, so the first water measurement was used as the background. These results were good for thicknesses up to 4 mm. The two 5-mm and first 6-mm measurements indicate that the instrument gain has drifted; note that the amplitude modulation caused by the oil on water is much larger than predicted by theory, even when excess T^B modulation is added to the theoretical prediction. After the first 6-mm measurement, the operator observed that the radiometer needed recalibration, which was done using the hot/cold load method. The new gain factors caused a slight change in the water reference temperature. This change was taken into account by observing the peak and minimum point on the resulting sinusoids, and estimating a corresponding water temperature.

Measurements of unknown thickness pools were included in this test. The results compare favorably with the operator's thickness observations.

3.2.2 16 August 1996 Results

A 0- to 10-mm oil-on-water data set was collected on 16 August; the results are presented in Table 3. The fourth number in the file naming convention specifies the expected oil thickness, e.g., 8165MMA.DAQ specifies that a volume of oil equal to a uniform layer of 5 mm was poured into the test tank.

The "B" water reference seems to be the best match to the data set; this is particularly indicated by the "A" water data set indicating an oil thickness though it was a water-only measurement. The 0.200 mm and the 0.000 mm theoretical curves differ only slightly in slope, making these difficult to separate analytically. The thin oil layers indicate mixed results while the thicker oil has good-to-excellent matches. The 10-mm oil thickness measurements appear to have some points lower than predicted; these channels may be experiencing a gain drift, indicating that the instrument should be recalibrated.

TABLE 2
Results from 12 August 1996 Test

FILE NAME	LMS	CORR	MN/SL	EST	METHOD	VIS	COMMENT
0MM812.DAQ							Water reference - precluded by use of 0MM812A.DAQ
0MM812A.DAQ	0.000	5.850	0.000	0.000	LMS & MN/SL	0.000	New water reference
1MM812A.DAQ	0.800	1.375	0.800	0.800	LMS & MN/SL	0.800	Good
1MM812B.DAQ	0.475	8.100	3.075	0.470	LMS only	0.475	Good
2MM812A.DAQ	2.125	1.975	2.075	2.100	LMS & MN/SL	2.100	Fair-to-good
2MM812B.DAQ	2.150	1.925	2.150	2.150	LMS & MN/SL	2.150	Good
4MM812A.DAQ	4.025	3.625	3.975	4.000	LMS & MN/SL	4.000	Fair
4MM812B.DAQ	3.850	3.825	0.375	3.825	LMS & CORR	3.800	Fair
5MM812A.DAQ	4.850	4.975	1.650	4.900	LMS & CORR	4.900	Fair when gain factor of 180% is used for theory
5MM812B.DAQ	4.750	4.900	1.425	4.825	LMS & CORR	4.800	Fair-to-good when gain factor of 200% is used for theory
6MM812A.DAQ	5.800	2.275	1.900	2.275	CORR only	5.800	Fair when gain factor of 200% is used for theory
6MM812B.DAQ	5.700	5.775	2.325	5.725	LMS & CORR	5.725	New water reference assumed for remaining files. Excellent
6MM812C.DAQ	5.775	5.775	2.450	5.775	LMS & CORR	5.775	Excellent
7MM812A.DAQ	6.700	3.250	2.550	6.700	LMS only	6.700	Excellent
7MM812B.DAQ	6.775	3.300	0.750	6.775	LMS only	6.775	Excellent
8MM812A.DAQ	7.675	7.675	0.875	7.675	LMS & CORR	7.675	Excellent
8MM812B.DAQ	7.750	7.775	0.850	7.750	LMS & CORR	7.750	Excellent
9MM812A.DAQ	8.675	1.800	0.775	8.675	LMS only	8.675	Excellent
9MM812B.DAQ	8.525	1.775	3.975	8.525	LMS only	8.525	Excellent
9MM812C.DAQ	8.575	1.775	3.925	8.575	LMS only	8.575	Excellent
10MM812B.DAQ	9.975	6.575	2.350	9.975	LMS only	9.975	Good-to-excellent
UNK1812A.DAQ	6.700	3.275	0.775	6.700	LMS only	6.700	Excellent
UNK1812B.DAQ	3.650	3.750	0.275	3.700	LMS & CORR	3.700	Good
UNK1812C.DAQ	3.575	3.650	0.150	3.600	LMS & CORR	3.600	Good
UNK1812D.DAQ	1.275	1.575	1.325	1.300	LMS & MN/SL	1.300	Good
UNK1812E.DAQ	0.000	0.500	0.000	0.000	LMS & MN/SL	0.000	Good-to-excellent
UNK1812F.DAQ	0.000	1.400	0.000	0.000	LMS & MN/SL	0.000	Excellent

3.2.3 21 August 1996 Results

The results of the 21 August data set are shown in Table 4. The fourth number in the file naming convention specifies the expected oil thickness, e.g., 8-20A7MM.DAT specifies that a volume of oil equal to a uniform layer of 7 mm was poured into the test tank. Although the file naming convention seems to indicate that the data sets were collected on 20 August, the actual collection occurred on 21 August.

TABLE 3
Results from 16 August 1996 Test

FILE NAME	LMS	CORR	MN/SL	EST	METHOD	VIS	COMMENT
8160MMB.DAQ							Water reference
8160MMA.DAQ	0.175	7.525	0.225	0.200	LMS & MN/SL	0.200	Excellent, however would have expected 0.000 mm
8161MMA.DAQ	1.000	3.950	1.000	1.000	LMS & MN/SL	1.000	Excellent
8161MMB.DAQ	1.350	0.525	1.475	1.400	LMS & MN/SL	1.400	Fair-to-good
8162MMA.DAQ	2.100	5.425	2.100	2.100	LMS & MN/SL	2.100	Fair-to-good
8162MMB.DAQ	1.900	1.825	1.975	1.850	LMS & CORR	1.850	Excellent
8163MMA.DAQ	3.000	2.900	0.125	2.950	LMS & CORR	2.950	Poor-to-fair
8163MMB.DAQ	3.000	2.925	0.225	2.950	LMS & CORR	2.950	Fair
8164MMA.DAQ	0.000	3.650	0.000	0.000	LMS & MN/SL	3.650	Good for correlation only estimate
8164MMB.DAQ	3.650	3.750	0.000	3.700	LMS & CORR	3.700	Good
8165MMA.DAQ	7.975	4.750	3.750	4.750	CORR only	4.750	Good
8165MMB.DAQ	4.250	4.725	3.925	4.725	CORR only	4.725	Good
8166MMA.DAQ	5.800	5.975	2.150	5.875	LMS & CORR	5.875	Good
8166MMB.DAQ	5.825	6.000	2.175	5.900	LMS & CORR	5.900	Good
8167MMA.DAQ	6.725	3.275	0.750	6.725	LMS only	6.725	Excellent
8167MMB.DAQ	6.775	3.300	0.775	6.775	LMS only	6.775	Excellent
8168MMA.DAQ	7.925	7.925	0.750	7.925	LMS & CORR	7.925	Excellent
8168MMB.DAQ	7.700	7.700	0.750	7.700	LMS & CORR	7.700	Excellent
8169MMA.DAQ	8.800	8.850	3.925	8.825	LMS & CORR	8.825	Excellent
8169MMB.DAQ	8.825	8.875	3.975	8.850	LMS & CORR	8.850	Good-to-excellent
81610MMA.DAQ	6.525	3.200	2.425	6.525	LMS only	10.000	Excellent if three outlying points disregarded
81610MMB.DAQ	6.550	6.550	2.450	6.550	LMS & CORR	10.000	Good if three outlying points disregarded

The results are quite favorable, indicating good curve matches (or better) from almost all the measurements. The water file 8160MMA.DAQ appears to be mislabeled; the raw data points appear to be very close to the measured values of 8160MMB.DAQ. The 3-mm curves are always difficult to discriminate from the 0 mm curves because the null of the T^B curve is being observed. There appears to be a drift in system gain during 5- or 6-mm data sweeps; by not applying a new (assumed) water background, the results of the thin unknown measurements seem to be skewed for thicker estimates. Some noisy data points are observed in the 10-mm curves. Overall, the results from the raw data measurements match the theoretical predictions well.

Table 4
Results from 21 August 1996 Testt

FILE NAME	LMS	CORR	MN/SL	EST	METHOD	VIS	COMMENT
8-20A0MM.DAT							Water reference
8-20A1MM.DAT	0.000	3.300	0.000	0.000	LMS & MN/SL	0.000	Appears to be 0.000 mm; file may be mislabeled
8-20A2MM.DAT	2.825	2.775	2.875	2.800	LMS & CORR	2.800	Good
8-20A3MM.DAT	2.250	2.600	2.100	2.175	LMS & MN/SL	2.600	Good (shape)
8-20A4MM.DAT	3.875	3.600	3.900	3.875	LMS & MN/SL	3.875	Good
8-20A5MM.DAT	4.675	4.725	1.300	4.700	LMS & CORR	4.700	Good
8-20A6MM.DAT	6.025	5.875	0.250	5.950	LMS & CORR	5.950	Fair-to-good
8-20B6MM.DAT	2.075	5.675	1.750	2.075	LMS only	6.000	Good - slightly above correlation-only estimate
8-20A7MM.DAT	10.00	3.250	2.200	3.250	CORR only	6.800	Good shape match to 6.800 mm
8-20A8MM.DAT	1.350	7.825	1.875	1.350	LMS only	7.800	Good match to correlation-only result
8-20A9MM.DAT	5.025	1.800	1.050	5.025	LMS only	8.800	Good, 8.800 mm chosen based on shape
8-20AXMM.DAT	1.925	6.525	1.675	1.800	LMS & MN/SL	9.950	Good, 9.950 mm chosen based on shape
8-20AUNK.DAT	1.500	7.625	1.675	1.575	LMS & MN/SL	1.575	Good for samples below 35 GHz.
8-20BUNK.DAT	1.425	4.050	1.650	1.525	LMS & MN/SL	1.525	Fair for samples below 36 GHz
8-20CUNK.DAT	1.425	4.100	1.650	1.525	LMS & MN/SL	1.525	Good for samples below 35 GHz
8-20DUNK.DAT	0.500	7.375	3.050	0.500	LMS only	0.500	Excellent but should be closer to 0.000 mm
8-20EUNK.DAT	3.275	3.300	3.275	3.275	LMS & MN/SL	0.200	Good-to-excellent but should be closer to 0.000 mm
8-20FUNK.DAT	3.350	7.175	3.300	3.325	LMS & MN/SL	0.300	Good-to-excellent but should be closer to 0.000 mm

4. CONCLUSIONS/RECOMMENDATIONS

4.1 CONCLUSIONS

The Oil Spill Radiometric Measurement System was tested under controlled conditions, using the small "calibrated" test tank at Lincoln Laboratory. On three occasions, the instrument was used to collect the T^B versus frequency signatures of oil on water for oil thicknesses from 0 mm to 10 mm in 1-mm increments. Additionally, measurements of unknown thicknesses were taken during two of the three tests. During posttest analysis, an automatic oil thickness estimation algorithm was used to analyze all the measurements and present a data analyst with thickness estimates. The analyst could compare the algorithm estimate to the data set or choose a better thickness estimate.

Based on the results from these three different test days, the system was able to measure the expected T^B versus frequency signatures for oil films within the 0- to 10-mm range. The instrument exhibits some gain variations over a long test period, however, the operator is able to recognize the excessive amplitude variation of the signature and recalibrate the instrument. These gain variations make thicknesses less than 1 mm difficult to estimate. Although the hardware for internal calibration is installed, more effort is needed for the internal calibration capability to be useable.

An automated oil thickness estimation algorithm was used to analyze each data set collected. The declared results from the algorithm compare favorably with the data analyst's results of visual comparison of the theoretical T^B versus frequency estimates.

4.2 RECOMMENDATIONS

Based on the successful testing under controlled conditions at Lincoln Laboratory, the instrument should be tested at OHMSETT under wave and chop conditions similar to those used in the October 1994 tests. If the instrument can successfully capture the T^B versus frequency signatures of oil on water under those conditions, larger (heavier) wave conditions should be chosen to find the upper limits of the instrument.

The results of the laboratory testing show some problems with gain drift over time during a long collection interval. The operator can recognize this drift and correct it by recalibrating the instrument. This drift is unexpected and might be heat related. Because of

this drifting, the system continues to use the proven hot/cold calibration procedure that utilizes liquid nitrogen. More testing is needed for the internal calibration to be useable.

Three channels have a low signal level at detector output resulting in the need for a high gain stage prior to the A/D conversion. The low signal level in these channels is caused by characteristics of the power splitters. An additional IF amplification stage should be added to increase the measured power at the detectors, which would allow the use of lower gain (i.e., buffer amplifiers) between the detector stage and the A/D conversion.

Although the results of the oil thickness estimation algorithm were favorable, the software was developed on an ad-hoc basis for the analysis of data collected at OHMSETT in October 1994. More work is needed to develop a more robust algorithm.

REFERENCES

1. G. L. Hover, T. J. Murphy, E. R. Brown, G. G. Hogan, O. B. McMahon, "Design, Construction, Test and Evaluation of a Frequency Scanning Radiometer for Measuring Oil Slick Thicknesses", Final Report, June 1994, Report No. CG-D-29-94, U.S. Department of Transportation, United States Coast Guard, Office of Engineering, Logistics, and Development.
2. T. J. Murphy, O. B. McMahon, G. L. Hover, "Test Tank Evaluation of a Frequency-Scanning Microwave Radiometer to Estimate Oil Slick Thickness and Physical Properties", Final Report, April 1996, Report No. (Pending), U.S. Department of Transportation, United States Coast Guard, Office of Research and Development.
3. F. T. Ulaby, R. K. Moore, A. K. Fung, Microwave Remote Sensing Active and Passive, Addison-Wesley, 1981, Vol. 1, pp. 355 - 356.

APPENDIX A
RECEIVER NOISE TEMPERATURE COMPUTATION

The receiver noise temperature was computed using Mathcad software. The following example illustrates the script used to compute the receiver noise temperature.

Radiometer Noise Temperature Computation

From Ulaby, Moore, Fung, Microwave Remote Sensing, Vol. 1, pp. 355 - 356.

Create gain and noise figure variables (units in dB). Set operating temperature to ambient conditions.

RF Amplifier	Mixer	IF Amplifier	Operating Temperature
Grf := 29	Gm := -7.5	Gif := 45	To := 295
Frf := 2.0	Fm := 5	Fif := 4	

Convert gain and noise figure to natural numbers.

$Grf := 10 \left(\frac{Grf}{10} \right)$	$Gm := 10 \left(\frac{Gm}{10} \right)$	$Gif := 10 \left(\frac{Gif}{10} \right)$
$Nrf := 10 \left(\frac{Frf}{10} \right)$	$Nm := 10 \left(\frac{Fm}{10} \right)$	$Nif := 10 \left(\frac{Fif}{10} \right)$

Change noise figure to noise temperature (°K).

$Trf := (Nrf - 1) \cdot To$ $Tm := (Nm - 1) \cdot To$ $Tif := (Nif - 1) \cdot To$

Compute receiver noise temperature (°K). Terms after IF amplifier will be much less than the Trf term, thus they will not affect the Trec.

$$Trec := Trf + \frac{Tm}{Grf} + \frac{Tif}{Grf \cdot Gm}$$

Print the computed noise temperature (°K).

Trec = 176.504

APPENDIX B
ANALYSIS OF RADIOMETRIC BRIGHTNESS TEMPERATURE
VERSUS FREQUENCY PLOTS

The Ka-band Oil Spill Radiometric Measurement System was tested at Lincoln Laboratory. Validation tests were conducted on 12, 16, and 21 August atop the Lincoln Laboratory Building-A/B roof. Measurements were conducted using a Lincoln Laboratory-constructed calibrated test tank, with diesel oil thicknesses ranging from 0 mm to 10 mm in steps of 1 mm.

The file naming convention is consistent over a test. Typically, the test date, expected oil thickness, and scan repetition are embedded in the file name to identify each data file.

The plots shown in this appendix are radiometric brightness temperature (T^B), expressed in Kelvin (K), as measured by the radiometer, versus the measurement frequency in GHz. Under the current radiometer hardware configuration, 12 equally spaced points between 26.5 and 40.0 GHz are sampled, with each scan period over all 12 channels taking approximately 0.5 s. These 12 points are plotted as “measured” points. For each data set, the oil thickness estimation algorithm [2] is used to estimate an oil film thickness. This algorithm-derived estimate is displayed with the smoothed curve and the declared result plotted over the actual measured points. The data analyst can then either choose to accept the algorithm estimate, or manually select a curve that may be a better fit to the measured data.

B.1 12 AUGUST 1996 ANALYSIS

The file naming convention used during this collection is explained below. Each file name has the form #MM812x.DAQ, where # indicates the intended oil thickness in millimeters for that measurement, and x is a letter representing repetitions over the same oil thickness. Thus 6MM812C.DAQ is the third of a series of measurements over an intended oil thickness of 6 mm. Measurements were also collected over oil targets of unknown thickness. The file naming convention for these have the form UNK1812x.DAQ where x is a letter representing repetitions over the unknown targets. Operator guess of the actual thickness is embedded in the comment line in the data set. Thus, UNK1812C.DAQ is the third measurement over an unknown thickness, and by viewing operator comments one would find that the operator estimate of thickness is 4 mm.

- 0MM812.DAQ – This plot is the water-only measurement, and is used as the baseline water temperature for the oil thickness estimation algorithm.
- 0MM812A.DAQ – This data set was collected after the 0MM812.DAQ data set. Based on the poor match between the theoretical water curve and the original data points, it is assumed that the instrument electronics were still warming up. The second plot of 0MM812A.DAQ shows the result when this curve is used as the baseline water temperature.
- 1MM812A.DAQ – This curve is a good match to the algorithm estimate of 0.800 mm when the 0MM812A.DAQ curve is used as the baseline water measurement.
- 1MM812B.DAQ – This curve is a good match to the algorithm estimate of 0.474 mm when the 0MM812A.DAQ curve is used as the baseline water measurement. Note that the difference between these two 1-mm measurements is a slight increase in the mean temperature with little difference in the slope of the curves. This is what makes the estimation of “thin” films difficult because small differences in temperature result in noticeably different estimates.
- 2MM812A.DAQ – This curve is a fair-to-good match to the algorithm estimate of 2.100 mm.
- 2MM812B.DAQ – This curve is a good match to the algorithm estimate of 2.150 mm.
- 4MM812A.DAQ – This curve is a fair match to the algorithm estimate of 4.000 mm. The actual data appear to have more amplitude variation than the theoretical curve predicts.
- 4MM812B.DAQ – This curve is a fair match to the algorithm estimate of 3.825 mm. The actual data appear to have more amplitude variation than the theoretical curve predicts, and the mean level of the curve seems to have shifted down.
- 5MM812A.DAQ – The amplitude variation of this curve is appreciably larger than theory predicts. It is assumed that the system gain may have drifted. The algorithm estimate for this curve is 4.900 mm. If the amplitude variation of the theoretical curve is increased, thereby increasing its “gain,” the 4.900-mm estimate is a fair match to the data set.

5MM812B.DAQ – The amplitude variation of this curve is appreciably larger than theory predicts. As with the 5MM812A.DAQ data set, it is assumed that the system gain may have drifted. The algorithm estimate for this curve is 4.825 mm; however, the peak value shown in this data set matches an estimate of 4.800 mm. When the amplitude variation of the theoretical curve is increased, thereby increasing its “gain,” the 4.800 mm estimate is a fair-to-good match to the data set.

6MM812A.DAQ – The amplitude variation of this curve is appreciably larger than theory predicts. As with the 5-mm data sets, it is assumed that the system gain may have drifted. The algorithm estimate for this curve is 2.275 mm; however, the LMS-only estimate is 5.800 mm. When the amplitude variation of the theoretical curve is increased, thereby increasing its “gain,” the 5.800-mm estimate is a somewhat fair match to the data set.

At this point in the collection, the instrument was recalibrated. Because there is oil in the test tank, no accompanying water reference is available. For the remaining cases, the water reference was determined by observing the peak/valley variations of the data sets, and estimating a new water reference temperature.

6MM812B.DAQ – This curve is an excellent match to the algorithm estimate of 5.725 mm.

6MM812C.DAQ – This curve is an excellent match to the algorithm estimate of 5.775 mm.

7MM812A.DAQ – This curve is an excellent match to the algorithm estimate of 6.700 mm.

7MM812B.DAQ – This curve is an excellent match to the algorithm estimate of 6.775 mm.

8MM812A.DAQ – This curve is an excellent match to the algorithm estimate of 7.675 mm.

8MM812B.DAQ – This curve is an excellent match to the algorithm estimate of 7.750 mm.

9MM812A.DAQ – This curve is an excellent match to the algorithm estimate of 8.675 mm.

9MM812B.DAQ – This curve is an excellent match to the algorithm estimate of 8.525 mm.

9MM812C.DAQ – This curve is an excellent match to the algorithm estimate of 8.575 mm.

10MM812B.DAQ – This curve is a good-to-excellent match to the algorithm estimate of 9.975 mm.

An unknown amount of oil was removed from the surface of the water using oil absorbent cloth.

UNK1812A.DAQ – This curve is an excellent match to the algorithm estimate of 6.700 mm. The operator estimated the oil thickness at 7.0 mm.

Again, an unknown amount of oil was removed from the surface of the water using oil absorbent cloth. For the following two measurements, the operator estimated the oil thickness at 4.0 mm.

UNK1812B.DAQ – This curve is a good match to the algorithm estimate of 3.700 mm.

UNK1812C.DAQ – This curve is a good match to the algorithm estimate of 3.600 mm.

Again, an unknown amount of oil was removed from the surface of the water using oil absorbent cloth.

UNK1812D.DAQ – This curve is a good match to the algorithm estimate of 1.300 mm. The operator estimated the oil thickness to be between 0.9 and 1.0 mm.

Again, an unknown amount of oil was removed from the surface of the water using oil absorbent cloth. For the next two measurements, the operator estimated the oil thickness at 0 mm, although a very thin sheen could be observed.

UNK1812E.DAQ – This curve is a good-to-excellent match to the algorithm estimate of 0.000 mm.

UNK1812E.DAQ – This curve is an excellent match to the algorithm estimate of 0.000 mm.

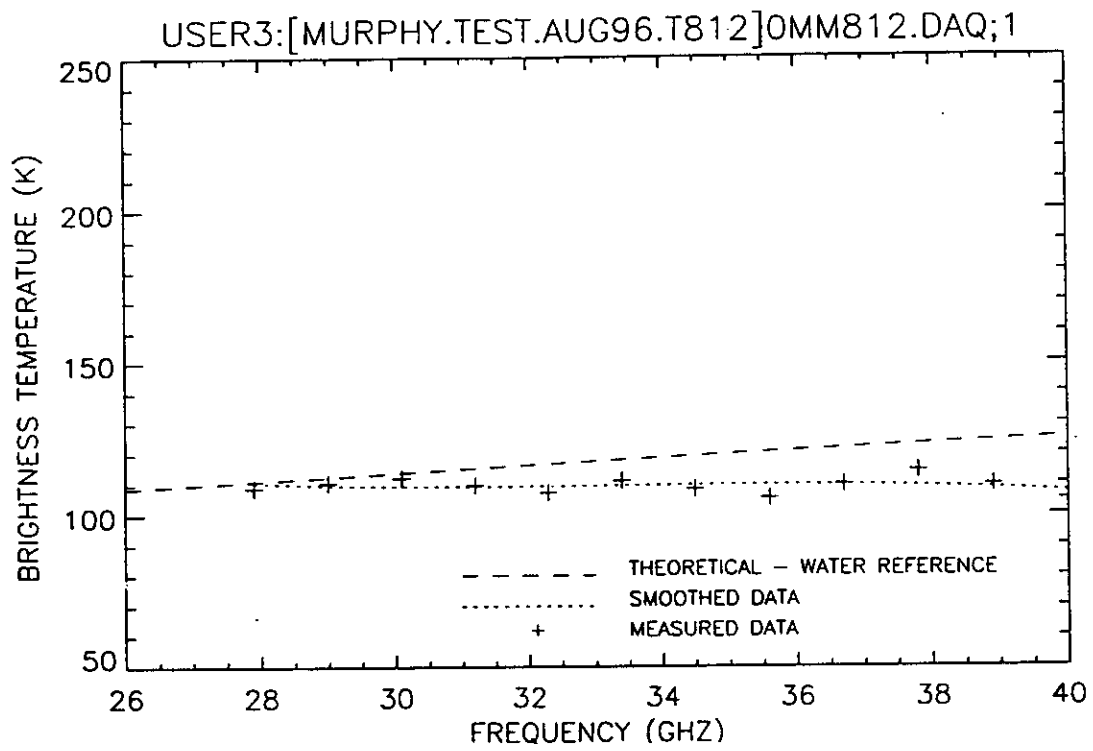


Figure B1. Plot of radiometric brightness temperature versus measurement frequency for water background, 12 August 1996.

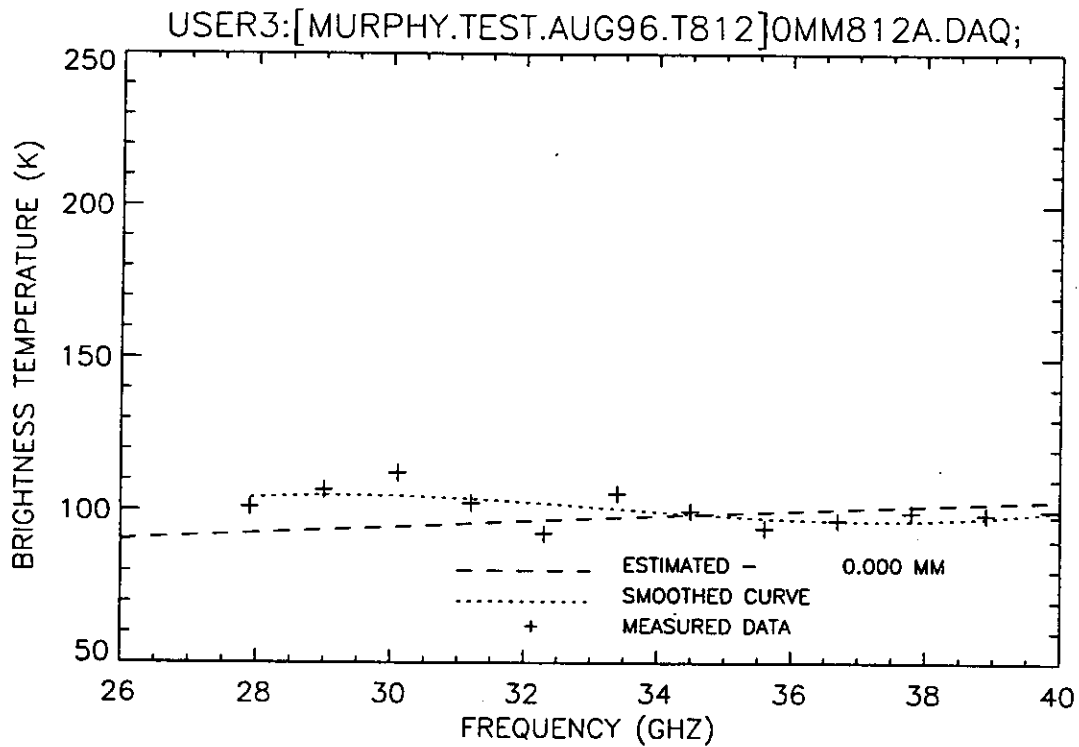
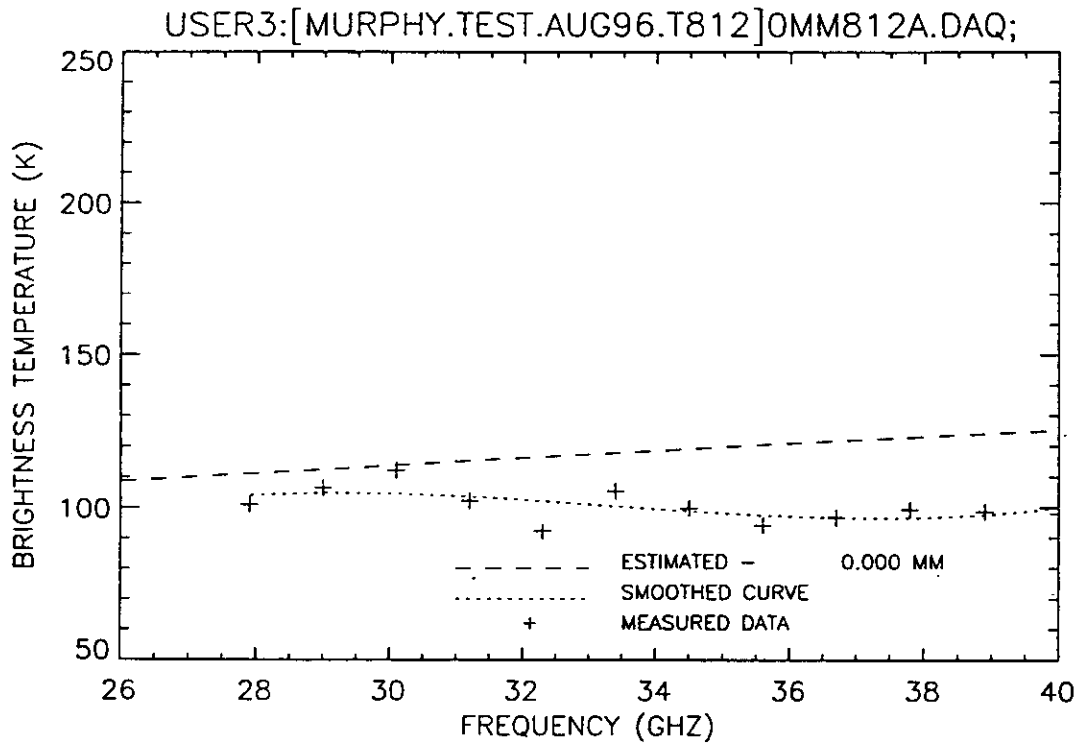


Figure B2. Plot of radiometric brightness temperature versus measurement frequency for water background, 12 August 1996 (a) shows the theoretical background curve from Figure B1, (b) shows the theoretical curve derived from this data set.

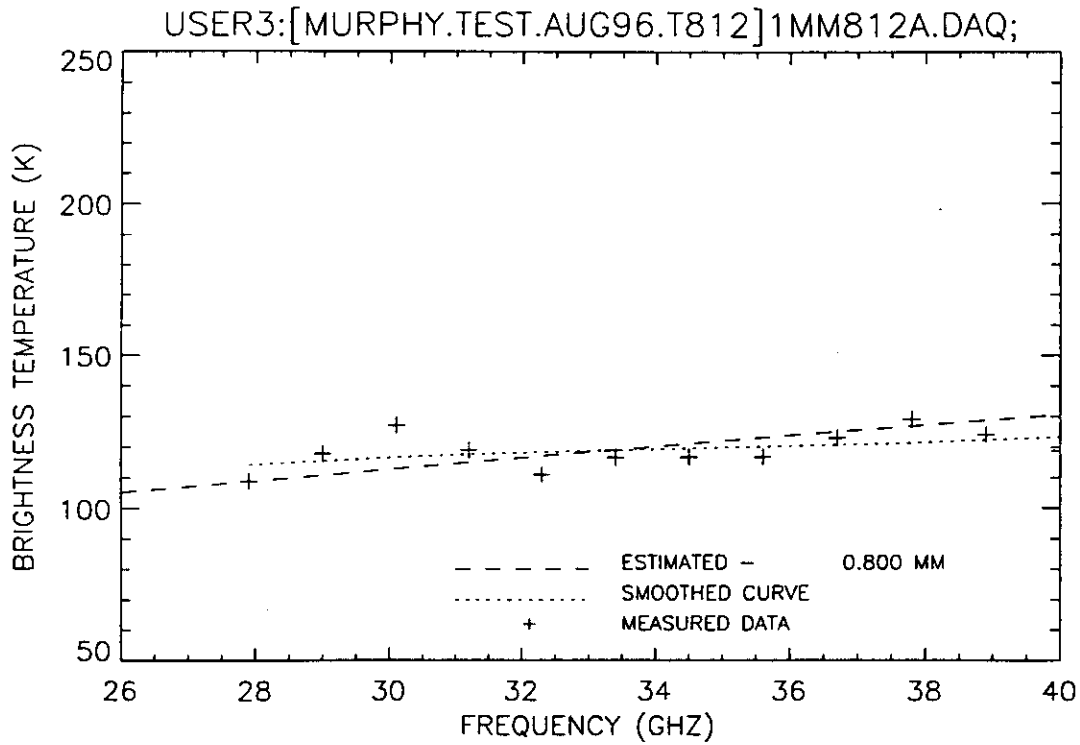


Figure B3. Plot of radiometric brightness temperature versus measurement frequency for 1.0 mm oil thickness, 12 August 1996.

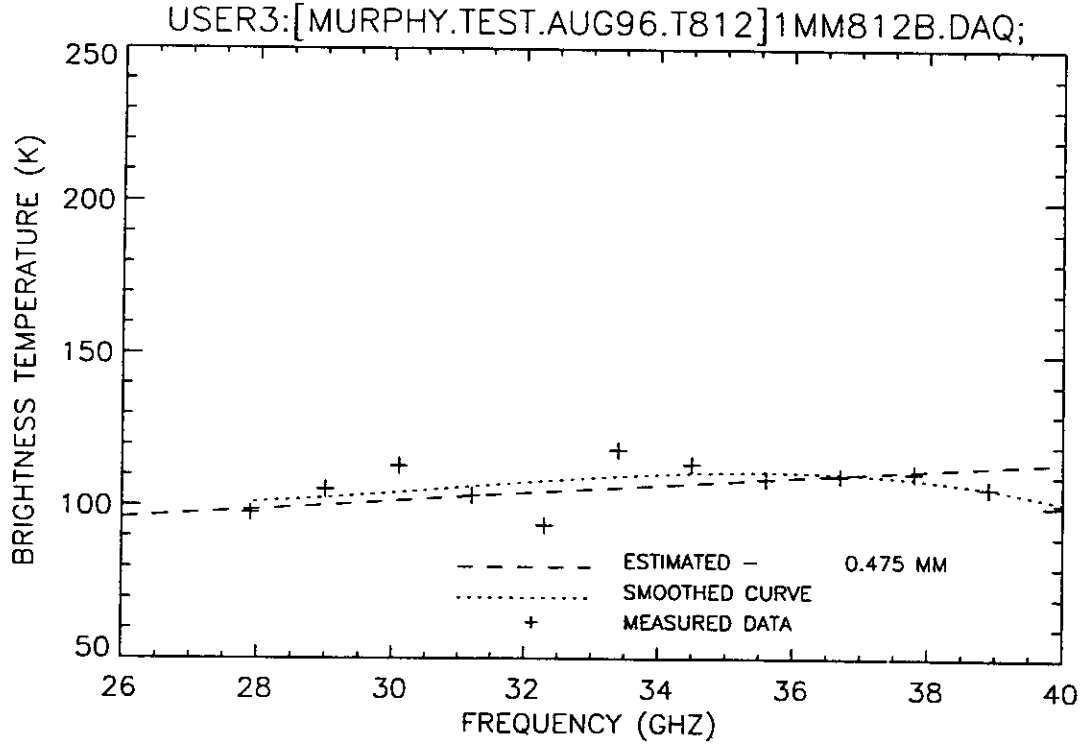


Figure B4. Plot of radiometric brightness temperature versus measurement frequency for 1.0 mm oil thickness, 12 August 1996.

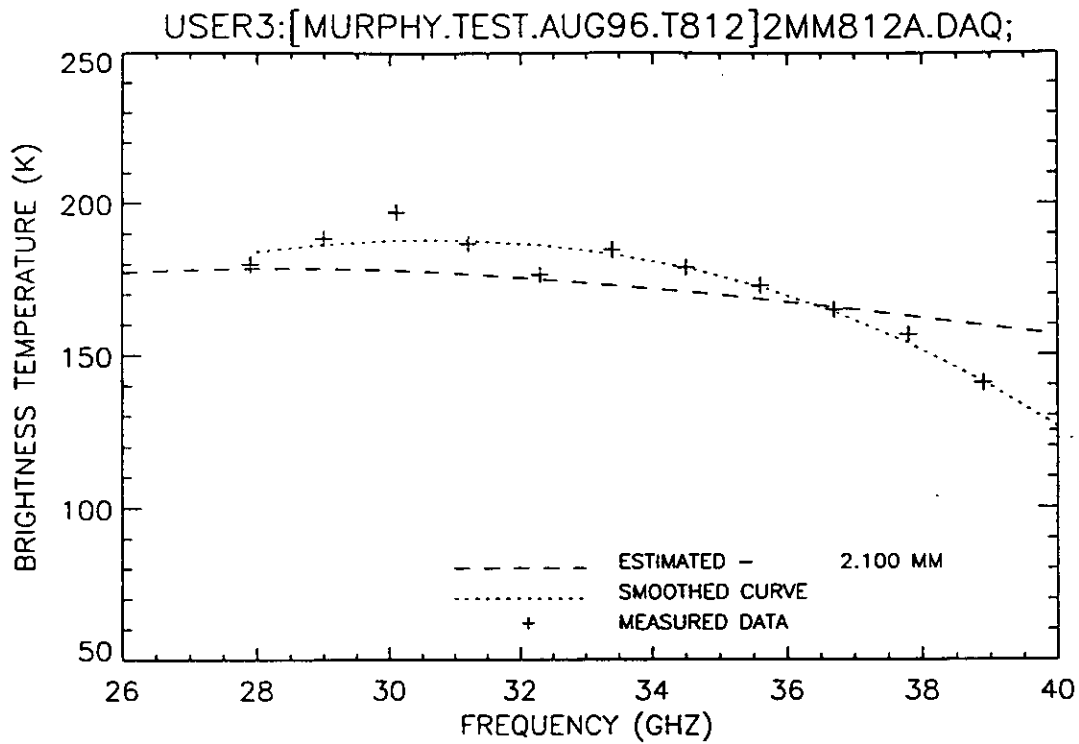


Figure B5. Plot of radiometric brightness temperature versus measurement frequency for 2.0 mm oil thickness, 12 August 1996.

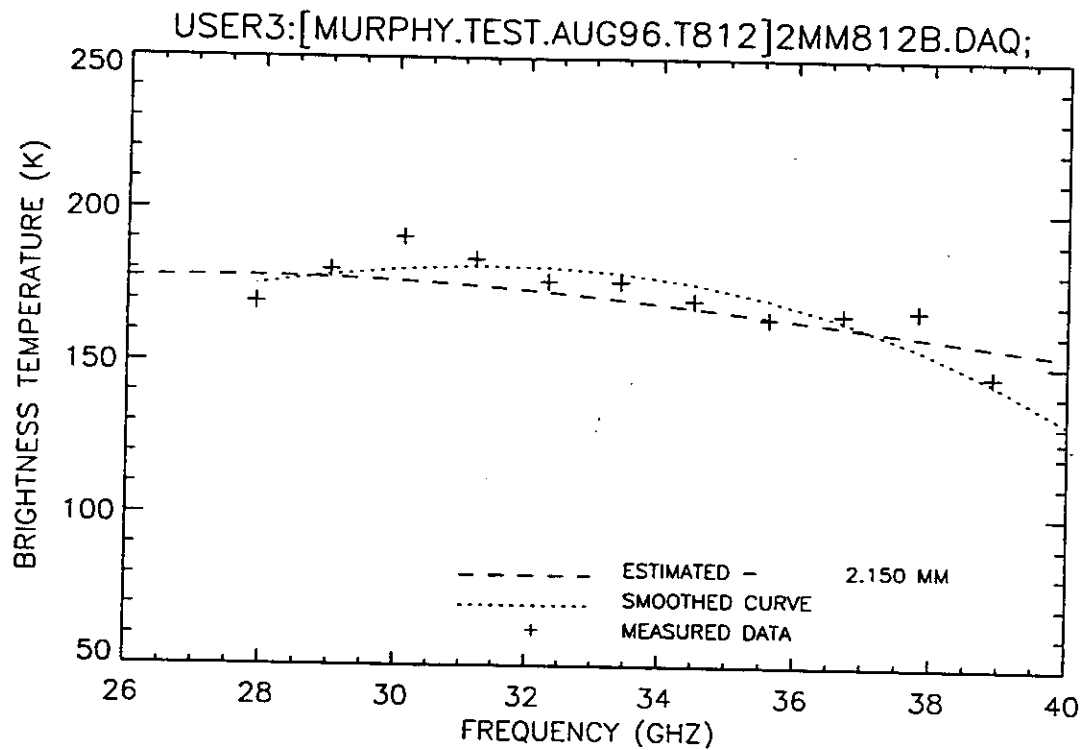


Figure B6. Plot of radiometric brightness temperature versus measurement frequency for 2.0 mm oil thickness, 12 August 1996.

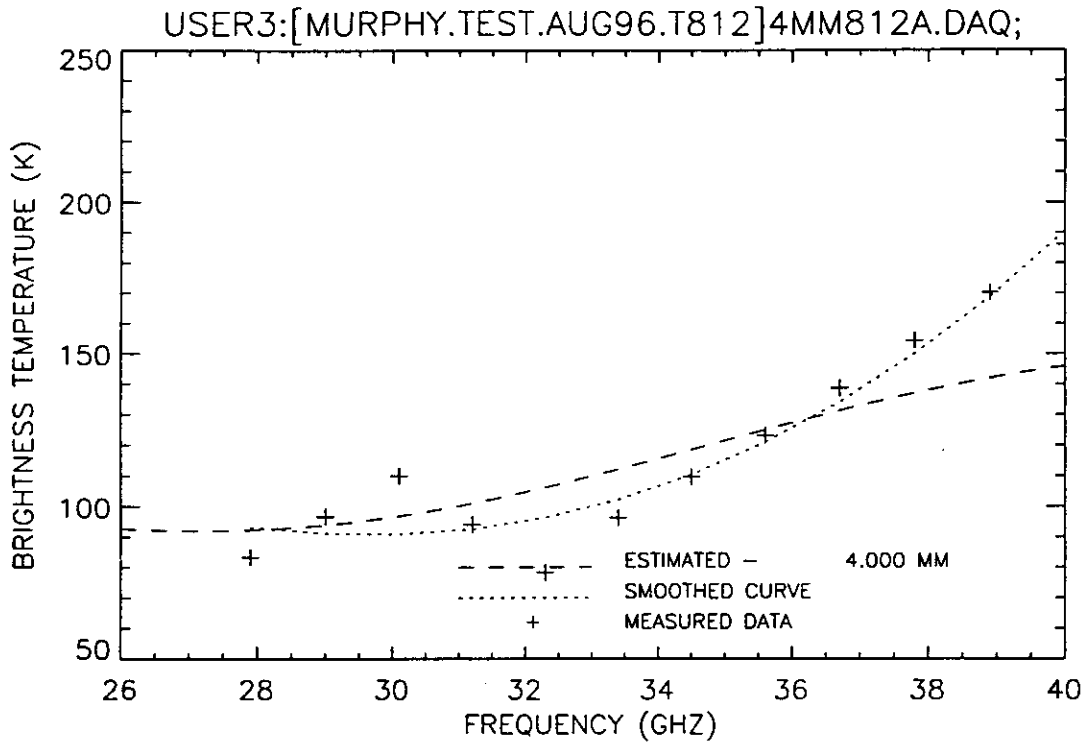


Figure B7. Plot of radiometric brightness temperature versus measurement frequency for 4.0 mm oil thickness, 12 August 1996.

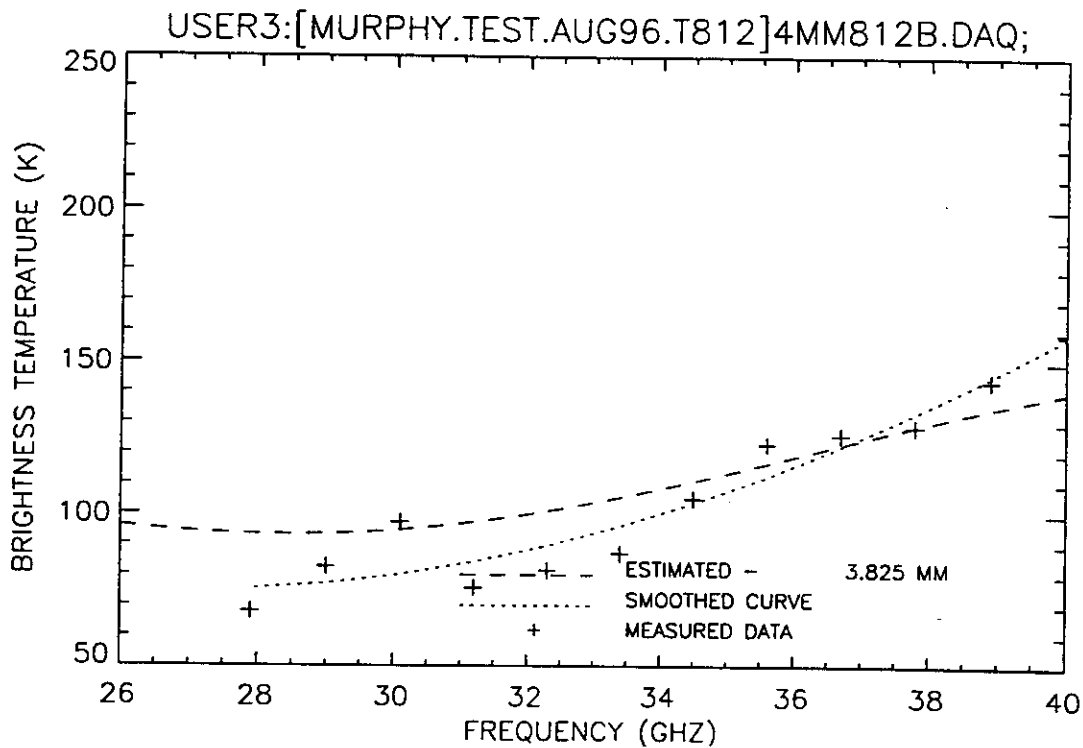


Figure B8. Plot of radiometric brightness temperature versus measurement frequency for 4.0 mm oil thickness, 12 August 1996.

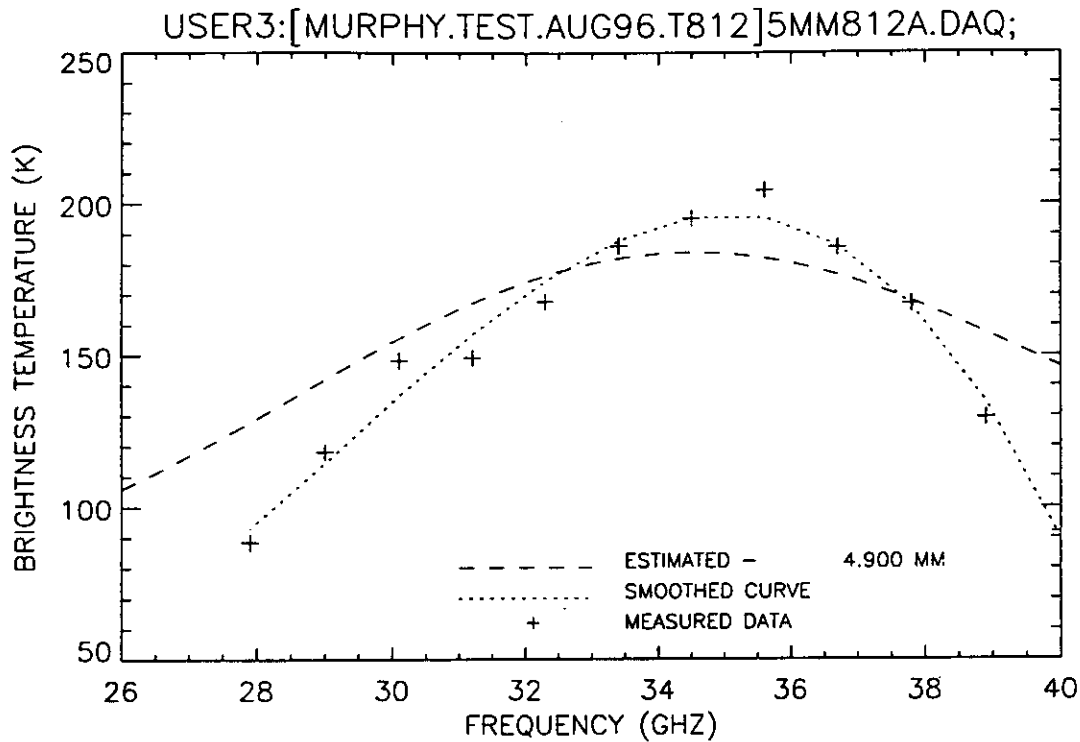


Figure B9. Plot of radiometric brightness temperature versus measurement frequency for 5.0 mm oil thickness, 12 August 1996.

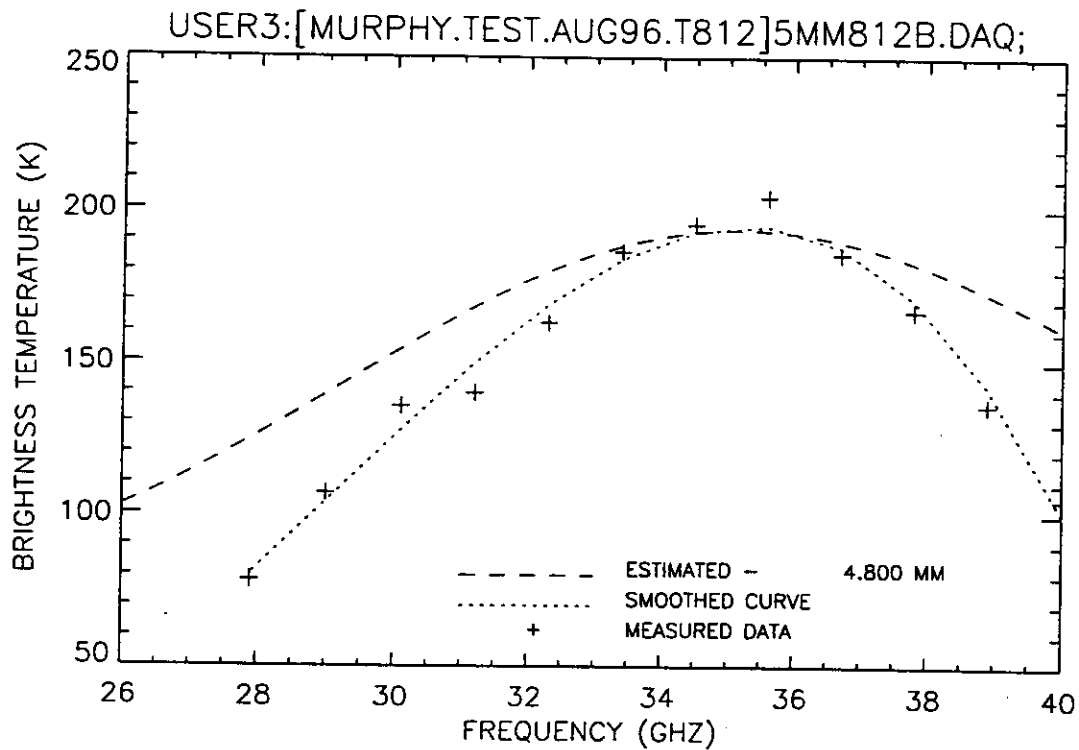


Figure B10. Plot of radiometric brightness temperature versus measurement frequency for 5.0 mm oil thickness, 12 August 1996.

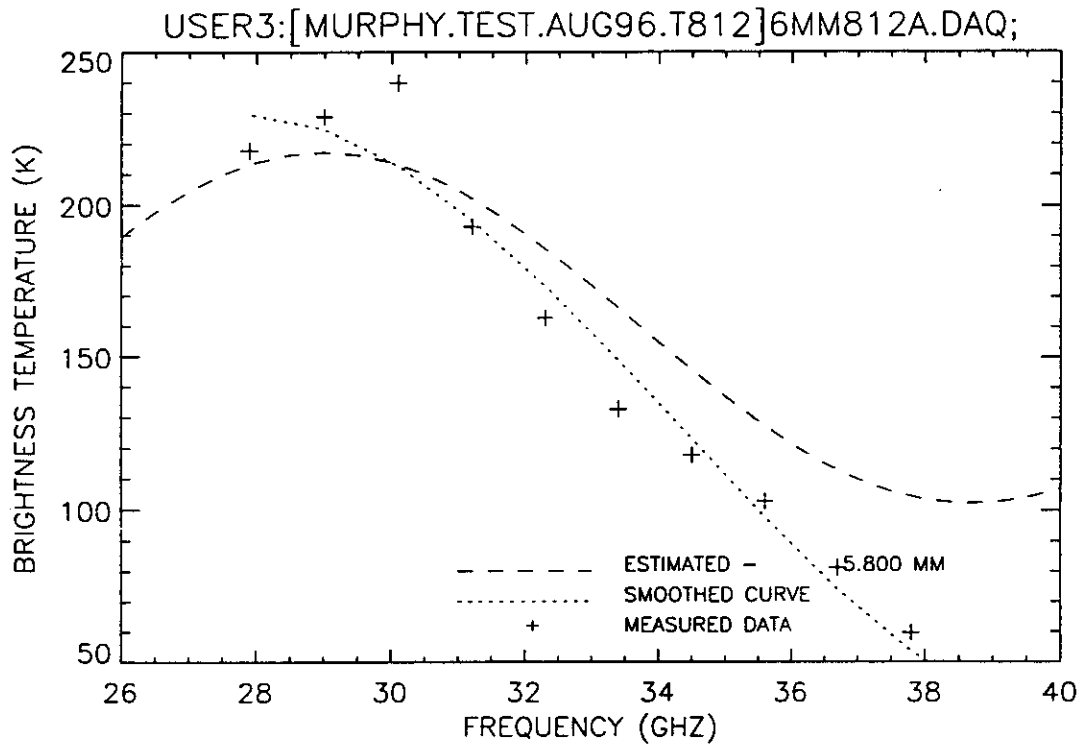


Figure B11. Plot of radiometric brightness temperature versus measurement frequency for 6.0 mm oil thickness, 12 August 1996.

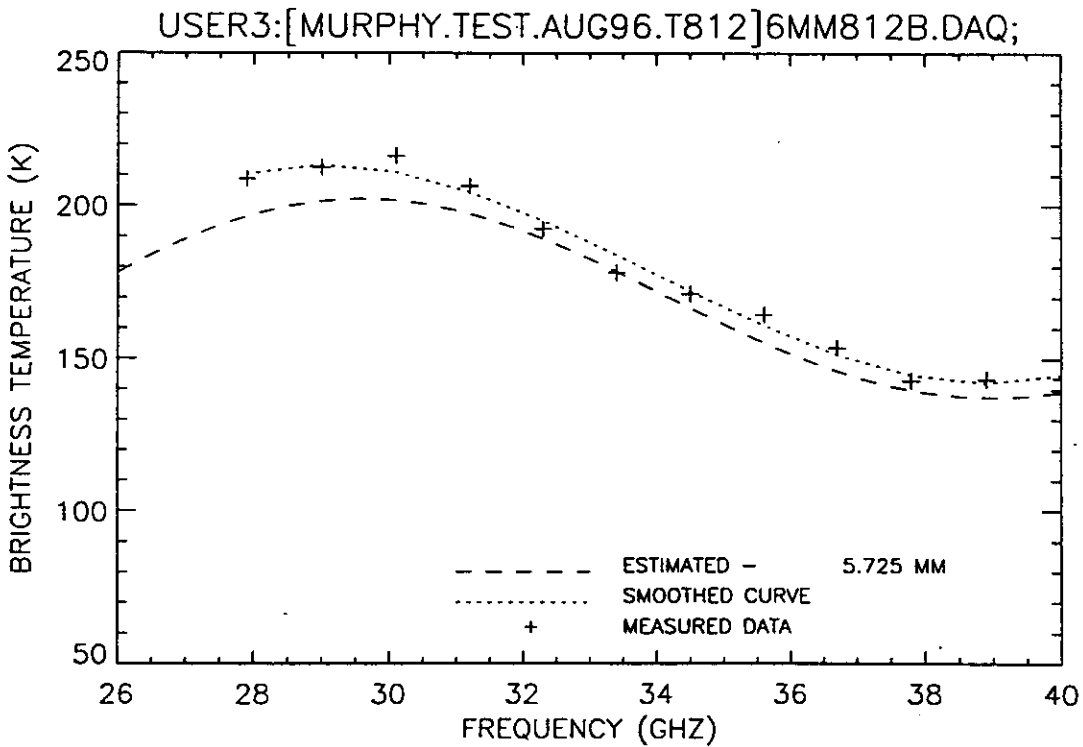


Figure B12. Plot of radiometric brightness temperature versus measurement frequency for 6.0 mm oil thickness, 12 August 1996.

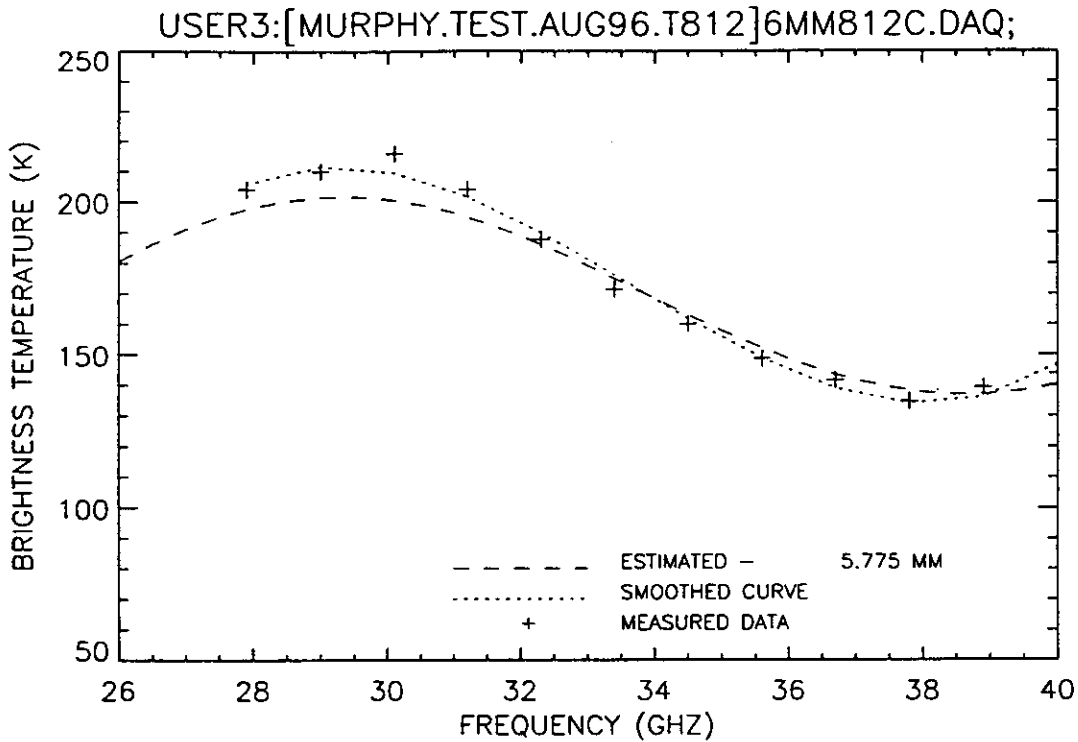


Figure B13. Plot of radiometric brightness temperature versus measurement frequency for 6.0 mm oil thickness, 12 August 1996.

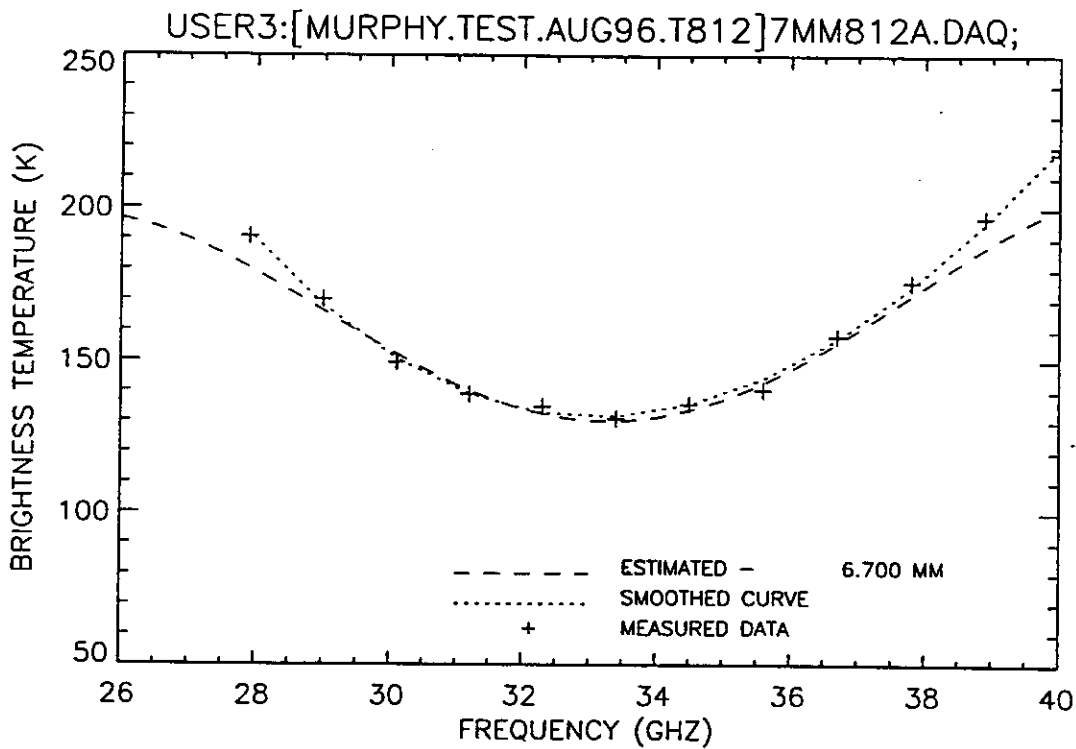


Figure B14. Plot of radiometric brightness temperature versus measurement frequency for 7.0 mm oil thickness, 12 August 1996.

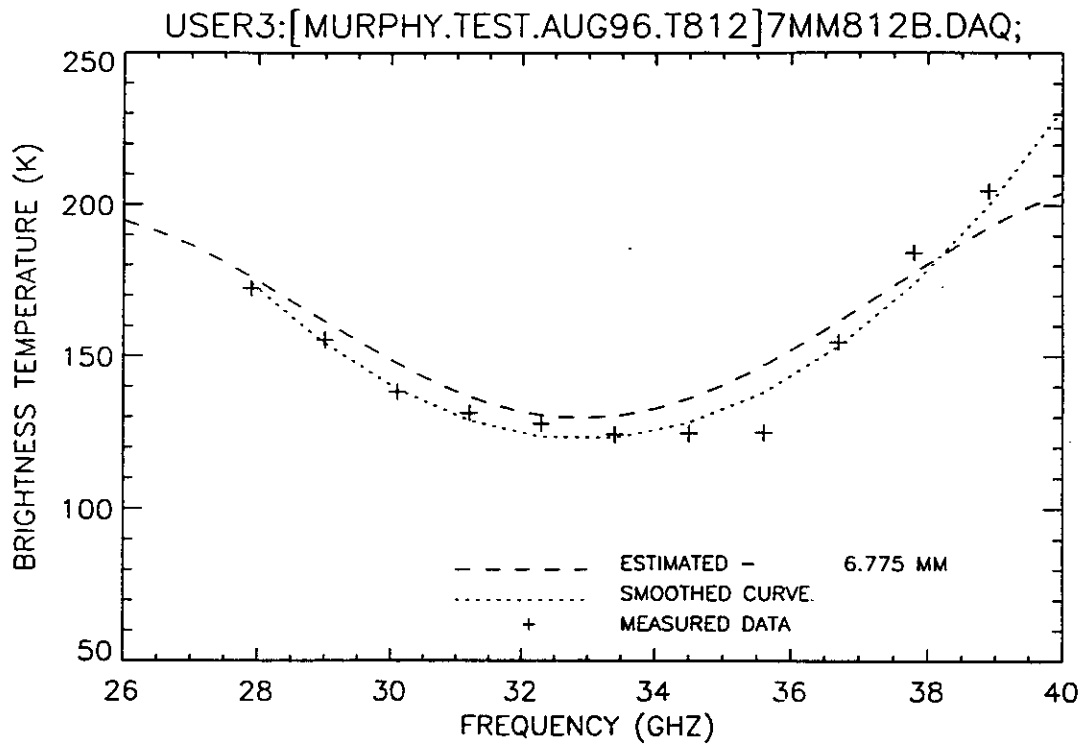


Figure B15. Plot of radiometric brightness temperature versus measurement frequency for 7.0 mm oil thickness, 12 August 1996.

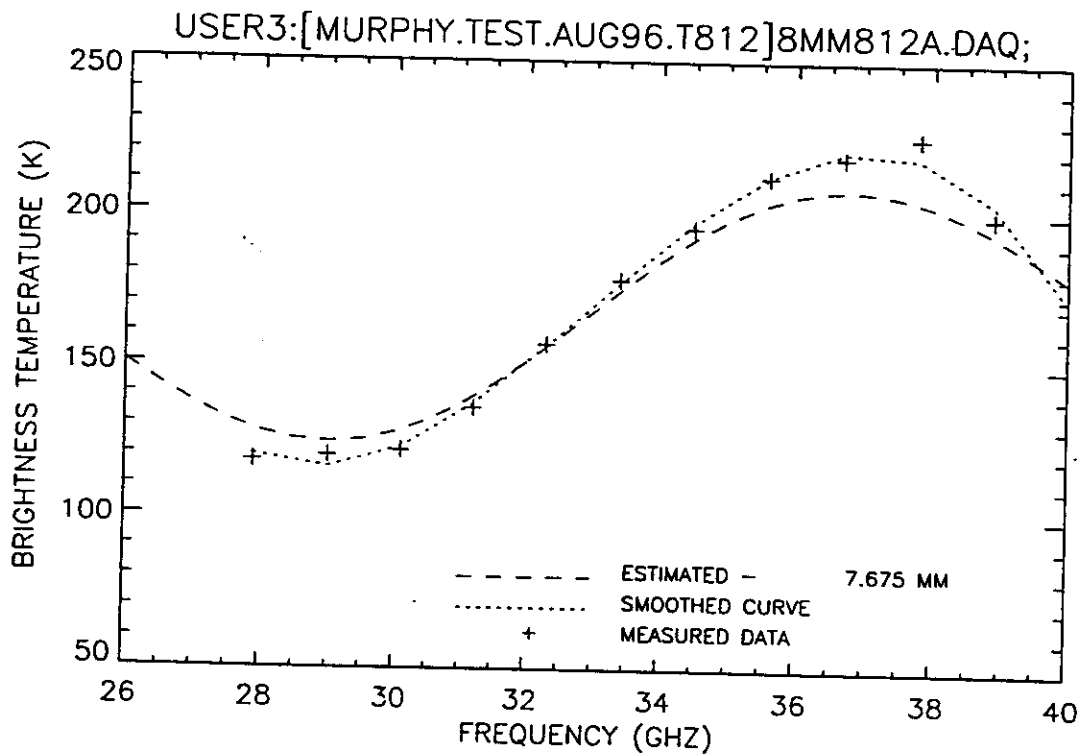


Figure B16. Plot of radiometric brightness temperature versus measurement frequency for 8.0 mm oil thickness, 12 August 1996.

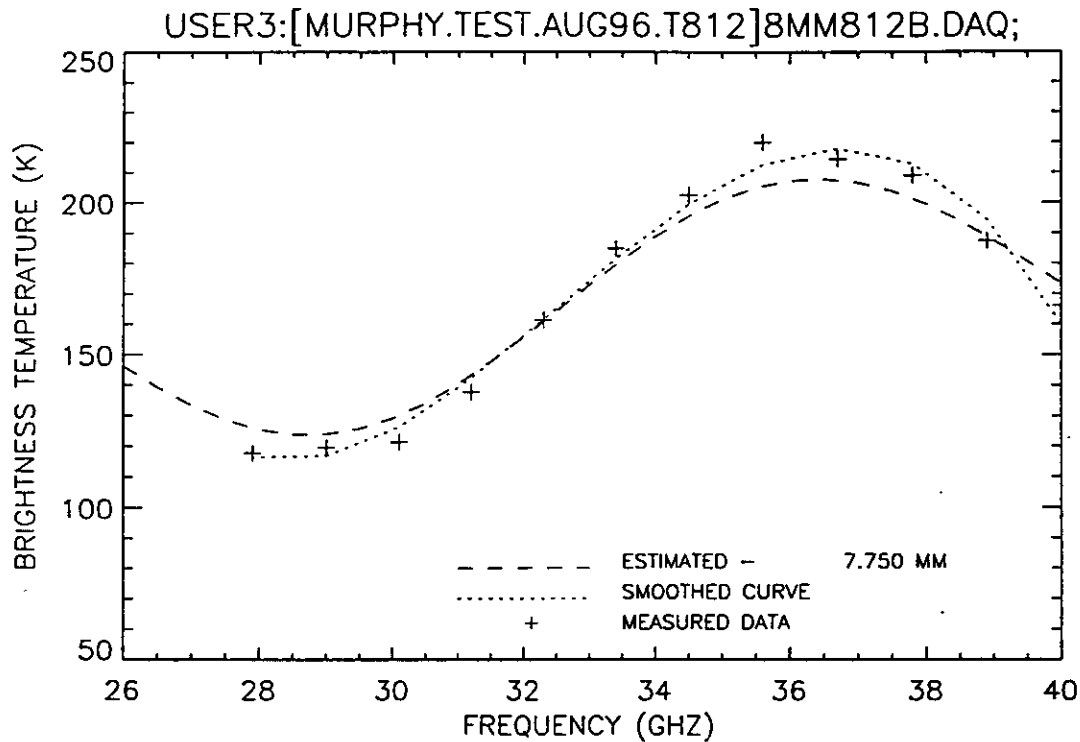


Figure B17. Plot of radiometric brightness temperature versus measurement frequency for 8.0 mm oil thickness, 12 August 1996.

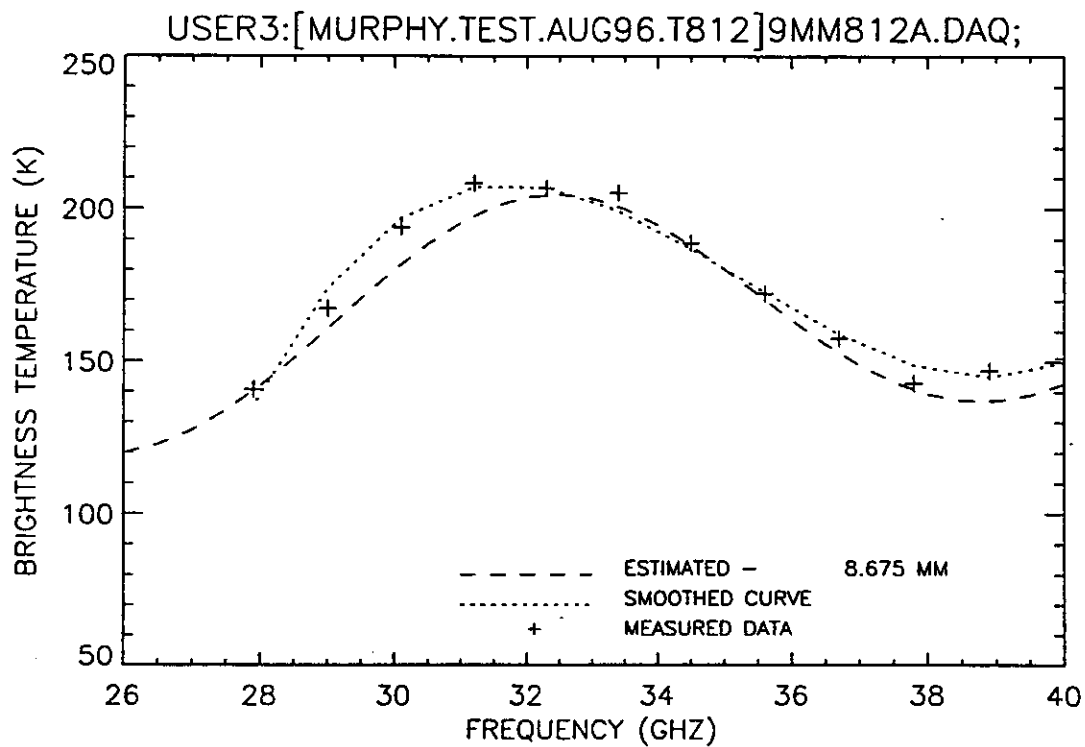


Figure B18. Plot of radiometric brightness temperature versus measurement frequency for 9.0 mm oil thickness, 12 August 1996.

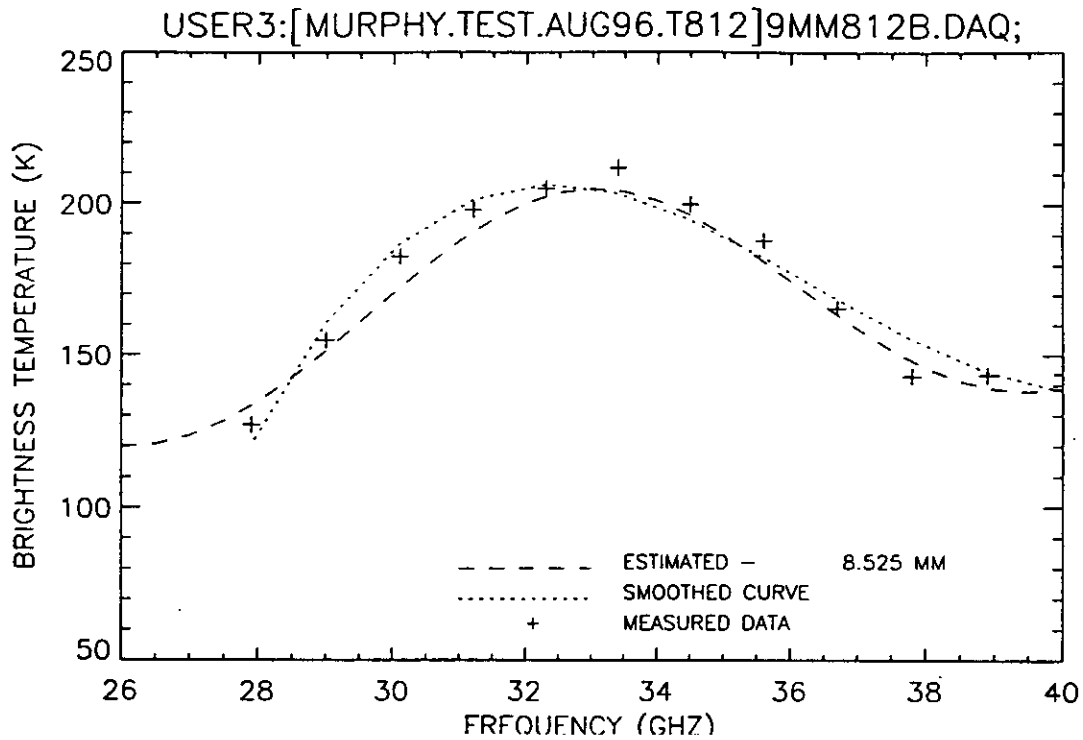


Figure B19. Plot of radiometric brightness temperature versus measurement frequency for 9.0 mm oil thickness, 12 August 1996.

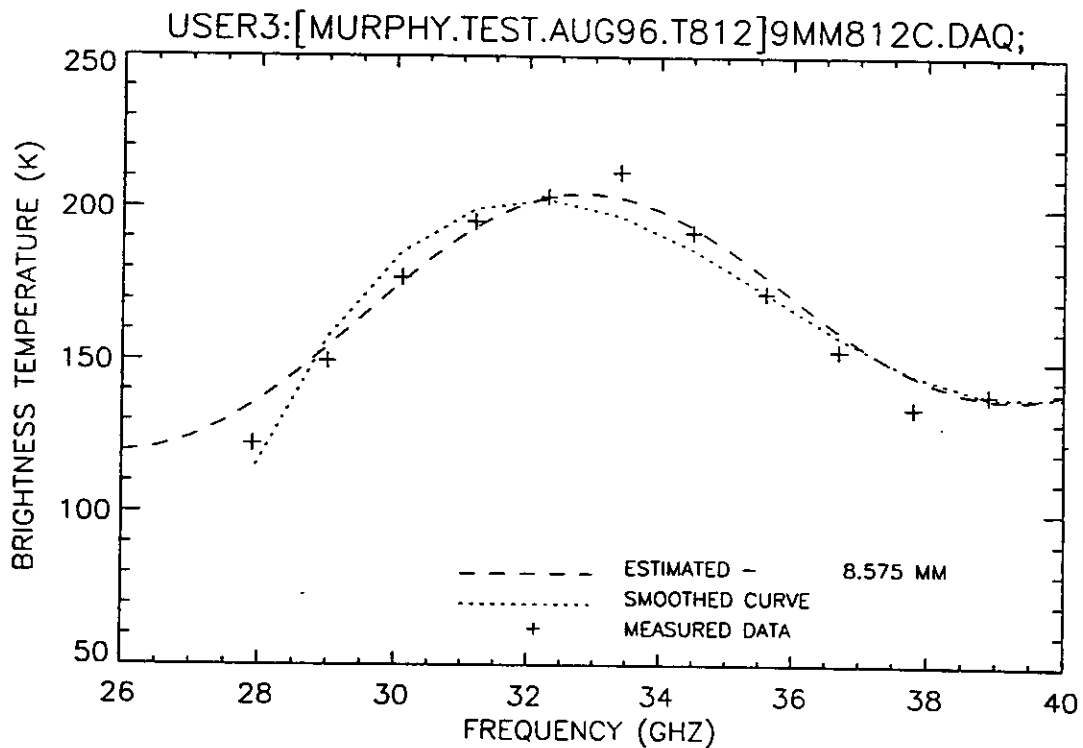


Figure B20. Plot of radiometric brightness temperature versus measurement frequency for 9.0 mm oil thickness, 12 August 1996.

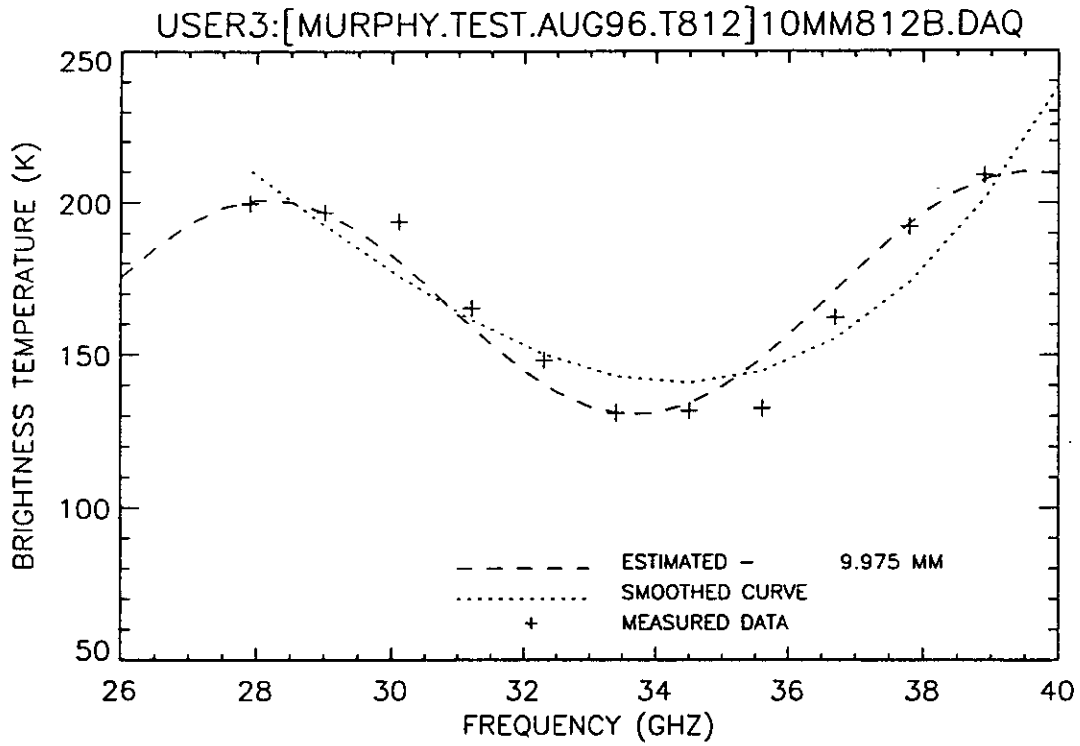


Figure B21. Plot of radiometric brightness temperature versus measurement frequency for 10.0 mm oil thickness, 12 August 1996.

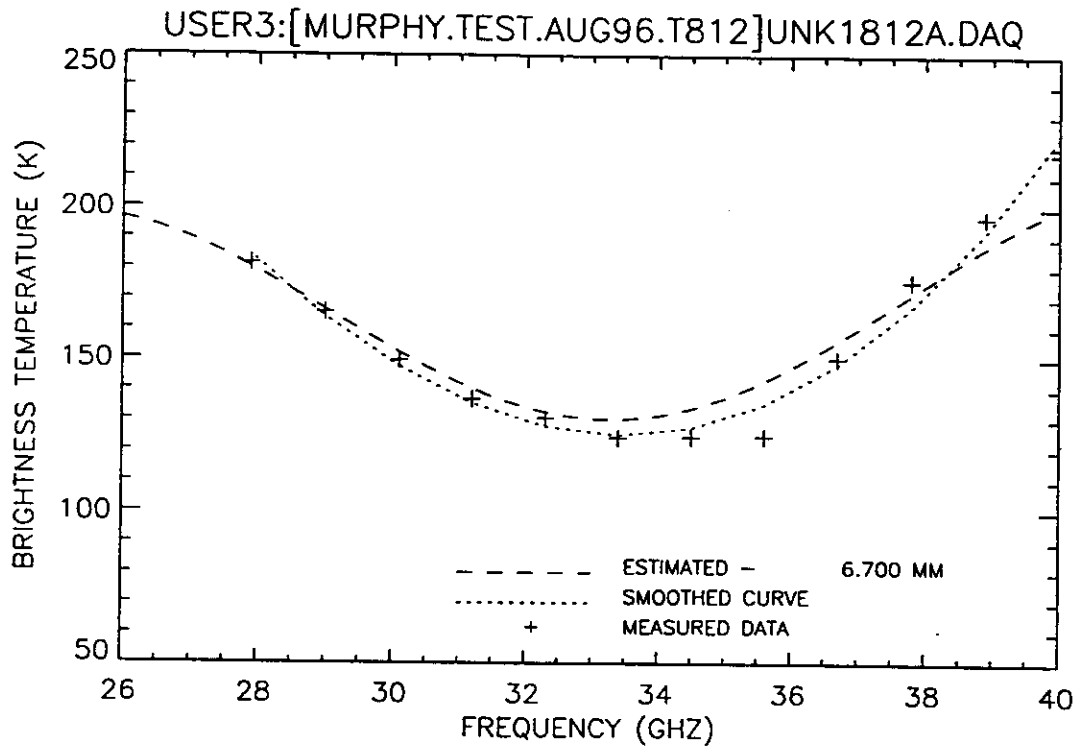


Figure B22. Plot of radiometric brightness temperature versus measurement frequency for an unknown oil thickness, 12 August 1996.

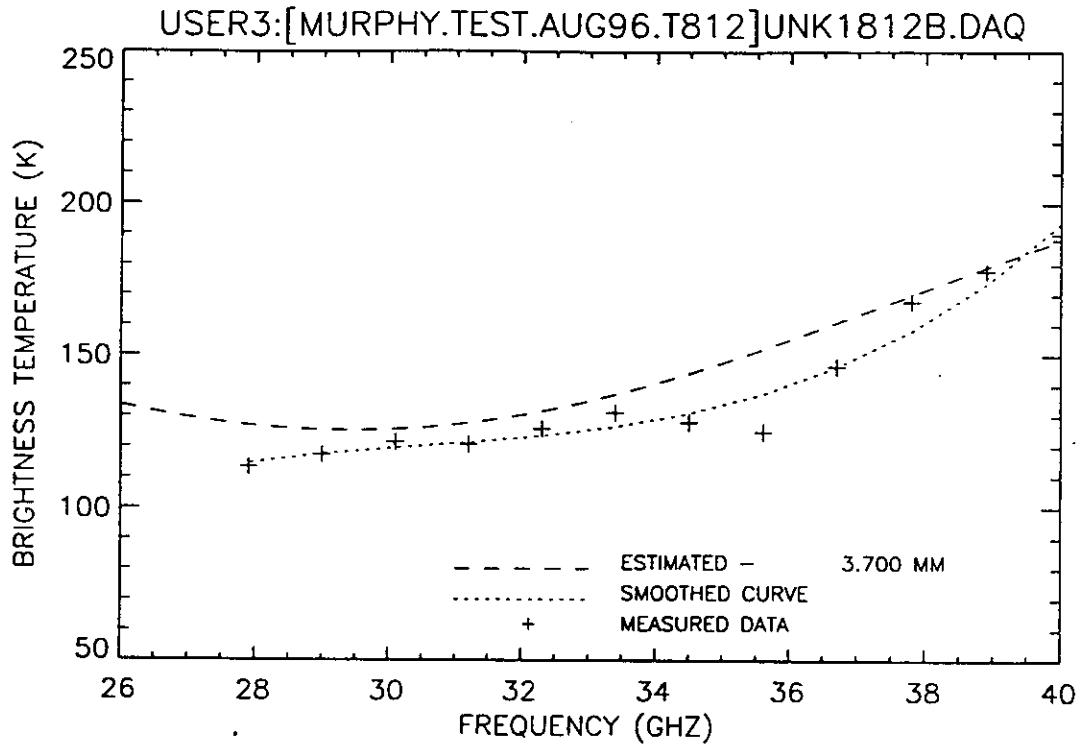


Figure B23. Plot of radiometric brightness temperature versus measurement frequency for an unknown oil thickness, 12 August 1996.

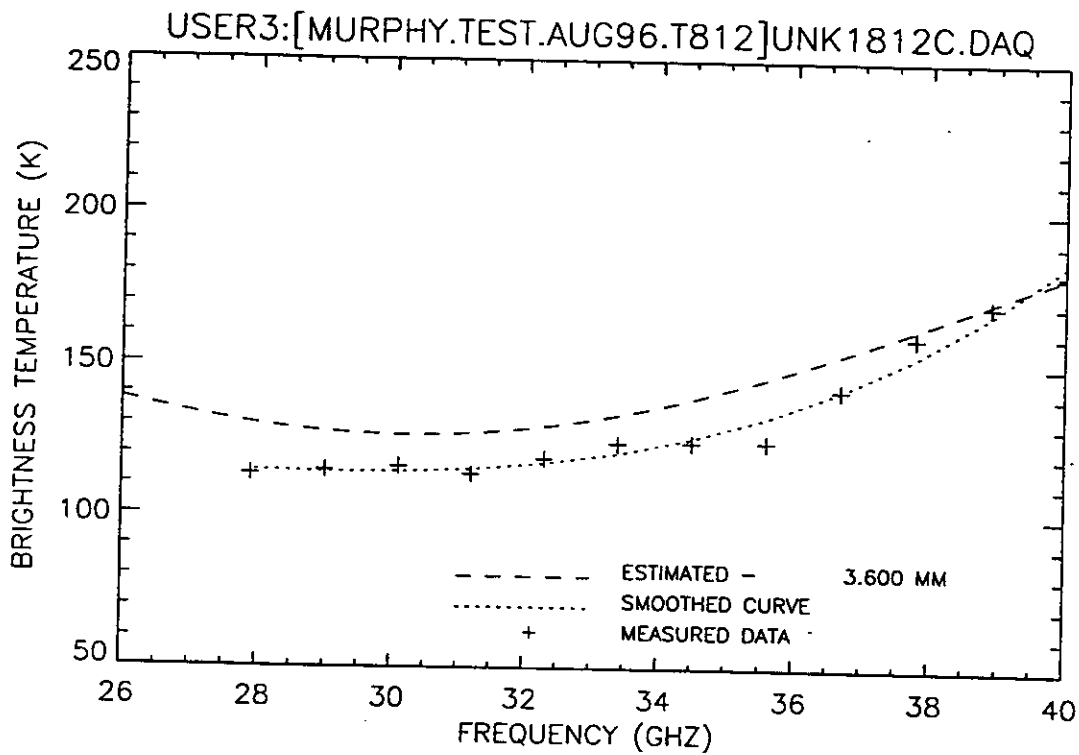


Figure B24. Plot of radiometric brightness temperature versus measurement frequency for an unknown oil thickness, 12 August 1996.

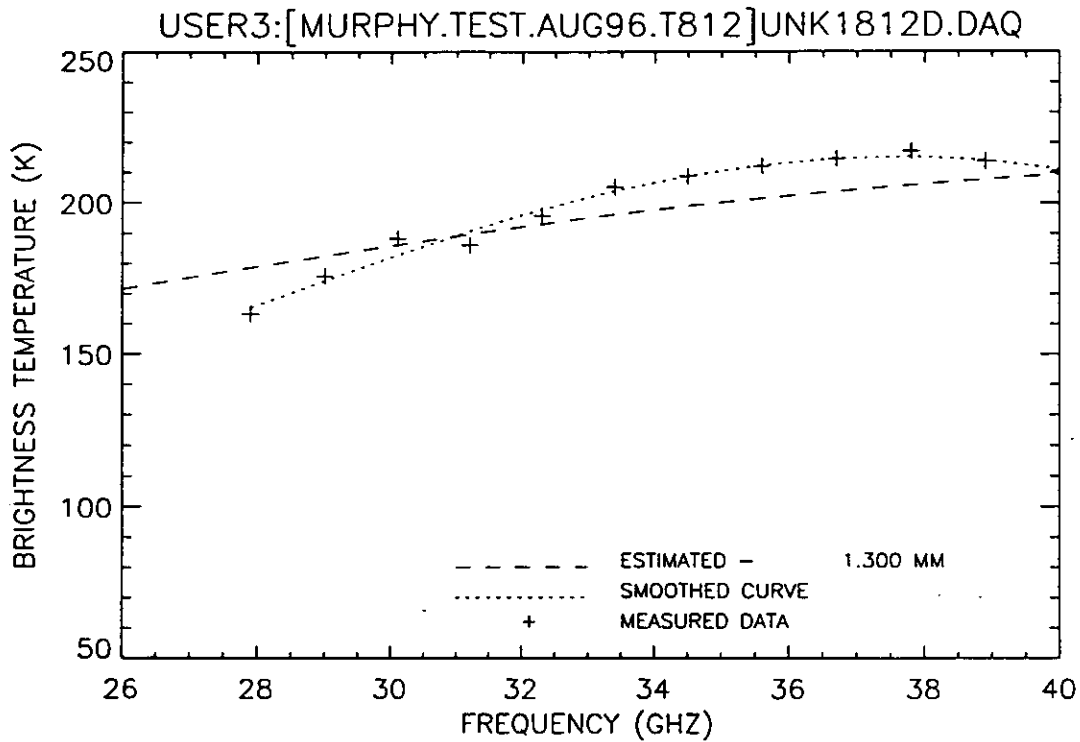


Figure B25. Plot of radiometric brightness temperature versus measurement frequency for an unknown oil thickness, 12 August 1996.

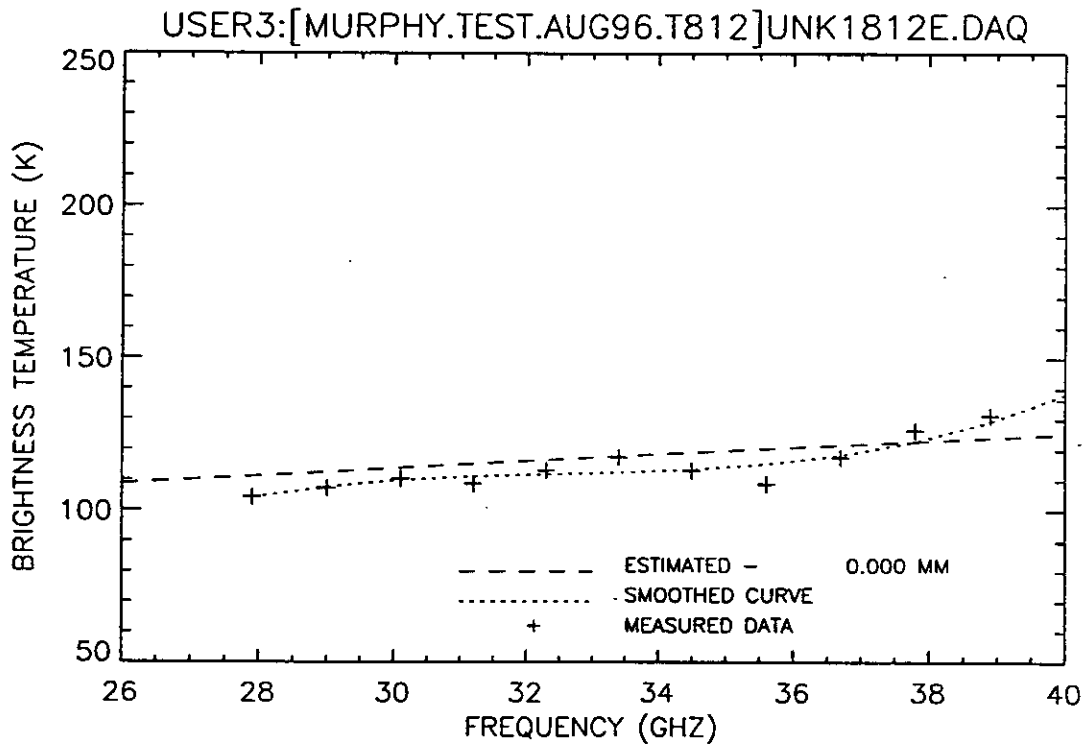


Figure B26. Plot of radiometric brightness temperature versus measurement frequency for an unknown oil thickness, 12 August 1996.

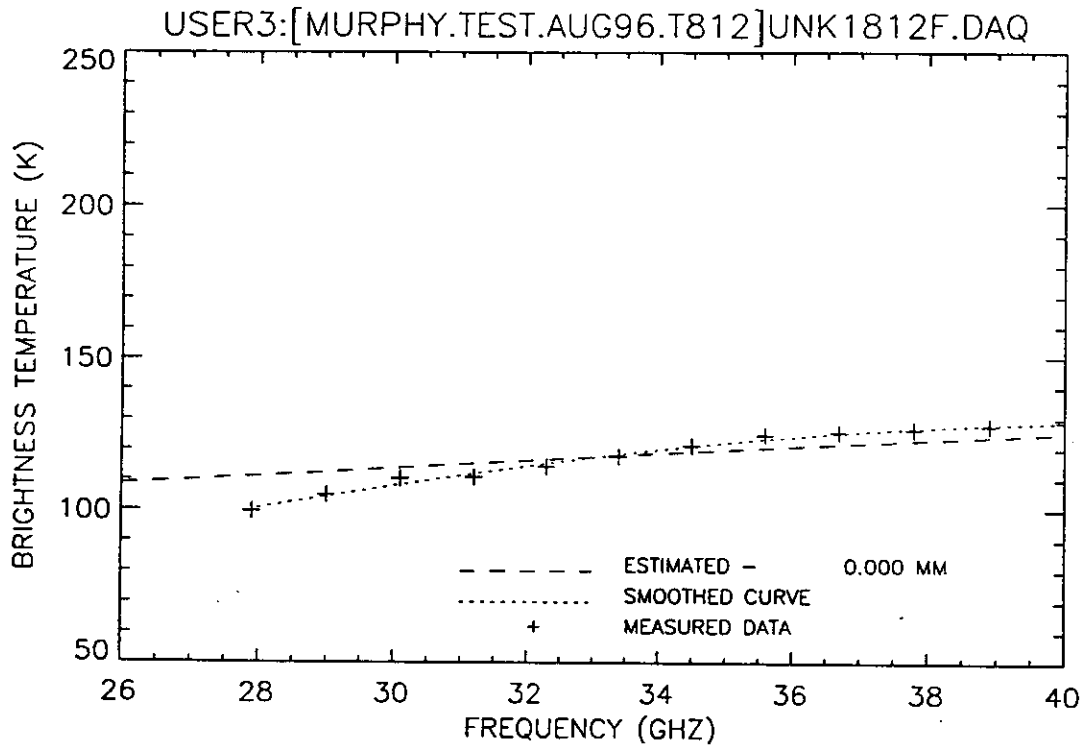


Figure B27. Plot of radiometric brightness temperature versus measurement frequency for an unknown oil thickness, 12 August 1996.

B.2 16 August 1996 Analysis

The file naming convention used during this collection is explained below. Each file name has the form 816#MMx.DAQ, where # indicates the intended oil thickness in millimeters for that measurement, and x is a letter representing repetitions over the same oil thickness. Thus 81610MMB.DAQ is the second of a series of measurements over an intended oil thickness of 10 mm.

8160MMB.DAQ – This plot is the water only measurement, and is used as the baseline water temperature for the oil thickness estimation algorithm.

8160MMB.DAQ – This curve was the initial water measurement. The algorithm estimate of 0.200 mm appears to be an excellent match. It appears that there was some additional warm-up needed for the receiver electronics to settle out.

8161MMA.DAQ – This curve is an excellent match to the algorithm estimate of 1.000 mm.

8161MMB.DAQ – This curve is a fair-to-good match to the algorithm estimate of 1.400 mm.

8162MMA.DAQ – This curve is a fair-to-good match to the algorithm estimate of 2.100 mm.

8162MMB.DAQ – This curve is an excellent match to the algorithm estimate of 1.850 mm.

8163MMA.DAQ – This curve is a poor-to-fair match to the algorithm estimate of 2.950 mm. It appears that the gain of the higher channels may have drifted. However, the overall curve shape, downward slope-to-inflection point, is typical of oil thicknesses in the 3-mm range.

8163MMB.DAQ – This curve is a somewhat better match to the algorithm estimate of 2.950 mm than the 8163MMA.DAQ. It appears that the gain of the higher channels may have a slight drift. However, the overall curve shape, downward slope-to-inflection point, is typical of oil thicknesses in the 3-mm range.

8164MMA.DAQ – This curve is a poor match to the algorithm estimate of 0.000 mm. It exhibits a good shape match to an estimate of 3.650 mm (as hinted by the correlation-only estimate of 3.650 mm) although the overall values for the theoretical

prediction are higher than the measured values. However, the overall curve shape, inflection-to-positive slope, is typical of oil thicknesses in the 3.5- to 4.0-mm range.

8164MMB.DAQ – This curve exhibits a good shape match to the algorithm estimate of 3.700 mm although the overall values for the theoretical prediction are higher than the measured values. However, the overall curve shape, inflection-to-positive slope, is typical of oil thicknesses in the 3.5 - 4.0 mm range.

8165MMA.DAQ – This curve exhibits a good shape match to the algorithm estimate of 4.750 mm although the overall values for the theoretical prediction are higher than the measured values. The overall convex curve shape is typical of oil thicknesses in the 5-mm range.

8165MMB.DAQ – This curve exhibits a good shape match to the algorithm estimate of 4.725 mm although the overall values for the theoretical prediction are higher than the measured values. The overall convex curve shape is typical of oil thicknesses in the 5-mm range.

8166MMA.DAQ – This curve exhibits a good shape match to the algorithm estimate of 5.875 mm although the overall values for the theoretical prediction are somewhat less than the measured values. At this thickness the curve is beginning to exhibit a true sinusoid shape.

8166MMB.DAQ – This curve exhibits a good shape match to the algorithm estimate of 5.900 mm although the overall values for the theoretical prediction are somewhat less than the measured values.

8167MMA.DAQ – This curve is an excellent match to the algorithm estimate of 6.725 mm.

8167MMB.DAQ – This curve is an excellent match to the algorithm estimate of 6.775 mm.

8168MMA.DAQ – This curve is an excellent match to the algorithm estimate of 7.925 mm.

8168MMB.DAQ – This curve is an excellent match to the algorithm estimate of 7.700 mm.

8169MMA.DAQ – This curve is an excellent match to the algorithm estimate of 8.825 mm.

8169MMB.DAQ - This curve is a good-to-excellent match to the algorithm estimate of 8.850 mm.

81610MMA.DAQ - If the three low points at 32, 36, and 37 GHz are disregarded, the measured data points exhibit an excellent match to an estimate of 10 mm.

81610MMB.DAQ - If the three low points at 32, 36, and 37 GHz are disregarded, the measured data points exhibit a good match to an estimate of 10 mm.

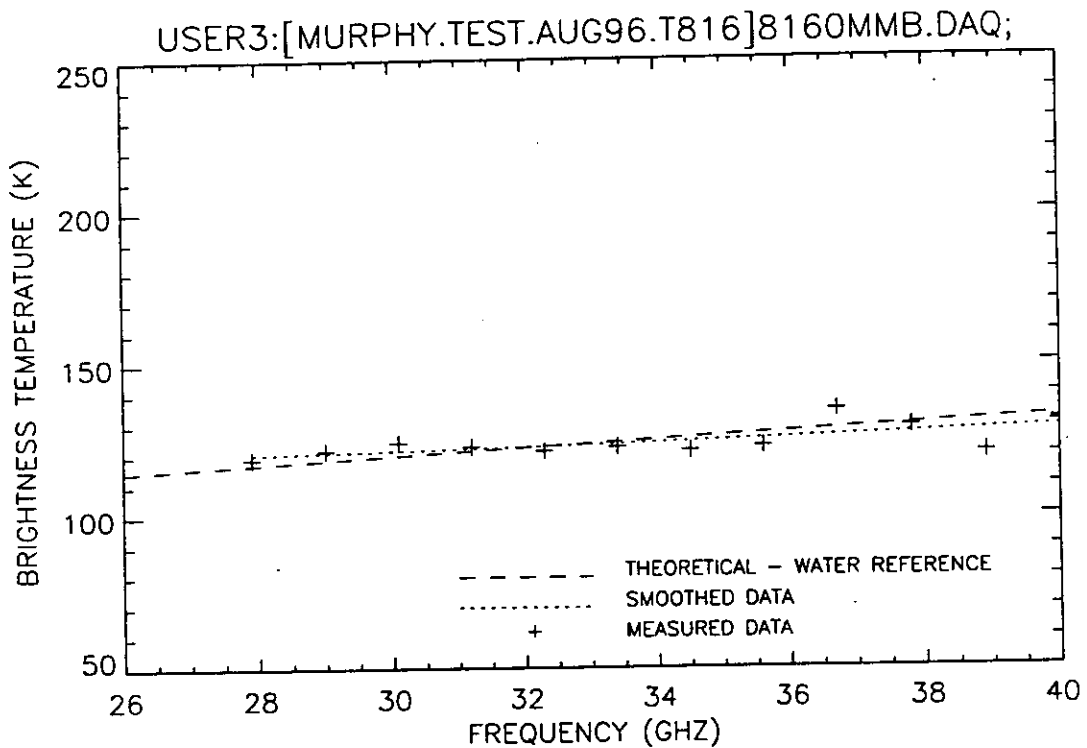


Figure B28. Plot of radiometric brightness temperature versus measurement frequency for water background, 16 August 1996.

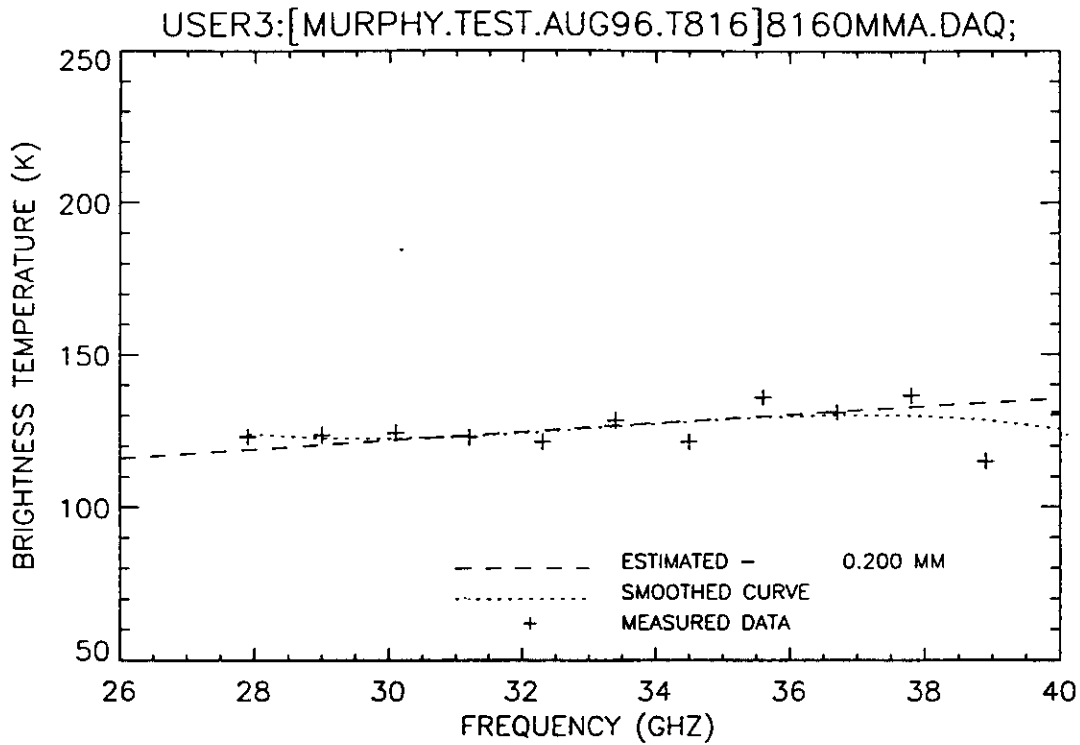


Figure B29. Plot of radiometric brightness temperature versus measurement frequency for water only measurement, 16 August 1996.

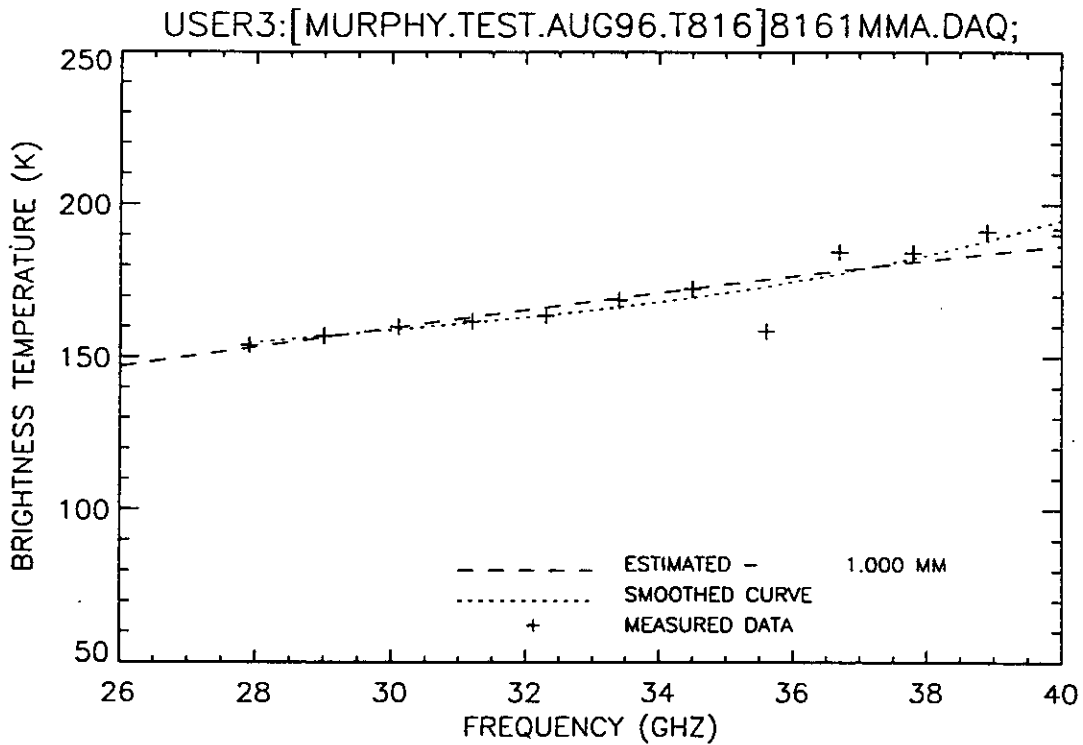


Figure B30. Plot of radiometric brightness temperature versus measurement frequency for 1.0 mm oil thickness, 16 August 1996.

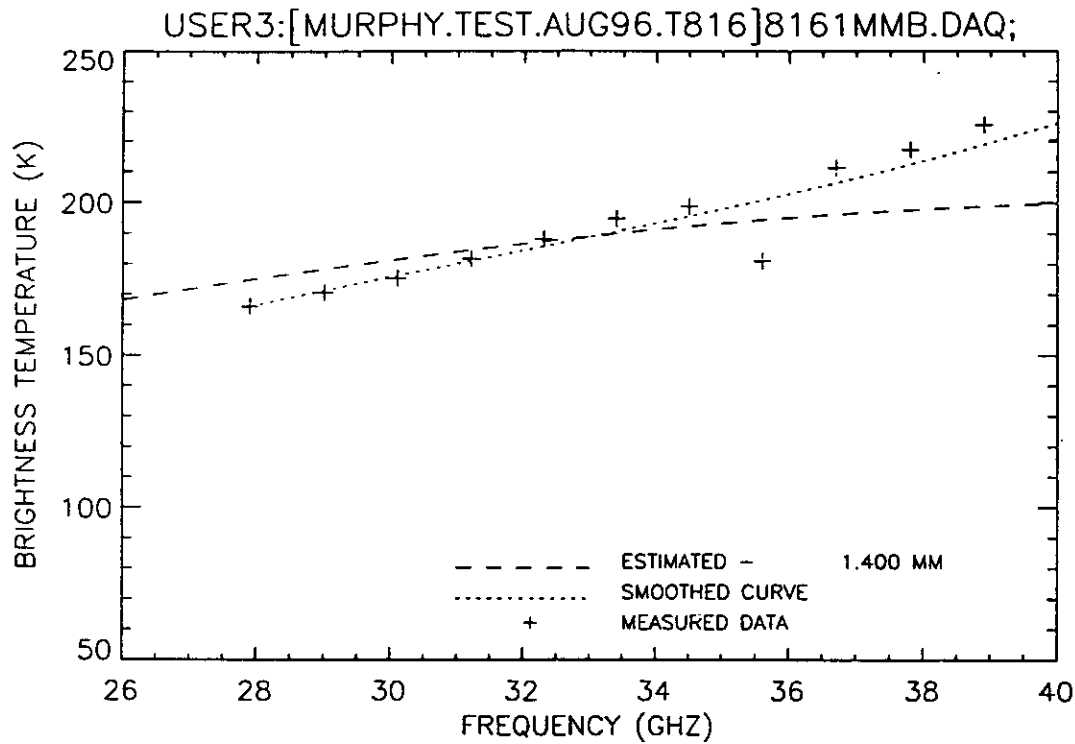


Figure B31. Plot of radiometric brightness temperature versus measurement frequency for 1.0 mm oil thickness, 16 August 1996.

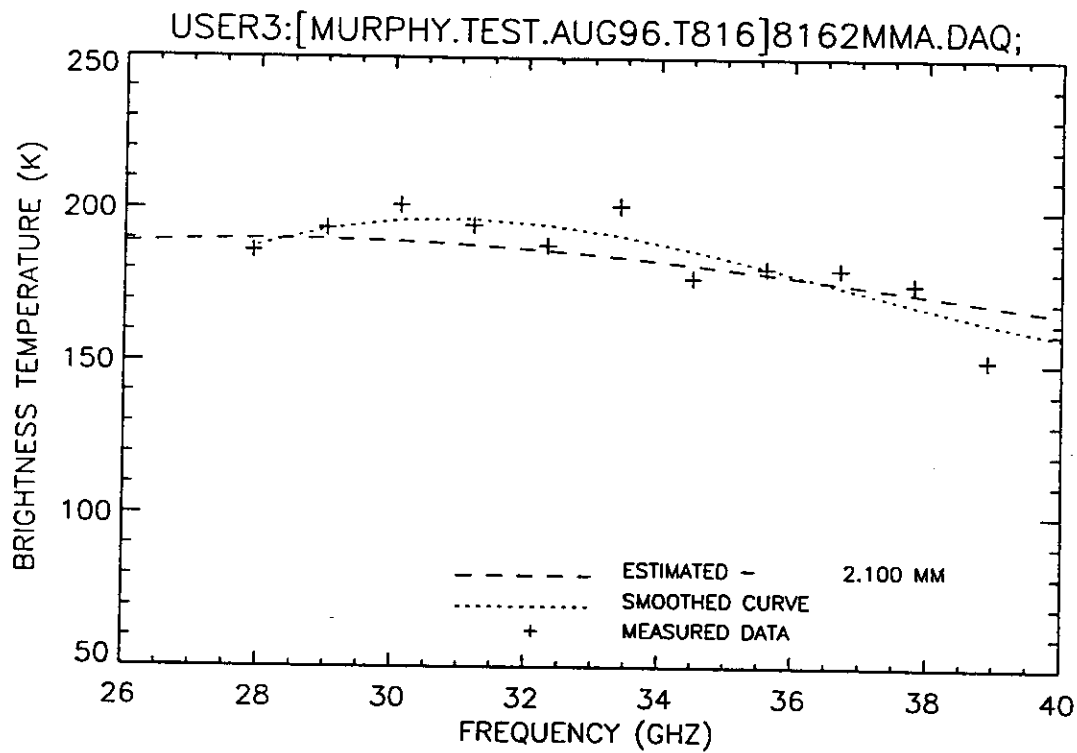


Figure B32. Plot of radiometric brightness temperature versus measurement frequency for 2.0 mm oil thickness, 16 August 1996.

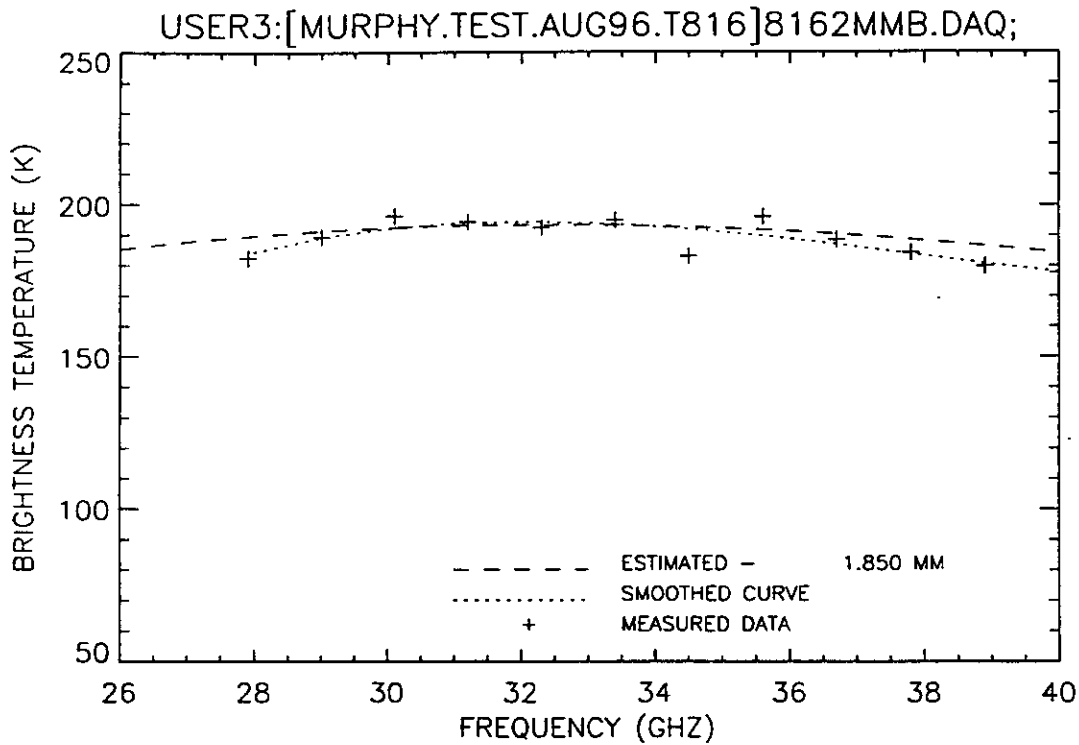


Figure B33. Plot of radiometric brightness temperature versus measurement frequency for 2.0 mm oil thickness, 16 August 1996.

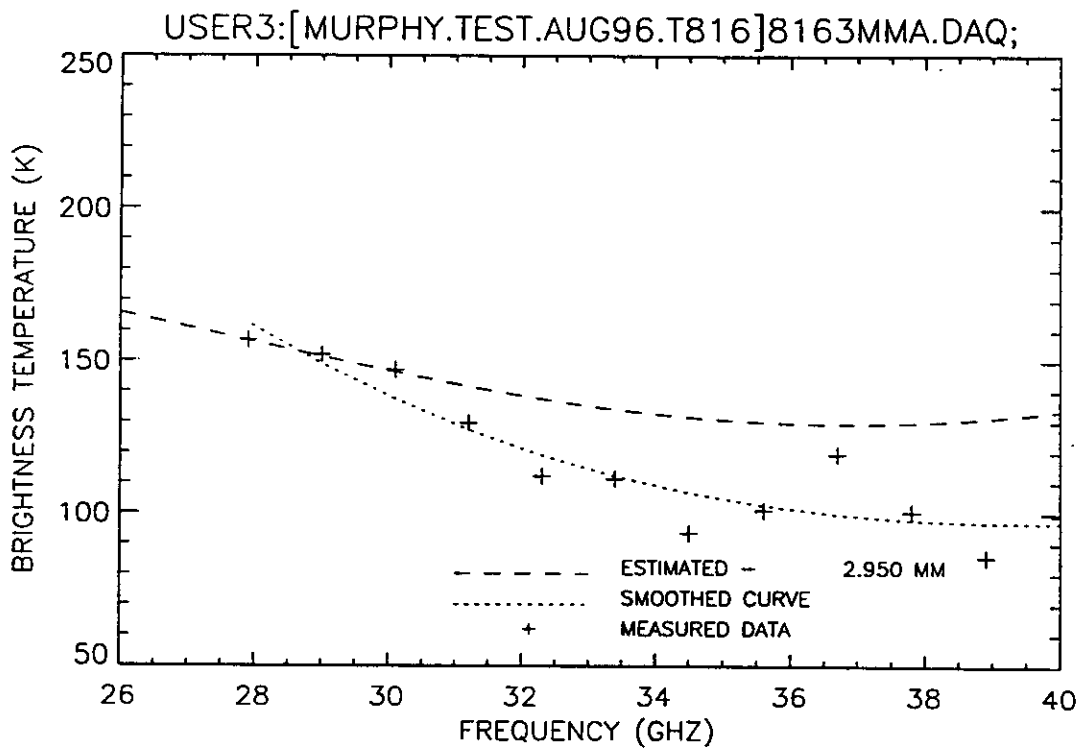


Figure B34. Plot of radiometric brightness temperature versus measurement frequency for 3.0 mm oil thickness, 16 August 1996.

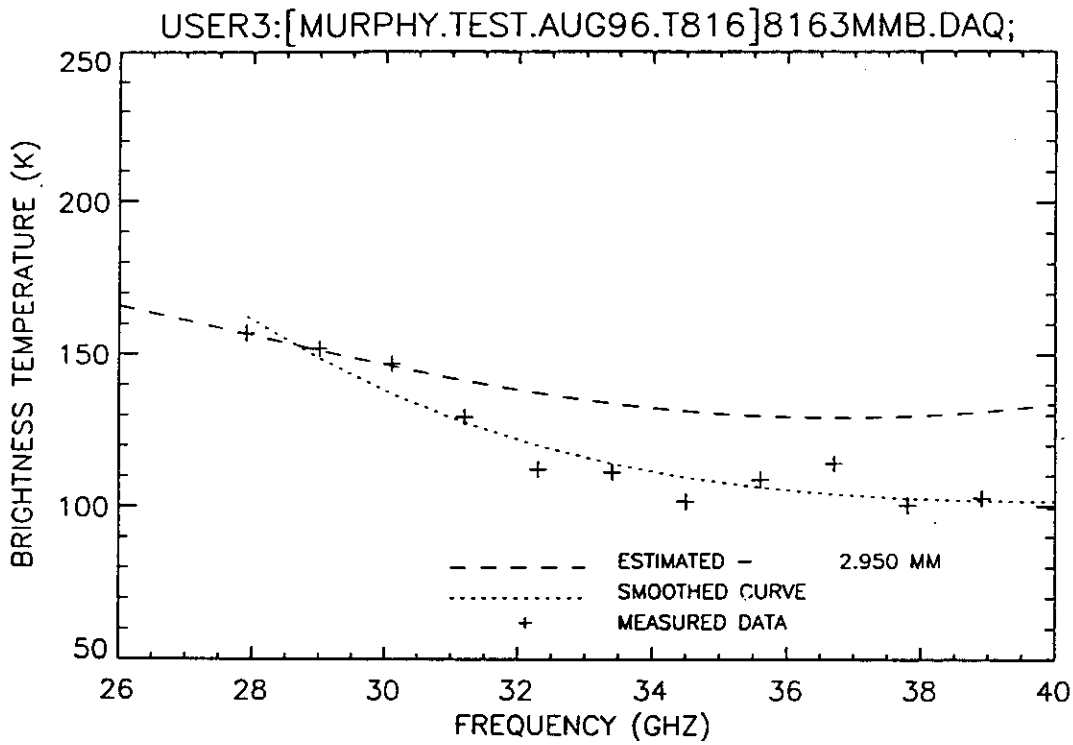


Figure B35. Plot of radiometric brightness temperature versus measurement frequency for 3.0 mm oil thickness, 16 August 1996.

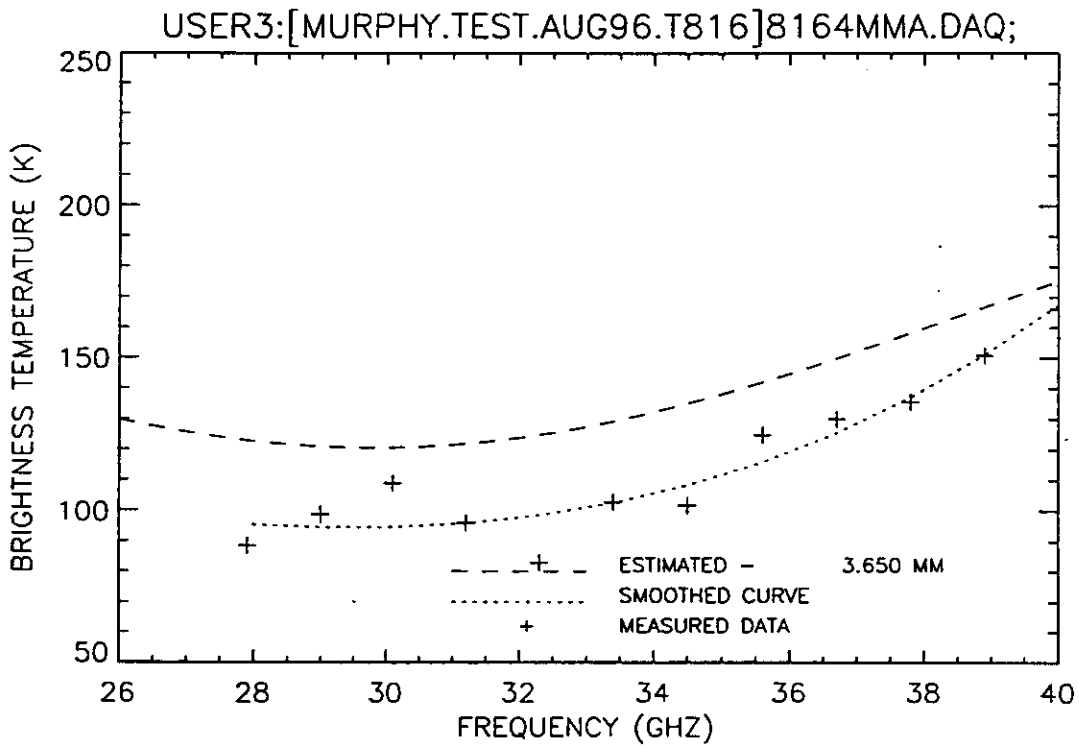


Figure B36. Plot of radiometric brightness temperature versus measurement frequency for 4.0 mm oil thickness, 16 August 1996.

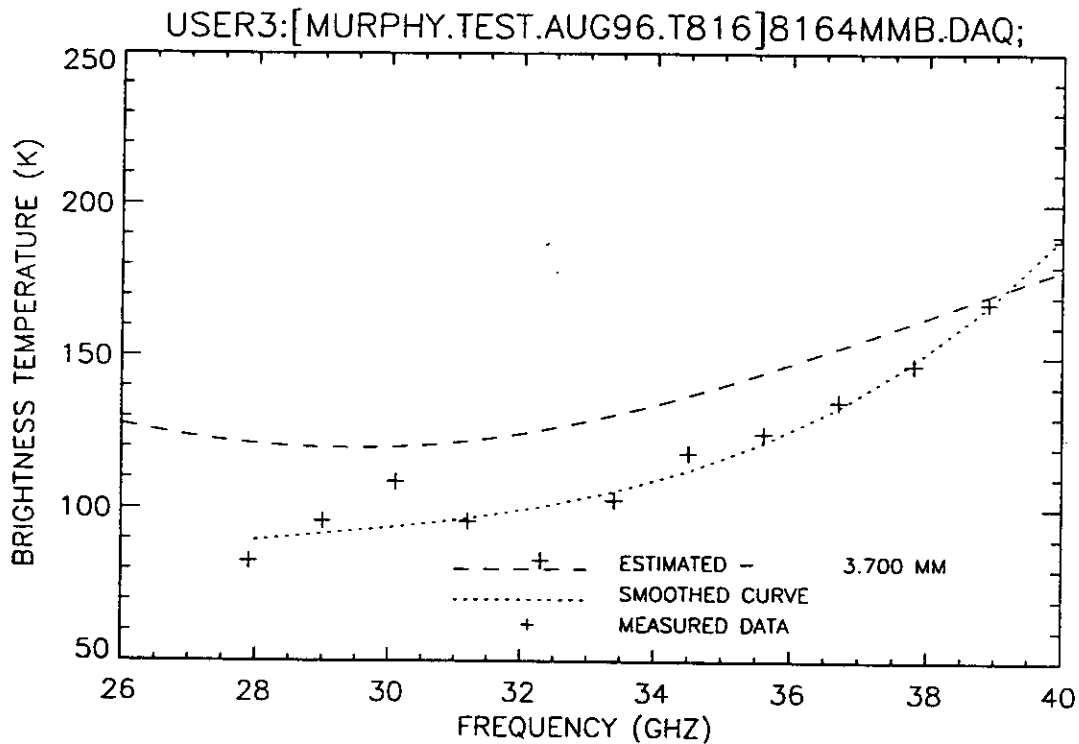


Figure B37. Plot of radiometric brightness temperature versus measurement frequency for 4.0 mm oil thickness, 16 August 1996.

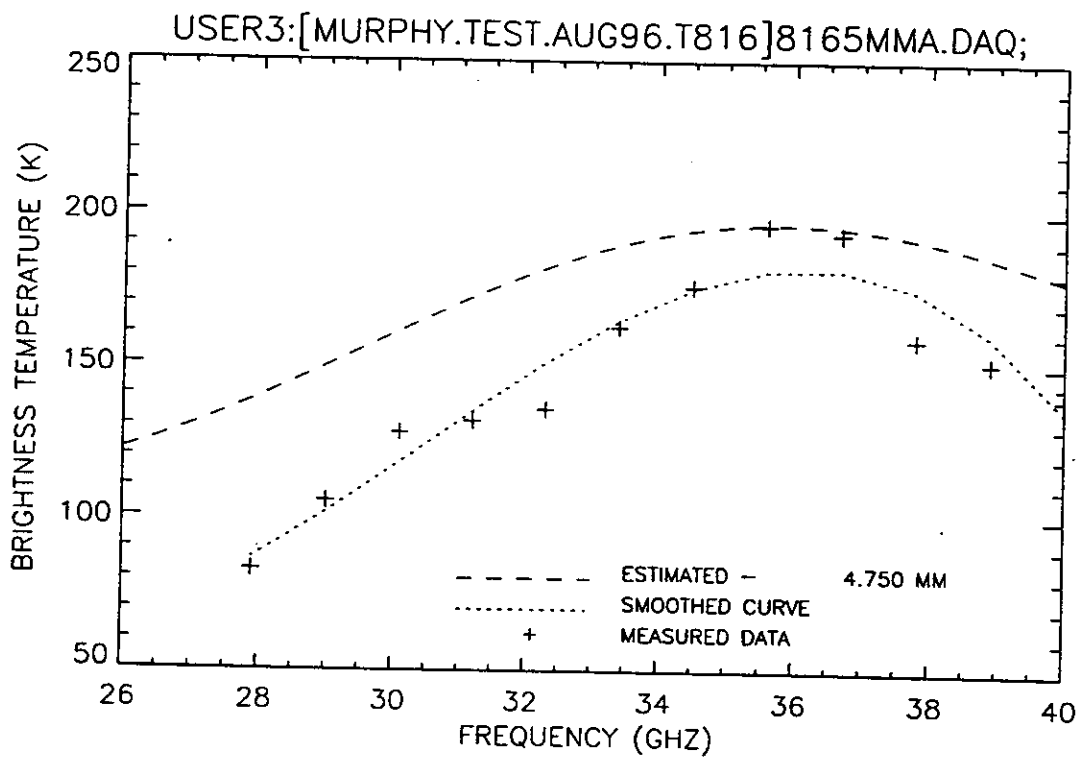


Figure B38. Plot of radiometric brightness temperature versus measurement frequency for 5.0 mm oil thickness, 16 August 1996.

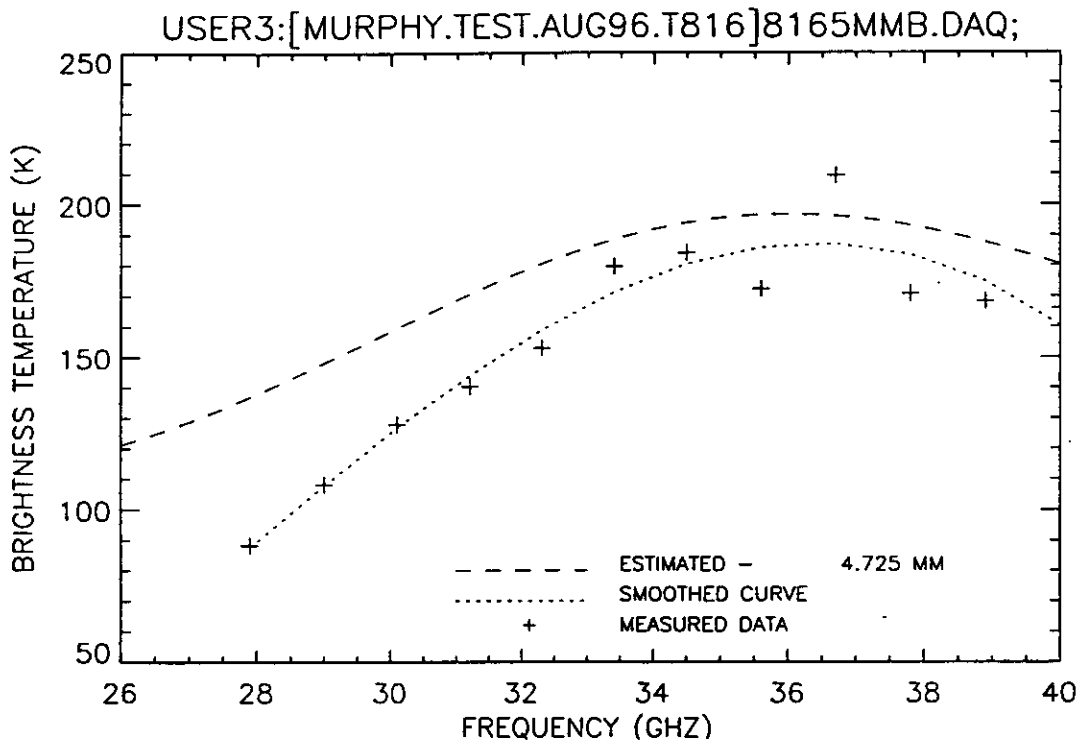


Figure B39. Plot of radiometric brightness temperature versus measurement frequency for 5.0 mm oil thickness, 16 August 1996.

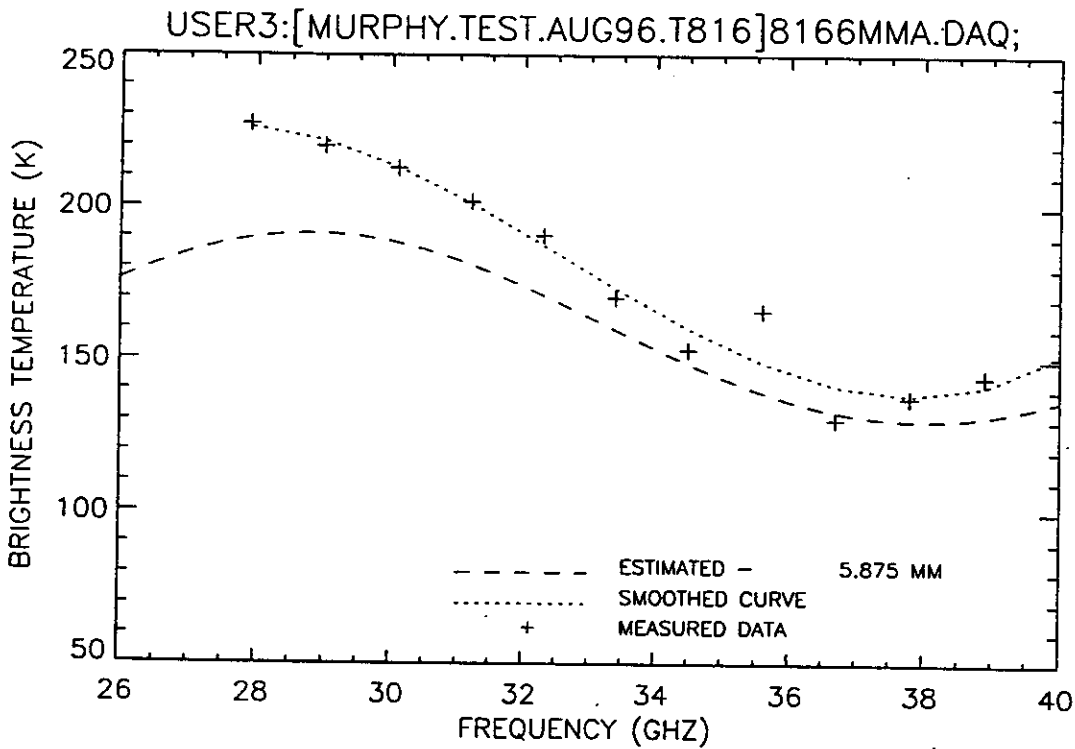


Figure B40. Plot of radiometric brightness temperature versus measurement frequency for 6.0 mm oil thickness, 16 August 1996.

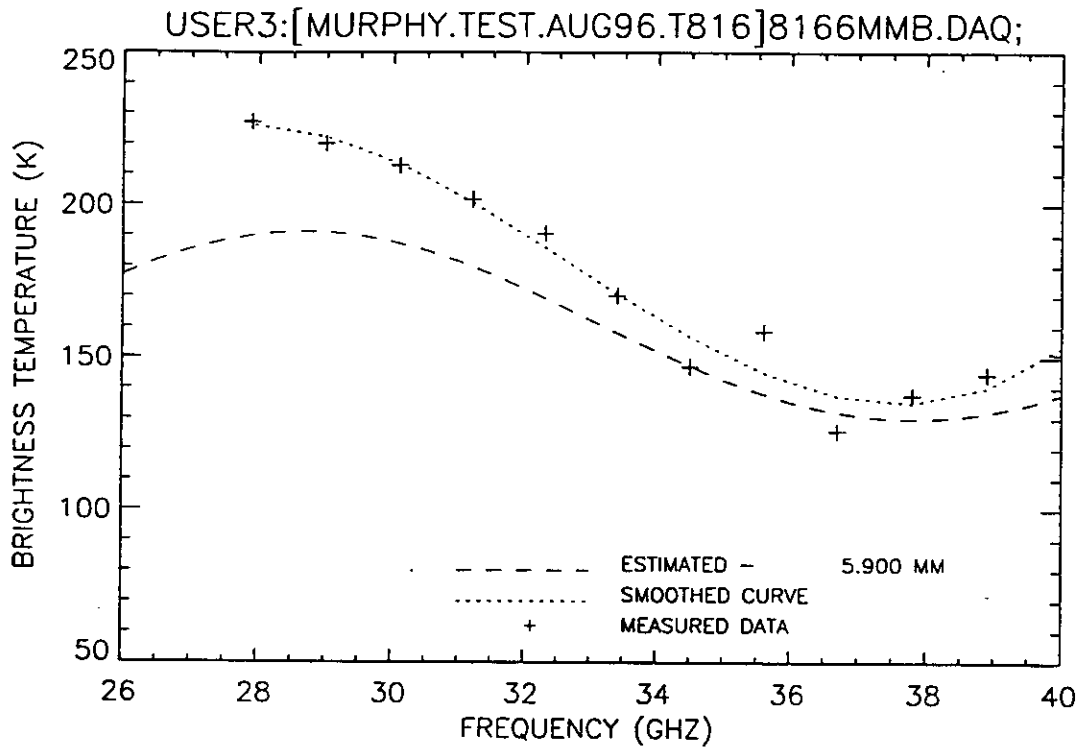


Figure B41. Plot of radiometric brightness temperature versus measurement frequency for 6.0 mm oil thickness, 16 August 1996.

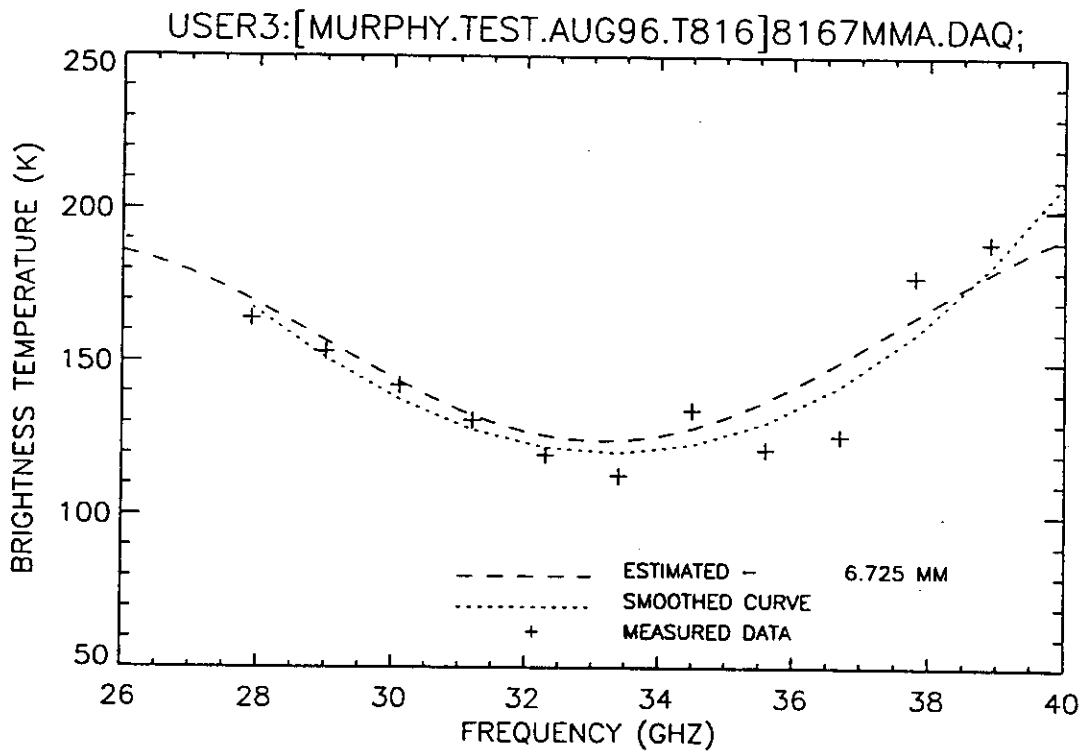


Figure B42. Plot of radiometric brightness temperature versus measurement frequency for 7.0 mm oil thickness, 16 August 1996.

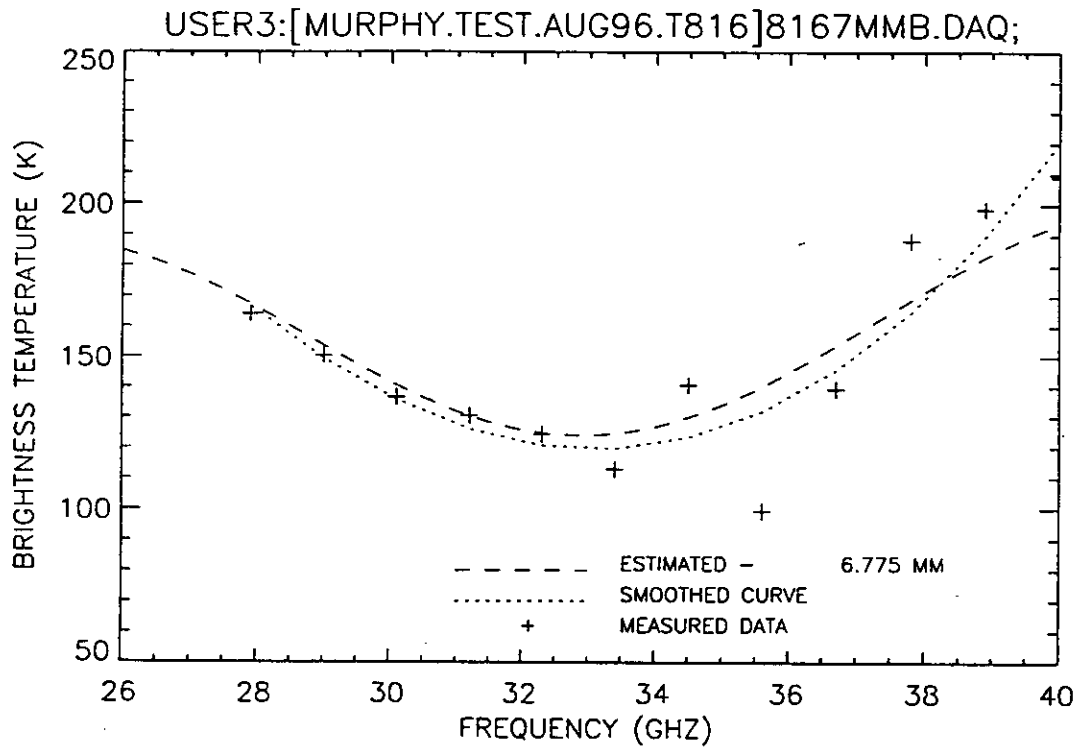


Figure B43. Plot of radiometric brightness temperature versus measurement frequency for 7.0 mm oil thickness, 16 August 1996.

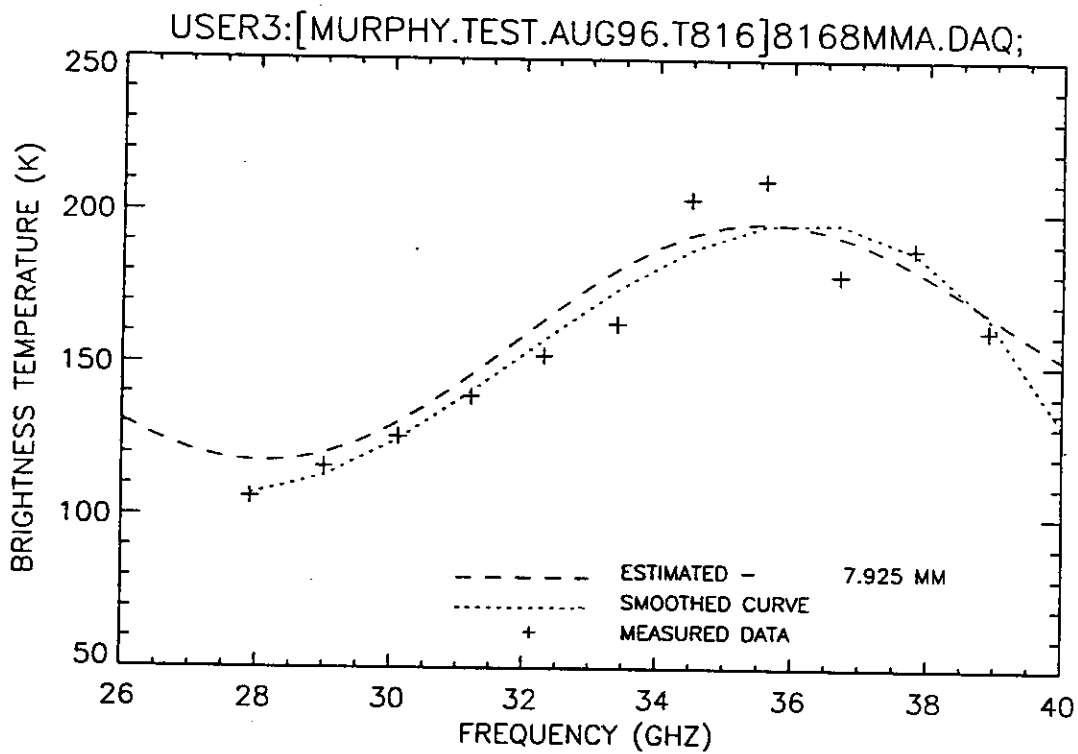


Figure B44. Plot of radiometric brightness temperature versus measurement frequency for 8.0 mm oil thickness, 16 August 1996.

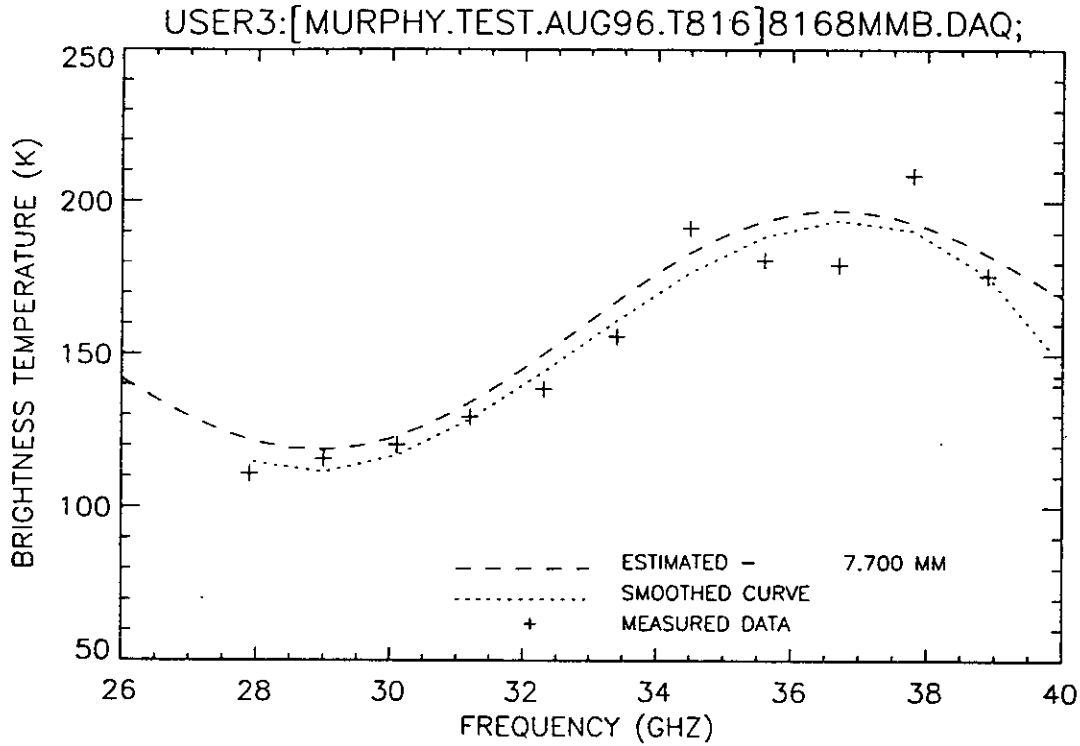


Figure B45. Plot of radiometric brightness temperature versus measurement frequency for 8.0 mm oil thickness, 16 August 1996.

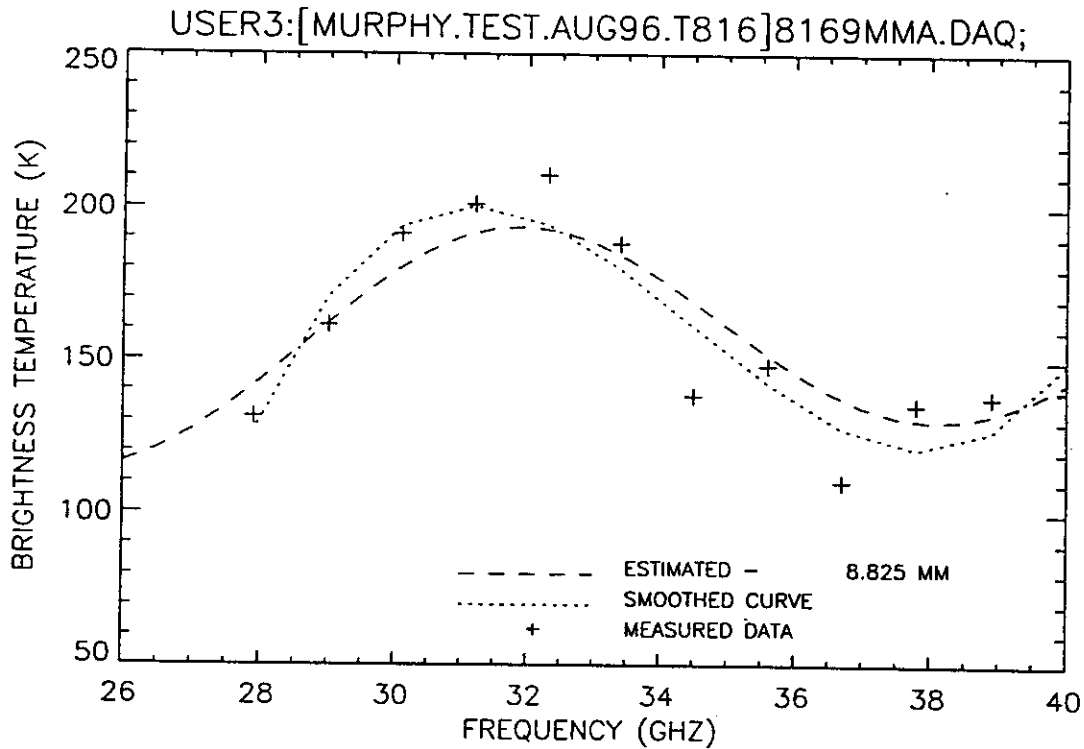


Figure B46. Plot of radiometric brightness temperature versus measurement frequency for 9.0 mm oil thickness, 16 August 1996.

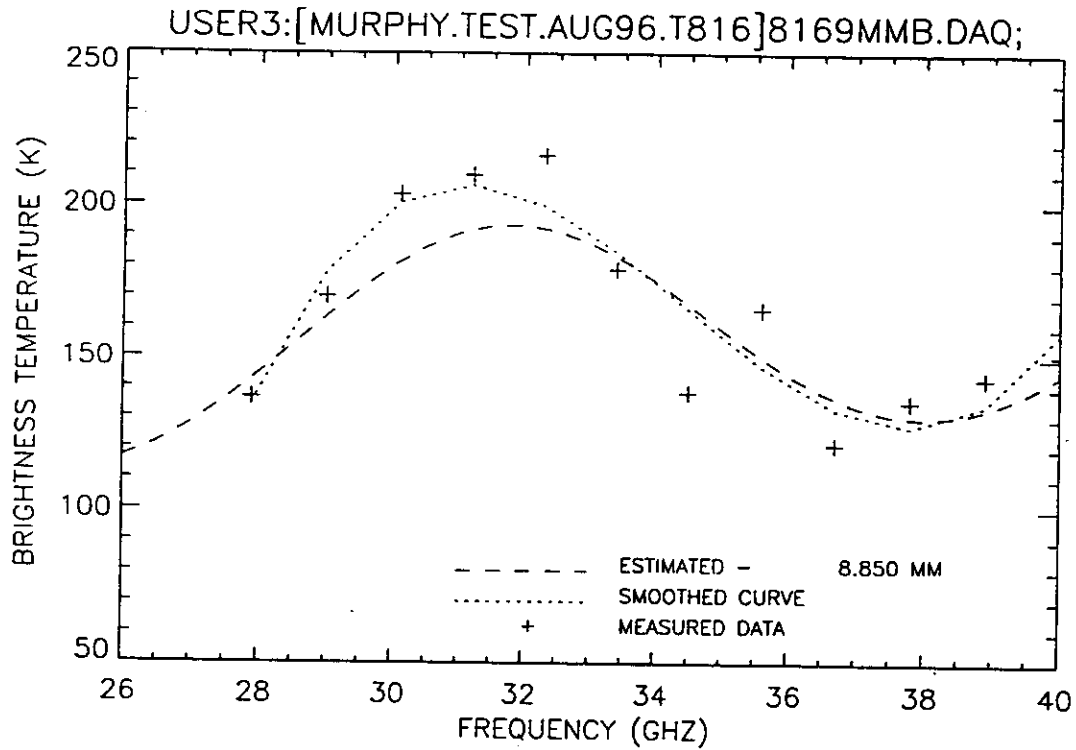


Figure B47. Plot of radiometric brightness temperature versus measurement frequency for 9.0 mm oil thickness, 16 August 1996.

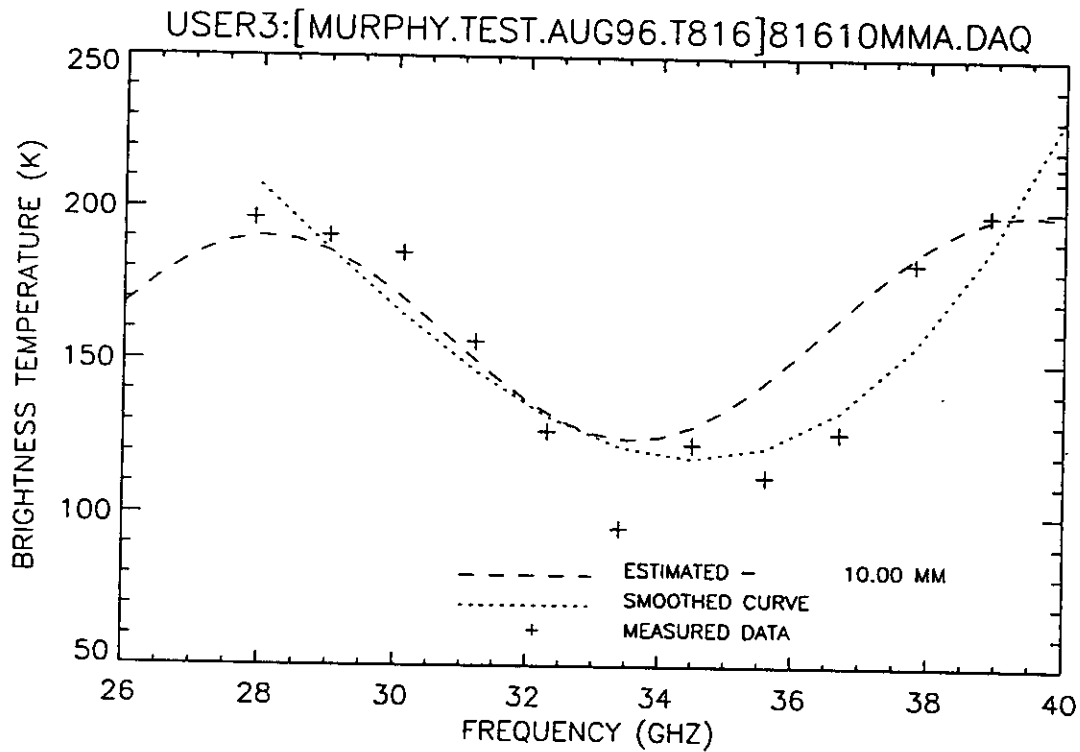


Figure B48. Plot of radiometric brightness temperature versus measurement frequency for 10.0 mm oil thickness, 16 August 1996.

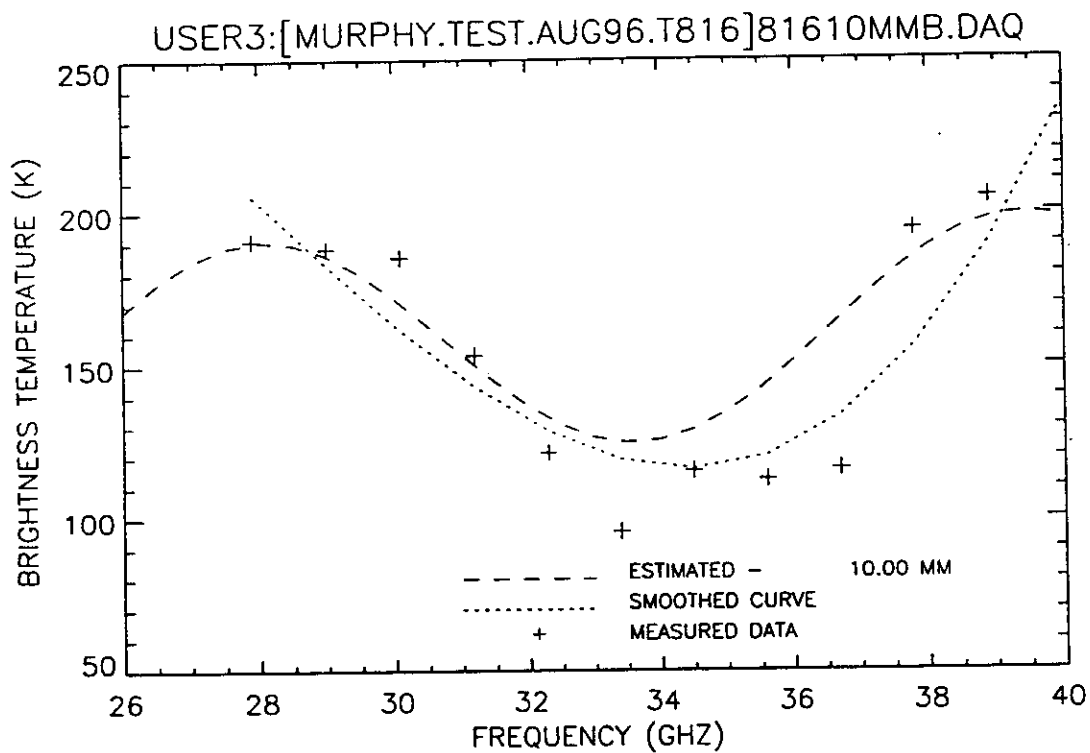


Figure B49. Plot of radiometric brightness temperature versus measurement frequency for 10.0 mm oil thickness, 16 August 1996.

B.3 21 August 1996 Analysis

This data collection was witnessed by representatives of the U.S. Coast Guard Research and Development Center as part of the pre-OHMSETT Test demonstration.

The file naming convention used during this collection is explained below. Each file name has the 8-20x#MM.DAT, where # indicates the intended oil thickness in millimeters for that measurement, and x is a letter representing repetitions over the same oil thickness. Thus 8-20AXMM.DAT is the first measurement over an intended oil thickness of 10 mm. Measurements were also collected over oil targets of unknown thickness. The file naming convention for these have the form 8-20xUNK.DAT where x is a letter representing repetitions over the unknown targets. Operator guess of the actual thickness is embedded in the comment line in the data set. Thus 8-20FUNK.DAT is the sixth measurement over an unknown thickness, and by viewing operator comments one would find that operator estimate of thickness is 0 mm.

8-20A0MM.DAT – This is the water background reference used for 20 August 1996.

8-20A1MM.DAT – It is believed that this curve is actually a 0 mm curve that was incorrectly identified in the file name as a 1-mm data set. The brightness temperatures of the data points are nearly identical to the 8-20A0MM.DAT data set. If this is the case, then the algorithm estimate of 0.000 mm is good.

8-20A2MM.DAT – This curve is a good match to the algorithm estimate of 2.800 mm.

8-20A3MM.DAT – This curve exhibits more amplitude variation than the theoretical curve would predict. A good shape match, downward sloping to inflection, is the correlation-only estimate of 2.600 mm.

8-20A4MM.DAT – This curve exhibits some noisy data points above 36 GHz. The algorithm estimate of 3.850 mm is a reasonably good shape match.

8-20A5MM.DAT – This curve exhibits more amplitude variation than the theoretical curve would predict. The algorithm estimate of 4.700 mm is a reasonably good shape match.

8-20A6MM.DAT – This curve exhibits much more amplitude variation than the theoretical curve would predict. The algorithm estimate of 5.95 mm is a fair-to-good shape match.

At this point, the instrument was recalibrated using the hot/cold load. The same water background temperature is assumed because the remaining known thickness curves all seem to have sufficient shape for comparison.

8-20B6MM.DAT – All the data points are slightly warmer than the theoretical curve would predict. The algorithm estimate of 2.075 mm was not a good match to the shape of the curve. The correlation-only result indicates a thicker estimate might be appropriate. An estimate of 6.000 mm provides a good shape match.

8-20A7MM.DAT – All of the data points are slightly warmer than the theoretical curve would predict. The algorithm estimate of 3.250 mm could be a possibility; however, the low point of the 3.250-mm estimate would be much closer to the background water temperature. An estimate of 6.800 mm provides a much better shape and temperature match.

8-20A8MM.DAT – The algorithm estimate of 1.350 mm was not a good match. The correlation-only estimate of 7.625 mm hints at a thicker oil film. The 7.800-mm estimate seems to be a good match to the peak and valley of the sinusoid.

8-20A9MM.DAT – The algorithm estimate of 5.025 mm was not a good match. Based on the curve shape, an 8.800-mm estimate seems to be a good shape match.

8-20AXMM.DAT – The algorithm estimate of 1.800 mm was not a good match. Based on the curve shape, a 9.950-mm estimate seems to be a good shape match.

Oil absorbent cloths were used to remove an unknown quantity of oil. For the next three measurements, the operator estimated the oil thickness at 1 mm.

8-20AUNK.DAT – It appears that the data points above 35 GHz may be noisy. The algorithm estimate of 1.575 mm appears to be a good match to the data points below 35 GHz.

8-20BUNK.DAT – It appears that the data points above 36 GHz may be noisy. The algorithm estimate of 1.525 mm appears to be a fair match to the data points below 36 GHz.

8-20CUNK.DAT – It appears that the data points above 35 GHz may be noisy. The algorithm estimate of 1.525 mm appears to be a good match to the data points below 35 GHz.

Again, an unknown quantity of oil was removed from the water surface. There was a noticeable sheen on the water, but visually its thickness was too thin to be measured.

8-20DUNK.DAT – This curve is an excellent match to the algorithm estimate of 0.500 mm. This estimate may be high because the instrument was recalibrated after the first 6 mm measurement and a new water background reference was not used.

8-20EUNK.DAT – The algorithm estimate of 3.275 was not a good match. This curve is a good-to-excellent match to an estimate of 0.200 mm. The 0.200 mm estimate may be high because the instrument was recalibrated after the first 6-mm measurement and a new water background reference was not used.

8-20FUNK.DAT – The algorithm estimate of 3.325 was not a good match. This curve is a good-to-excellent match to an estimate of 0.300 mm. The 0.300 mm estimate may be high because the instrument was recalibrated after the first 6-mm measurement and a new water background reference was not used.

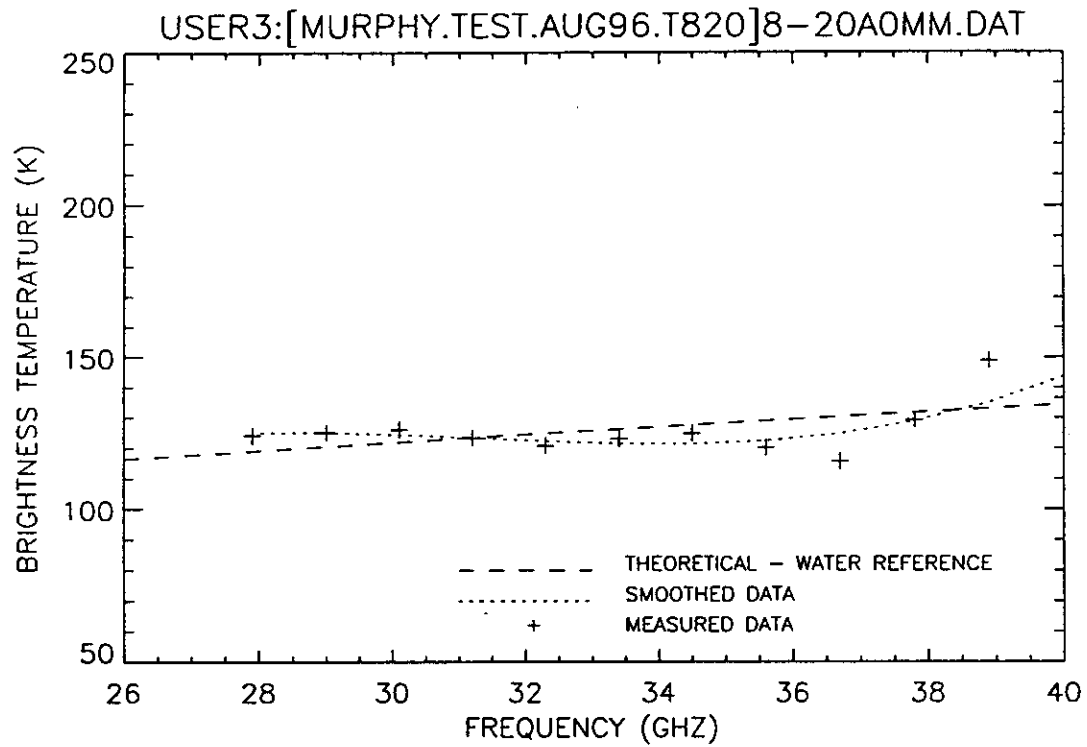


Figure B50. Plot of radiometric brightness temperature versus measurement frequency water background, 21 August 1996.

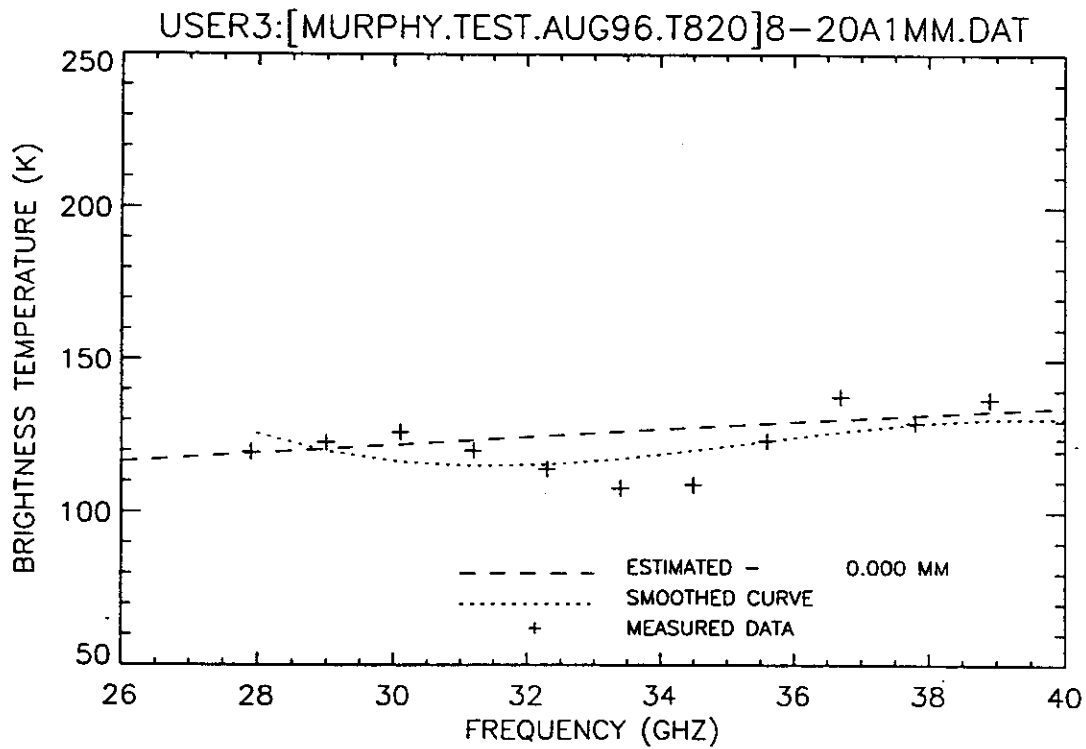


Figure B51. Plot of radiometric brightness temperature versus measurement frequency for 1.0 mm oil thickness, 21 August 1996.

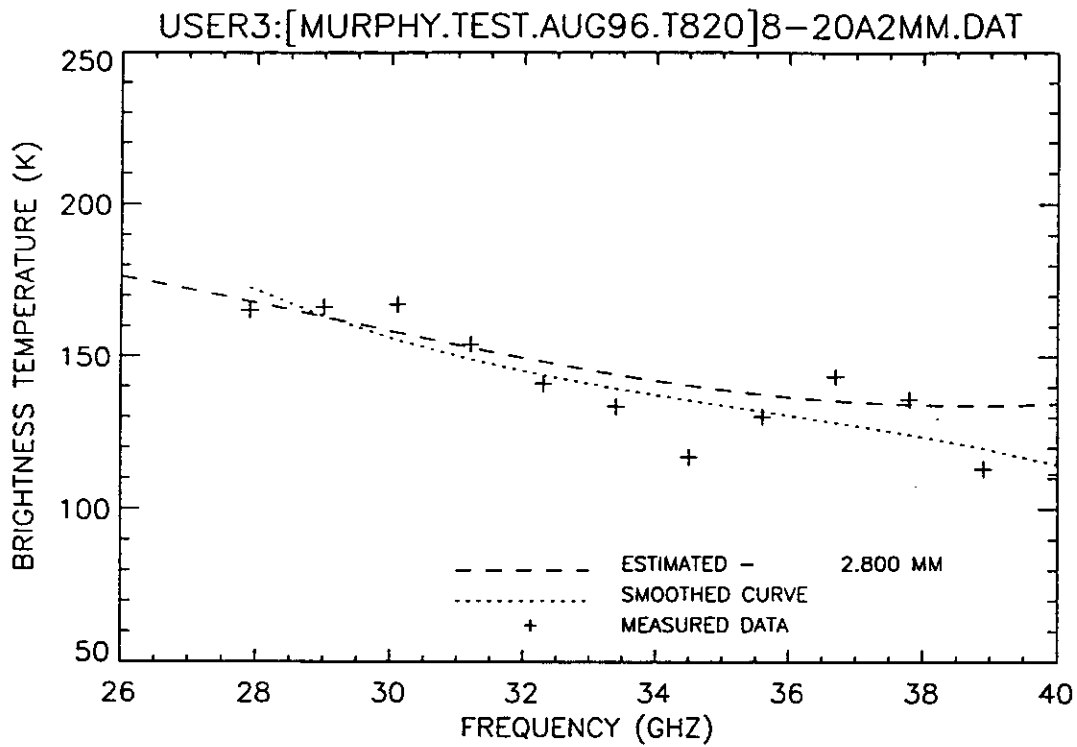


Figure B52. Plot of radiometric brightness temperature versus measurement frequency for 2.0 mm oil thickness, 21 August 1996.

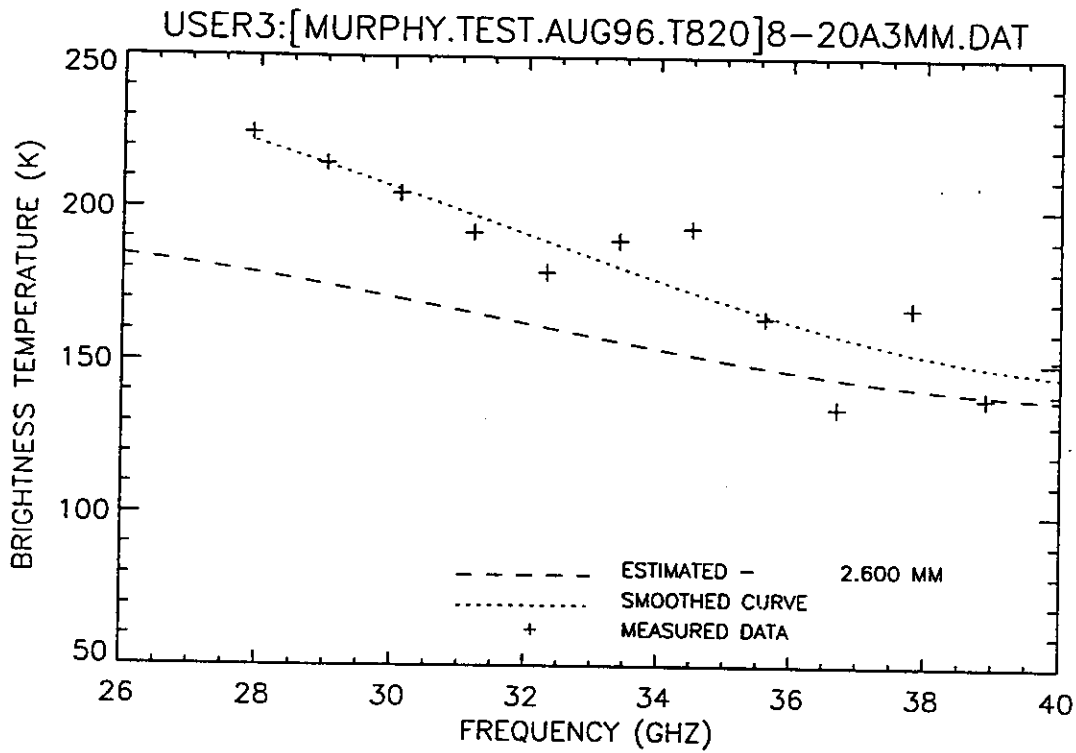


Figure B53. Plot of radiometric brightness temperature versus measurement frequency for 3.0 mm oil thickness, 21 August 1996.

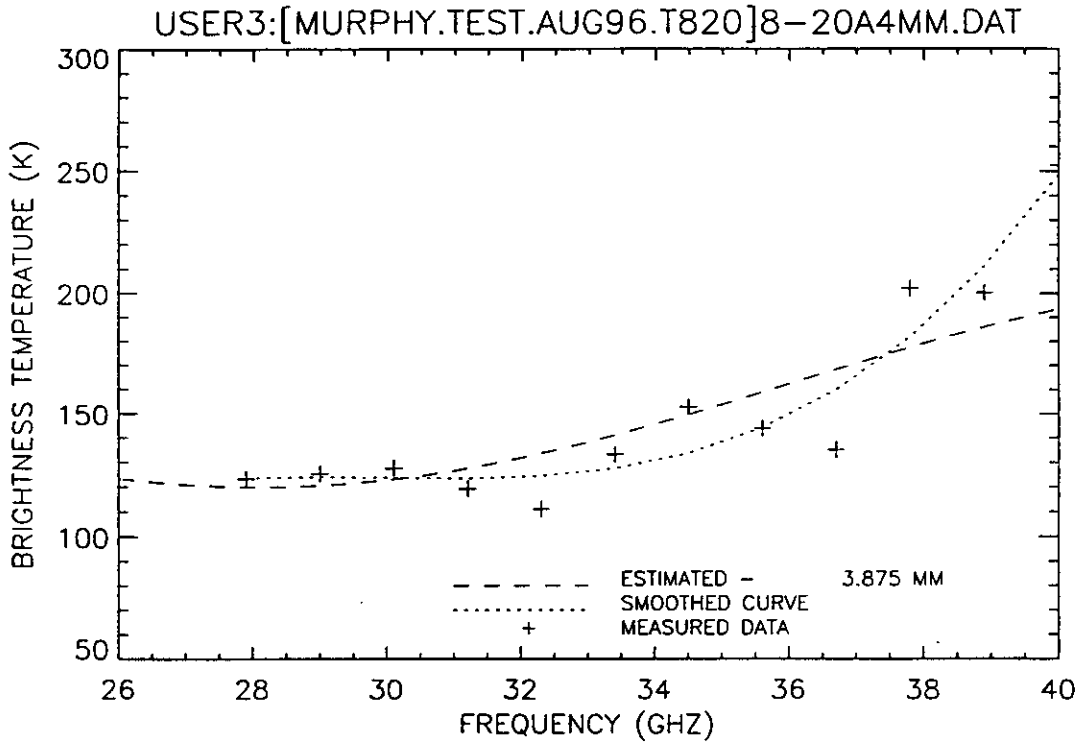


Figure B54. Plot of radiometric brightness temperature versus measurement frequency for 4.0 mm oil thickness, 21 August 1996.

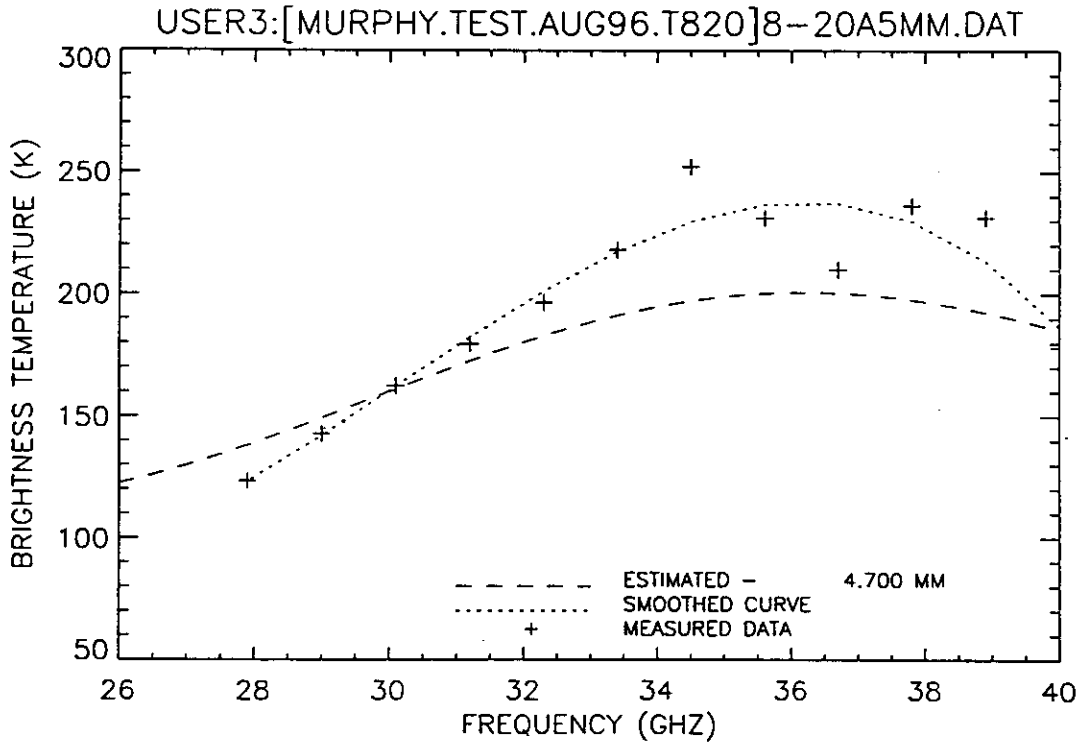


Figure B55. Plot of radiometric brightness temperature versus measurement frequency for 5.0 mm oil thickness, 21 August 1996.

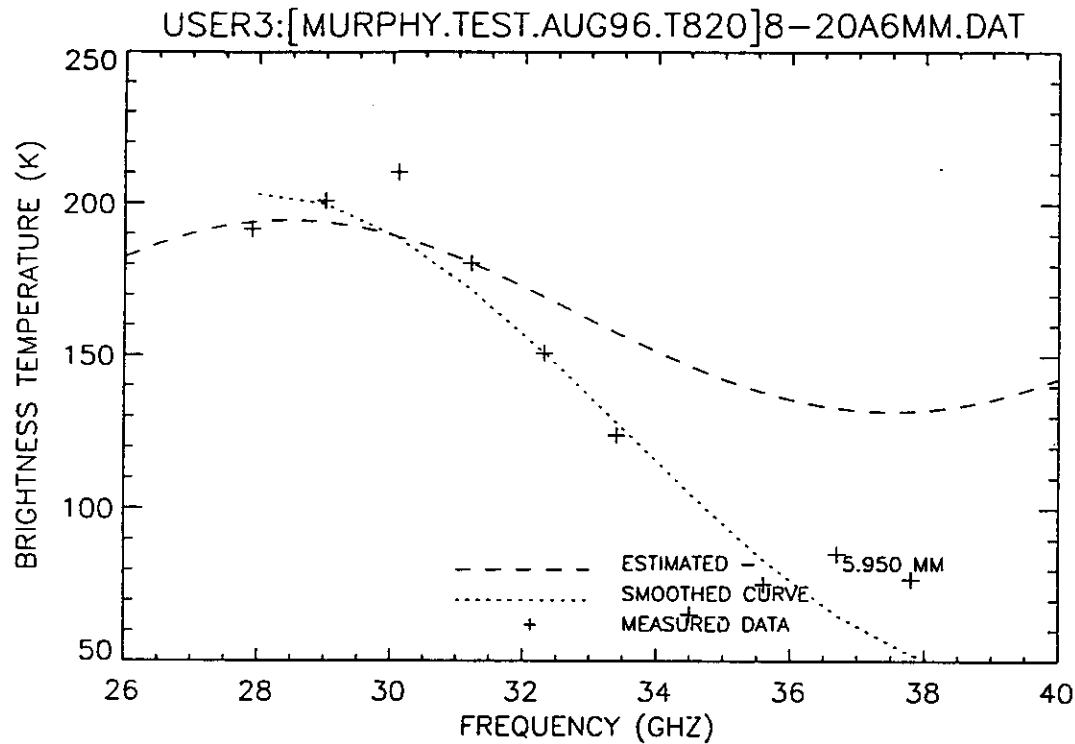


Figure B56. Plot of radiometric brightness temperature versus measurement frequency for 6.0 mm oil thickness, 21 August 1996.

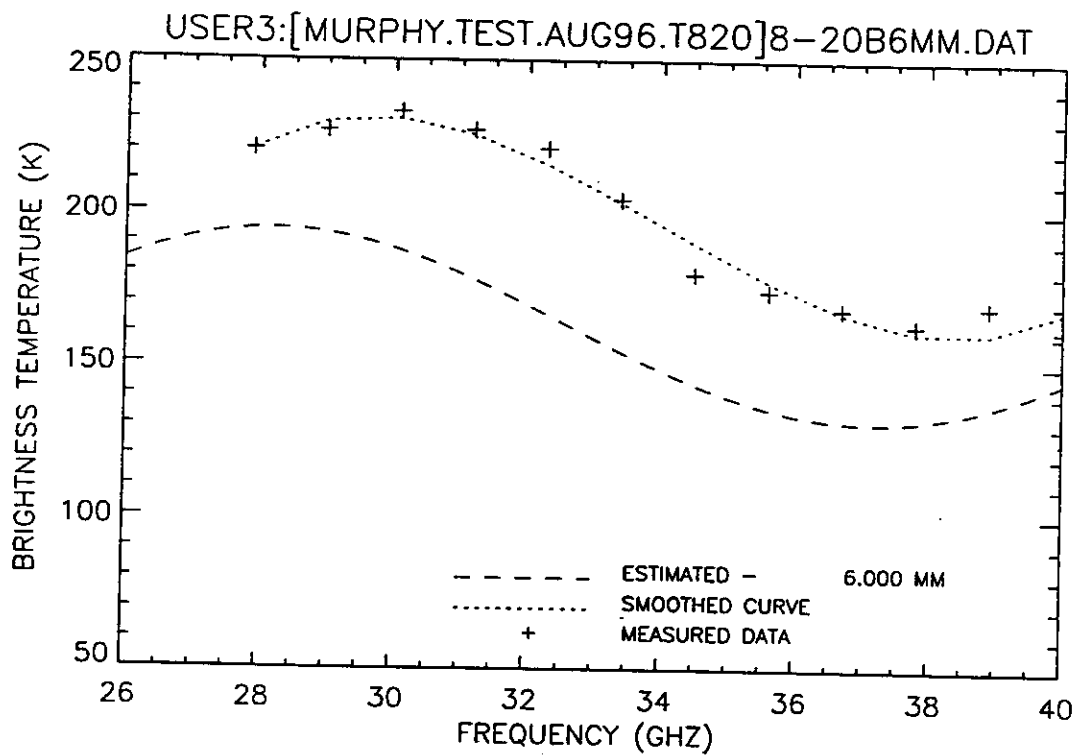


Figure B57. Plot of radiometric brightness temperature versus measurement frequency for 6.0 mm oil thickness, 21 August 1996.

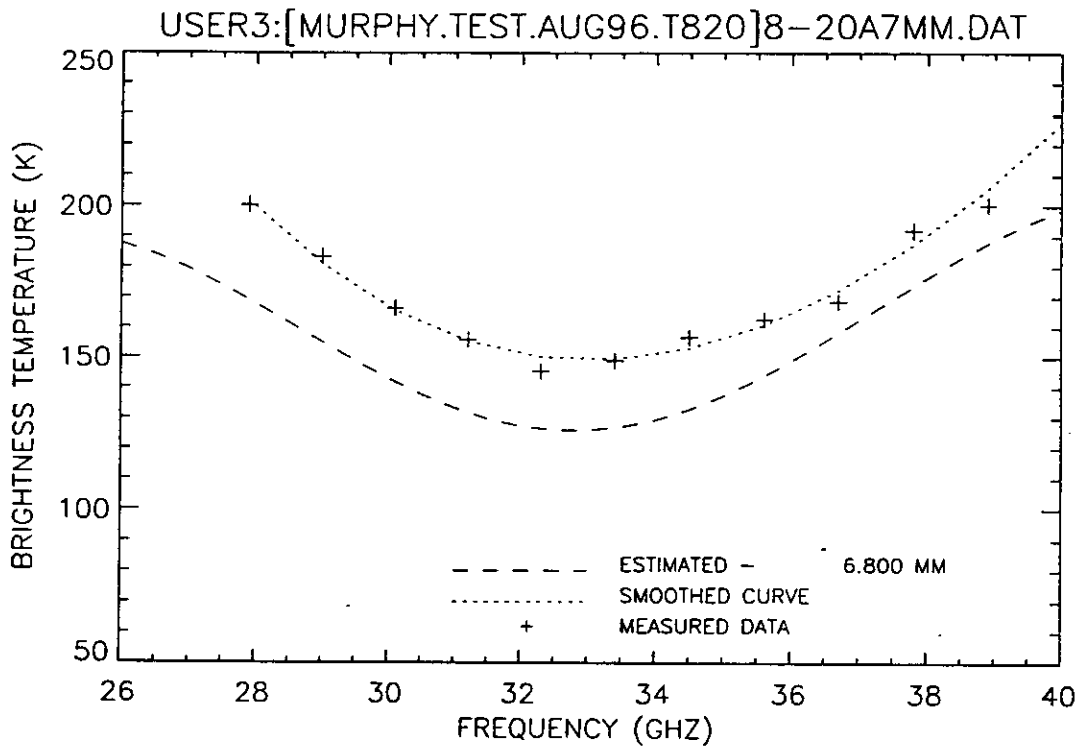


Figure B58. Plot of radiometric brightness temperature versus measurement frequency for 7.0 mm oil thickness, 21 August 1996.

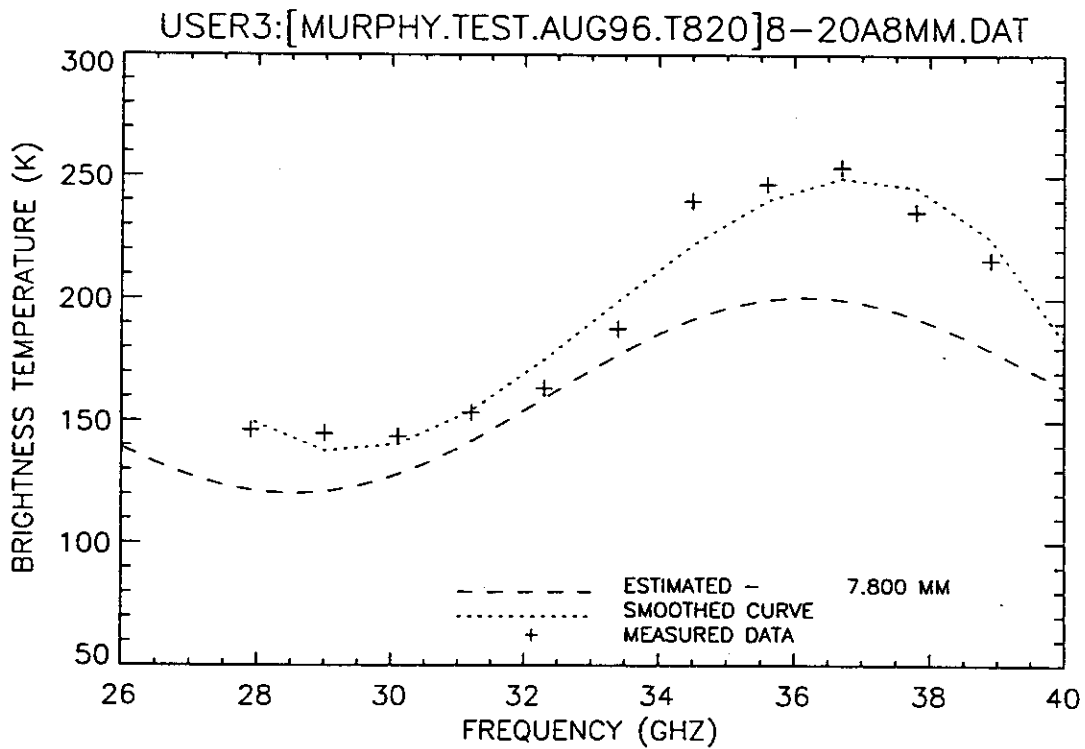


Figure B59. Plot of radiometric brightness temperature versus measurement frequency for 8.0 mm oil thickness, 21 August 1996.

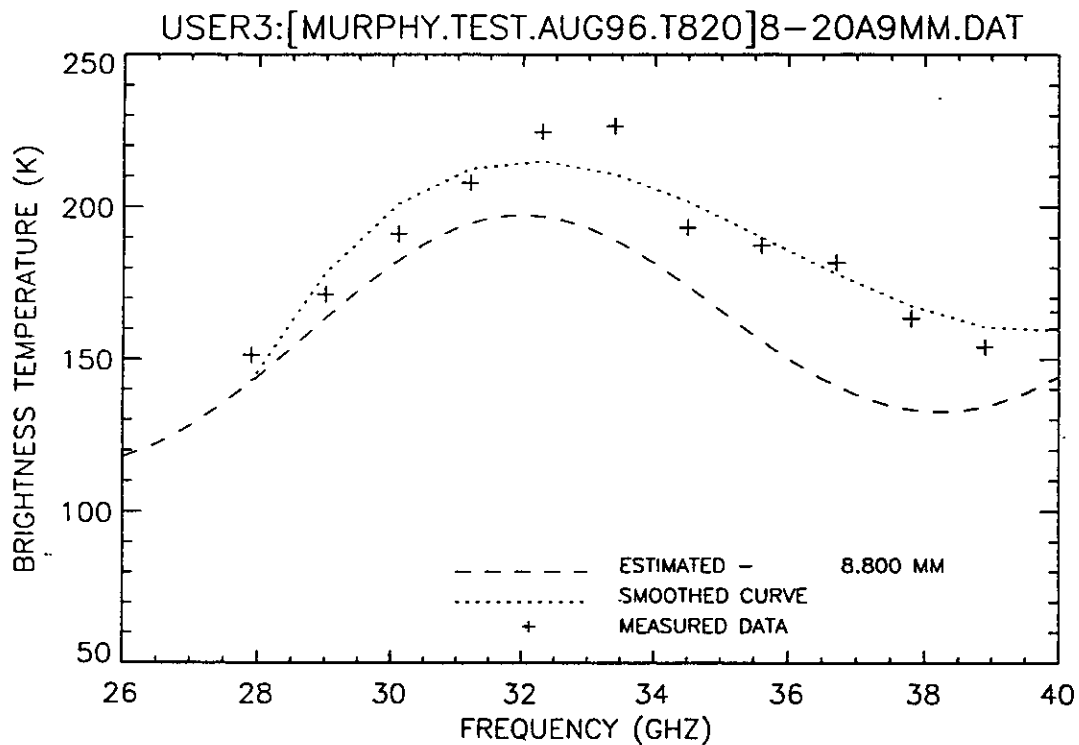


Figure B60. Plot of radiometric brightness temperature versus measurement frequency for 9.0 mm oil thickness, 21 August 1996.

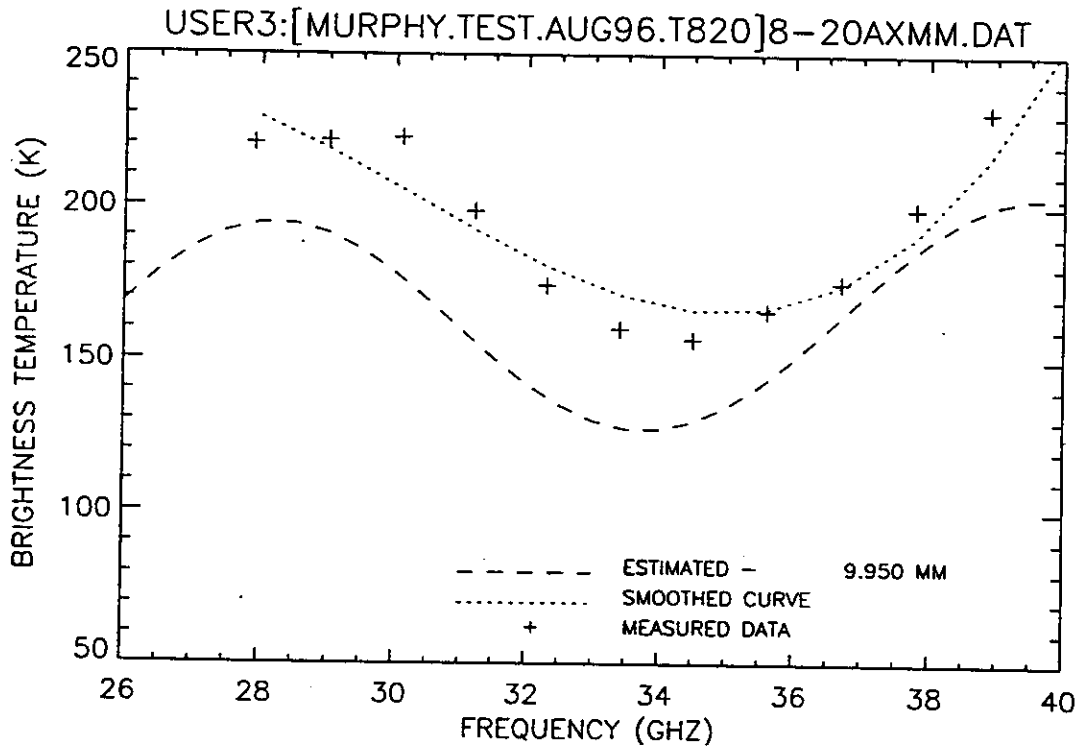


Figure B61. Plot of radiometric brightness temperature versus measurement frequency for 10.0 mm oil thickness, 21 August 1996.

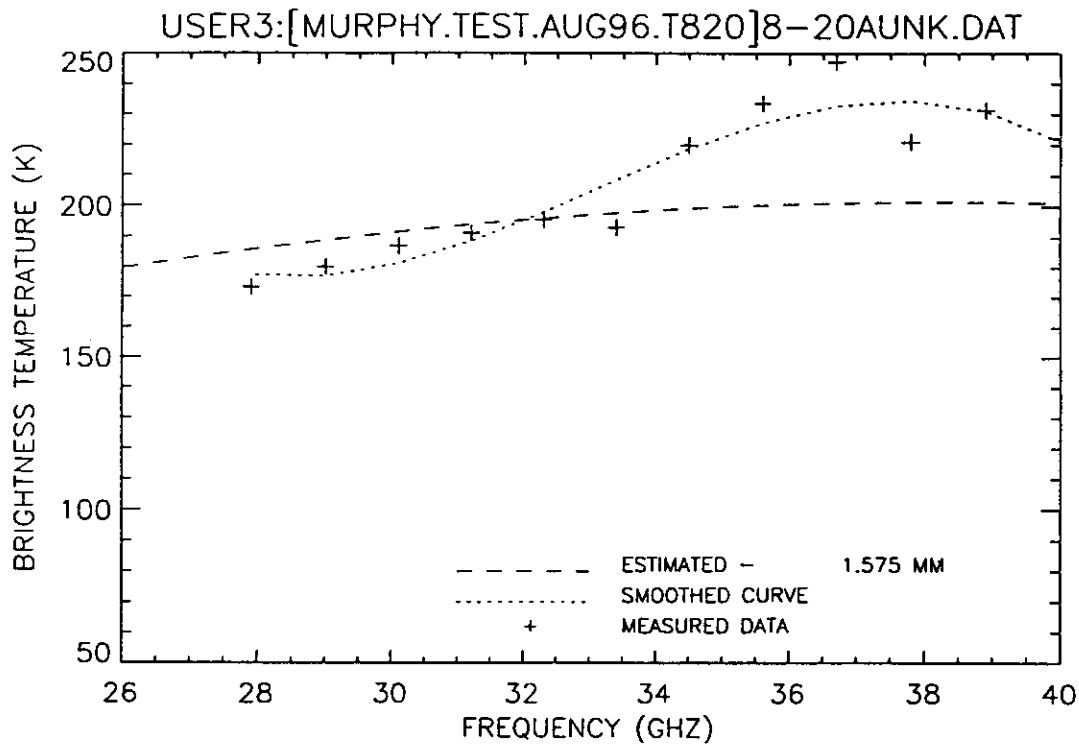


Figure B62. Plot of radiometric brightness temperature versus measurement frequency for an unknown oil thickness, 21 August 1996.

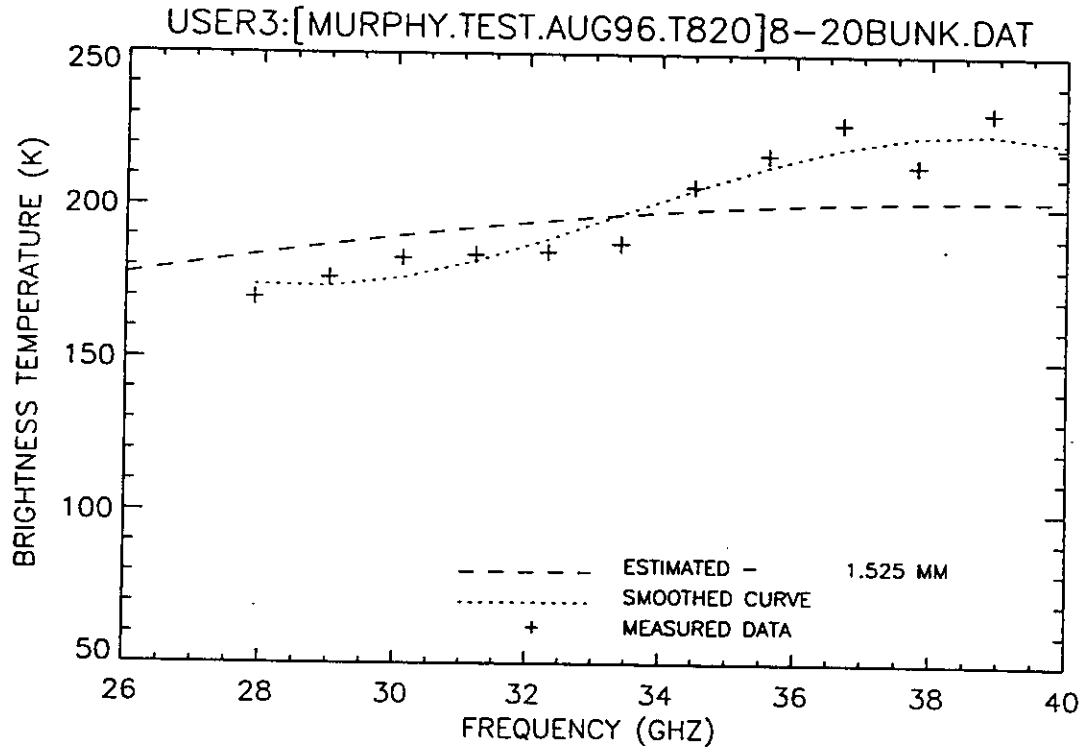


Figure B63. Plot of radiometric brightness temperature versus measurement frequency for an unknown oil thickness, 21 August 1996.

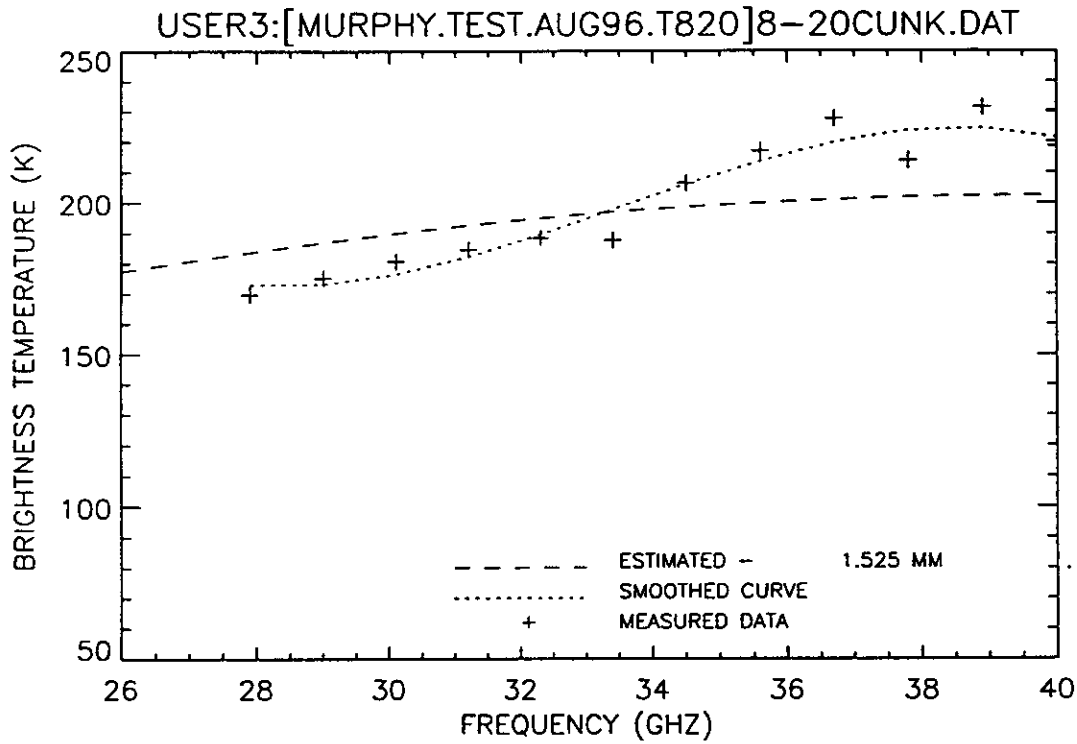


Figure B64. Plot of radiometric brightness temperature versus measurement frequency for an unknown oil thickness, 21 August 1996.

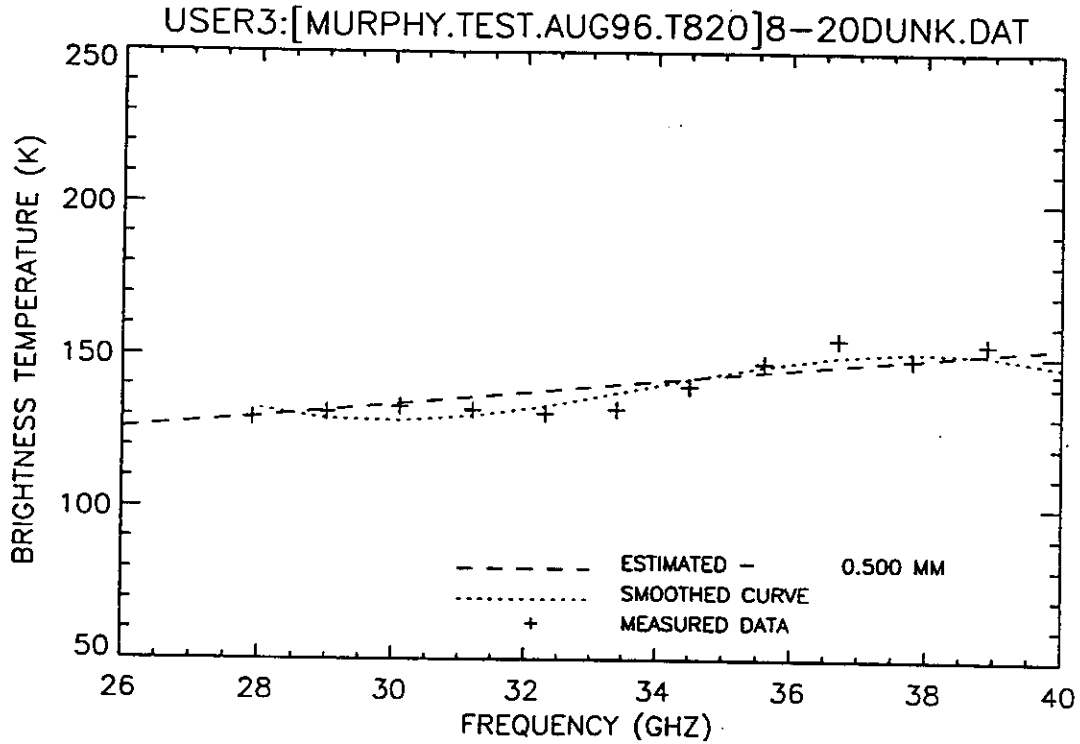


Figure B65. Plot of radiometric brightness temperature versus measurement frequency for an unknown oil thickness, 21 August 1996.

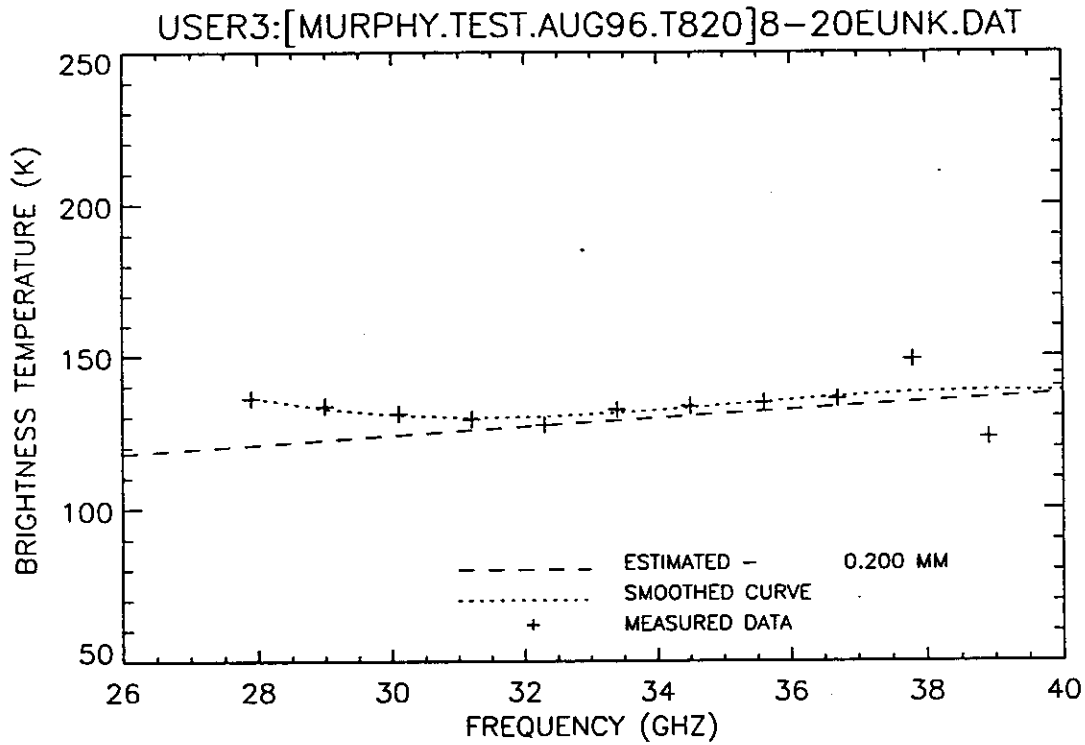


Figure B66. Plot of radiometric brightness temperature versus measurement frequency for an unknown oil thickness, 21 August 1996.

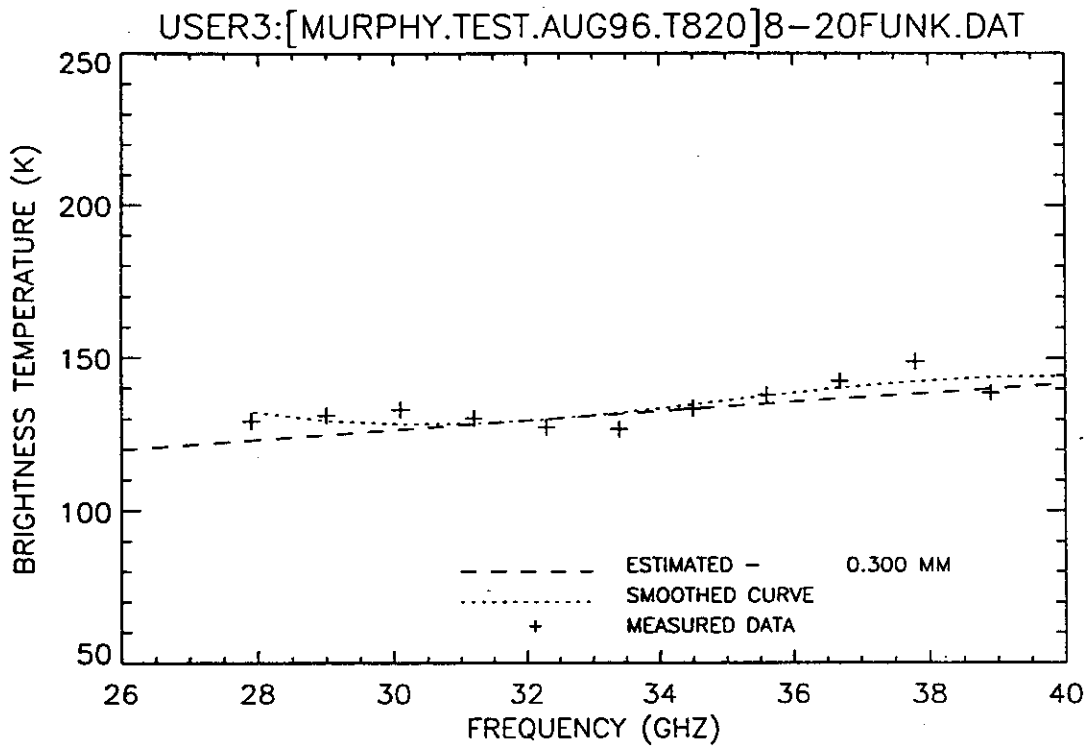


Figure B67. Plot of radiometric brightness temperature versus measurement frequency for an unknown oil thickness, 21 August 1996.

